$2(mix)$

NASA CR-130085

ATMOSPHERE EXPLORER MISSIONS C, D, & E

Spacecraft/Experiment
Interface Definition Study

Prepared by
RCA, Government and Commercial Systems
Astro-Electronics Division, Princeton, N.J.

March 30, 1972
Final Report for Period May–November 1971
NAS5-11432

Prepared for
Goddard Space Flight Center
National Aeronautics and Space Administration
Washington, D.C.

RCA

AED R-3816F

ATMOSPHERE EXPLORER MISSIONS C, D, & E

Spacecraft/Experiment
Interface Definition Study

Prepared by
RCA, Government and Commercial Systems
Astro-Electronics Division, Princeton, N.J.

March 30, 1972
Final Report for Period May—November 1971
NAS5-11432

Prepared for
Goddard Space Flight Center
National Aeronautics and Space Administration
Washington, D.C.

AED R-3816F

TABLE OF CONTENTS

TABLE OF CONTENTS (Continued)

LIST OF ILLUSTRATIONS

LIST OF TABLES

SECTION I
INTRODUCTION AND SUMMARY

This report describes, in summary form, the work accomplished under the Atmosphere Explorer Missions C, D, & E Spacecraft/Experiment Interface Definition Study, NASA Contract NAS 5-11432. The objectives of the study included an analysis of the accommodation requirements of the experiments for the three missions, an assessment of the overall effect of these requirements on the spacecraft system design and performance, and the detailed definition of all experiment/spacecraft electrical, mechanical, and environmental interfaces. In addition, the study included the identification and definition of system characteristics required to ensure compatibility with the consolidated STADAN and MSFN communications networks.

At the time of preparation of this report a few details relating to the experiment interfaces remain to be finalized. However, sufficient work has been accomplished to define all the principal spacecraft design features required to accommodate the experiments identified for Missions C, D, and E. As the "C" mission includes the full complement of experiments selected for the program, emphasis has been placed on this spacecraft configuration during the study period.

Some significant study results are the following:

- The full complement of fifteen experiments identified for the "C" mission together with the support equipment has been successfully accommodated within a 53.5 inch diameter spacecraft envelope.

- All field-of-view requirements have been met including critical requirements for a clear 2π field-of-view for the forward-looking experiments.

- An overall spacecraft height of 45 inches has been shown to provide sufficient solar array area to satisfy the power requirements of the selected complement of experiments.

- The spacecraft command subsystem has been designed to provide significant experiment programming flexibility (by inclusion of redundant command memories), and the capability of accommodating a variety of types of experiment command interfaces.

- A capability to remotely program the format of the telemetry main frame has been included.

- With the provision of an active thermal controller, improved thermal performance and greater margin for experiment operation can be achieved over the full range of mission conditions.

- The communications subsystem has been designed to be compatible with the present understanding of the new standards to be adopted for the combined MSFN/STADAN network. VHF command has been deleted in favor of S-band command. Fully redundant transponders provide the capability for simultaneous ranging (with either GRARR or MSFN stations) command, real time telemetry and playback telemetry.

The spacecrafts system configuration and performance which has been evolved during the study is described herein in terms of modifications to the system as defined at the outset of the study and summarized in Attachment A.* The revised system configuration updated to reflect the status at the completion of the study is presented in Attachment B.** A brief summary of overall system design and performance is also given under Section II in the main body of the report.

Section III outlines the key results of the experiment accommodation analyses. It includes the layout of the experiments on the AE-C spacecraft, addresses the reasons for particular locations selected and any special accommodation considerations which influenced the mounting arrangement. Command, telemetry, and power interfaces are also discussed, highlighting the achievement of standardization in this area to the greatest degree practicable. The section concludes with a summary of environmental characteristics embracing the thermal, magnetic, and aerodynamic accommodation analyses which have been completed during the study period. Complete details of the standarized spacecraft/experiment interfaces are given in the General Interface Specification (RCA No. 2260216). This document, prepared under the study, has been approved for formal usage on the Atmosphere Explorer Program.

In Section IV, revisions to the spacecraft to meet the experiment requirements, the communications network changes, and other system considerations are discussed by subsystem. Further details on areas unaffected by changes arising from the accomodation studies are given in the Phase B/C Study Report. Throughout the report, references are made to Design Notes generated during the study period. These are included in Attachment C and provide additional details in selected subsystem areas.

---

*Attachment A is "Atmosphere Explorer (AE) Spacecraft Experiment Interface Definition Study: Spacecraft Baseline Design Summary".
**Attachment B is "The AE Spacecraft System Description".

SECTION II
SYSTEM SUMMARY

As stated in the Introduction to this report, the spacecraft system configuration which has evolved from the experiment accommodation requirements and network changes identified during the study period is described herein in terms of changes to a baseline established at the outset of the Interface Definition Study. This baseline, which is in essence the configuration as defined in the earlier Phase B/C Atmosphere Explorer studies, is described in Attachment A. The revised system configuration, together with associated performance data, which has resulted from the present accommodation studies is described in Attachment B, "The AE Spacecraft System Description". In the following paragraphs, the key features of the updated configuration extracted from Attachment B are outlined, showing the manner in which experiment characteristics have influenced the system design and the impact of their operational requirements on overall system performance.

A.   GENERAL CONFIGURATION

The general configuration of the spacecraft shown in Figure II-1 is essentially unchanged from that established prior to the study. It is a sixteen-sided polyhedron, 53.5" in outside diameter and 45" in height. The side surfaces of the spacecraft, except for experiment viewing ports, and one end (the lower or +z surface) comprise the solar array. The remaining upper, or +z surface of the spacecraft provides the principal thermal control surface, under which are mounted four independent rotating louver-type active thermal controllers. The solar array and thermal surface are divided into two individual assemblies or "hats" separated at the equator of the spacecraft by an omni-directional S-band belt antenna. A four element VHF turnstile antenna is mounted on the upper surface together with one of two Cylindrical Electrostatic Probes. The ground plane of the S-band antenna, and selected exposed conductive areas on the sides of the array in the vicinity of experiment ports provide the bare area required for plasma grounding. An 18-inch diameter separation ring on the +z end forms the mounting interface between the two-stage Delta booster and the spacecraft. Spacecraft all-up-weight is currently estimated at 1282 lbs.

In mission orientation, the spacecraft is maintained with its z-axis normal to the orbit plane, and is designed to operate in either a despun (1 revolution per orbit) or spin-controlled mode at body rates between 0.5 and 10 rpm. It is of a compact and symmetric geometry, in order to minimize the effects of aerodynamic disturbances during low perigee operations.
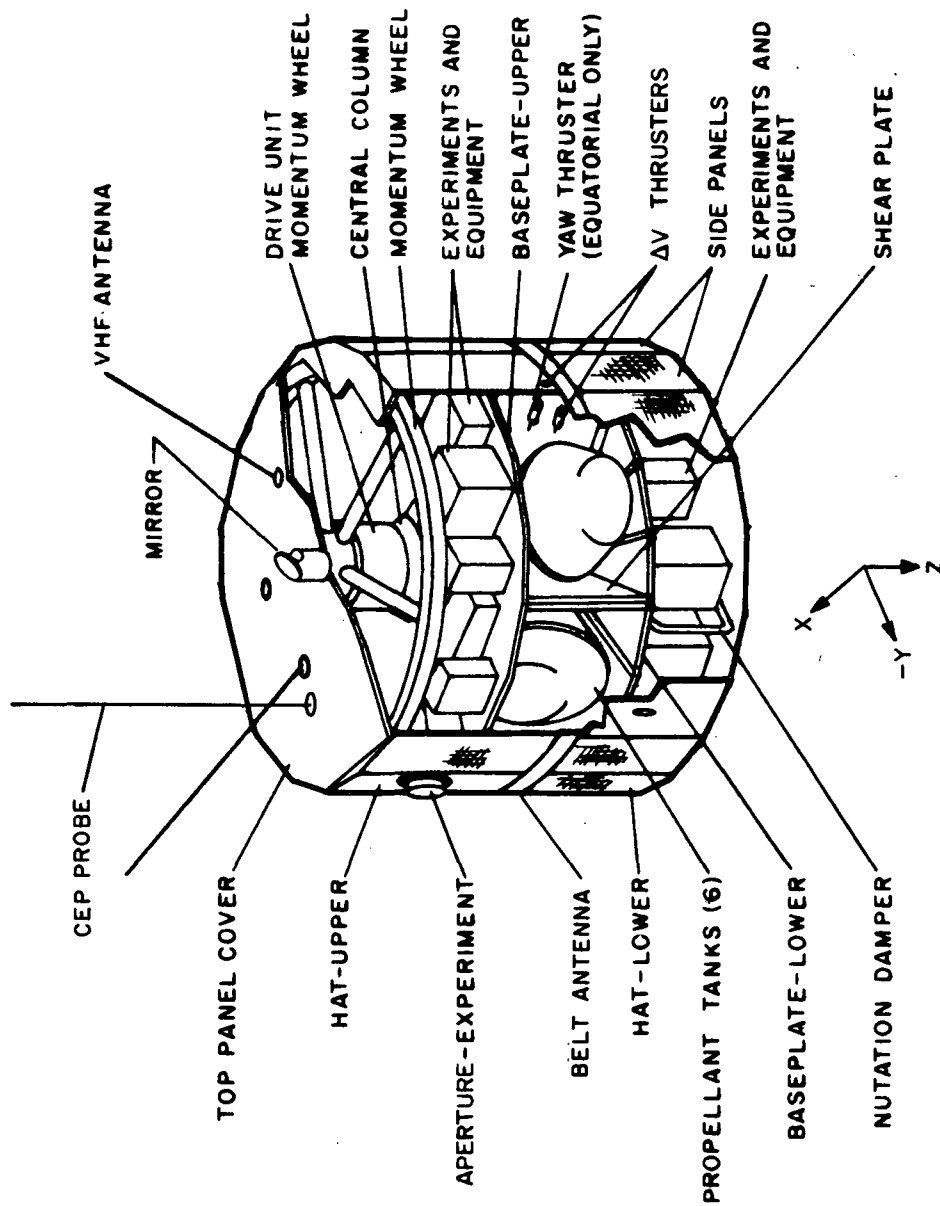
Figure II-1. Spacecraft Configuration

One new feature of the revised configuration, shown in Figure II-1, is the inclusion of an extended flat on the forward facing segment of the spacecraft (+x direction) to provide additional mounting area for those experiments (six in number) which require to face into the aerodynamic ram. The chordal flat, 18 inches in width, is equivalent in area to two adjacent array side panels. The rearward facing segment has been similarly modified for experiment accommodation.

The spacecraft internal arrangement is also partially shown in Figure II-1. Mounting surfaces for the experiments and spacecraft support equipment are provided by two machined magnesium baseplates attached to a center column, the lower end of which mates with the spacecraft adapter. Experiments are mounted on the periphery of each baseplate and, in general, view radially outwards. Their actual location on the AE-C spacecraft is shown in Figure III-1 of Section III. (For a complete listing of the experiments for each of the three missions, C, D and E, see Table III-1 of Section III.) Spacecraft support equipment is also divided between baseplates, inboard of the experiments, in a manner to best satisfy thermal control, balance, and signal routing requirements.

The center column, the main structural support member, extends from the separation adapter, through the two baseplates to support the momentum wheel assembly, the principal component of the attitude control subsystem. It encloses the miniature electrostatic accelerometer (MESA) experiment, the sensitive elements of which must be located at or close to the spacecraft center of mass. One experiment, the Extreme Ultra Violet Spectrometer, (EUVS) which requires precise solar orientation, is located on a gimballed platform (the Solar Pointing Subsystem or SPS) within the spacecraft adapter section.

Six propellant tanks, with associated plumbing, valving and thruster assemblies, comprising the Orbit Adjust Propulsion Subsystem (OAPS), occupy the bay separating the baseplates. Six structural sheet metal webs, interleaved between the tanks, provide a shear tie between the two baseplates.

B.   OPERATIONAL CHARACTERISTICS

The spacecraft is designed to operate in orbit of any inclination between 15° and 105°, both elliptical (nominal 4000 km apogee, 150 km perigee altitude) and circular orbits between 300 km and 800 km altitude. The propulsion subsystem provides the capability to compensate for aerodynamic drag losses, to make occasional perigee altitude adjustments (down to 120 km) and to accomplish the transition between elliptical and circular orbit phases of the mission. A velocity capability in excess of 2000 ft/sec is provided. Specific orbit profiles for the three missions remain to be defined in detail.

Experiments are operated in general in the low altitude regions of the elliptic orbit, with an occasional full orbit operation during the low circular-orbit phase. On-board tape recorders provide several orbits worth of data storage capability. Data can be read-out in real time via a VHF telemetry link or in either real-time or playback mode over an S-band link. The communication subsystem is designed to be fully compatible with the integrated MSFN/STADAN communications network.

C. SPACECRAFT SUBSYSTEMS

The spacecraft overall block diagram is shown in Figure II-2 and the equipment family tree in Figure II-3. In addition to the structural components, the spacecraft comprises the following subsystems:

- Thermal Control
- Attitude Control
- Orbit Adjust Propulsion (OAPS)
- Power
- Communication
- Command & Data Handling
- Solar Pointing Subsystem

1. Thermal Subsystem

The spacecraft thermal design is based on an active control system employing louver-type controllers, baseplate heaters, OAPS heaters and appropriate insulation and finishes. Active control represents a revision from the Phase B/C baseline design. It has been added to increase thermal performance margins for the selected experiments and housekeeping equipment. The controller, which consists of four independent rotating louver-type assemblies mounted beneath the -z skin of the spacecraft, provides a means of varying the effective emissivity of the principal external thermal control surface.

Louver rotation is achieved by applying heat to bimetallic elements supporting the louvers, under the control of thermistor detectors mounted on the upper baseplate. The assemblies are designed to operate full-open to full-closed over a temperature variation of less than 2°C. OAPS heaters are provided to maintain
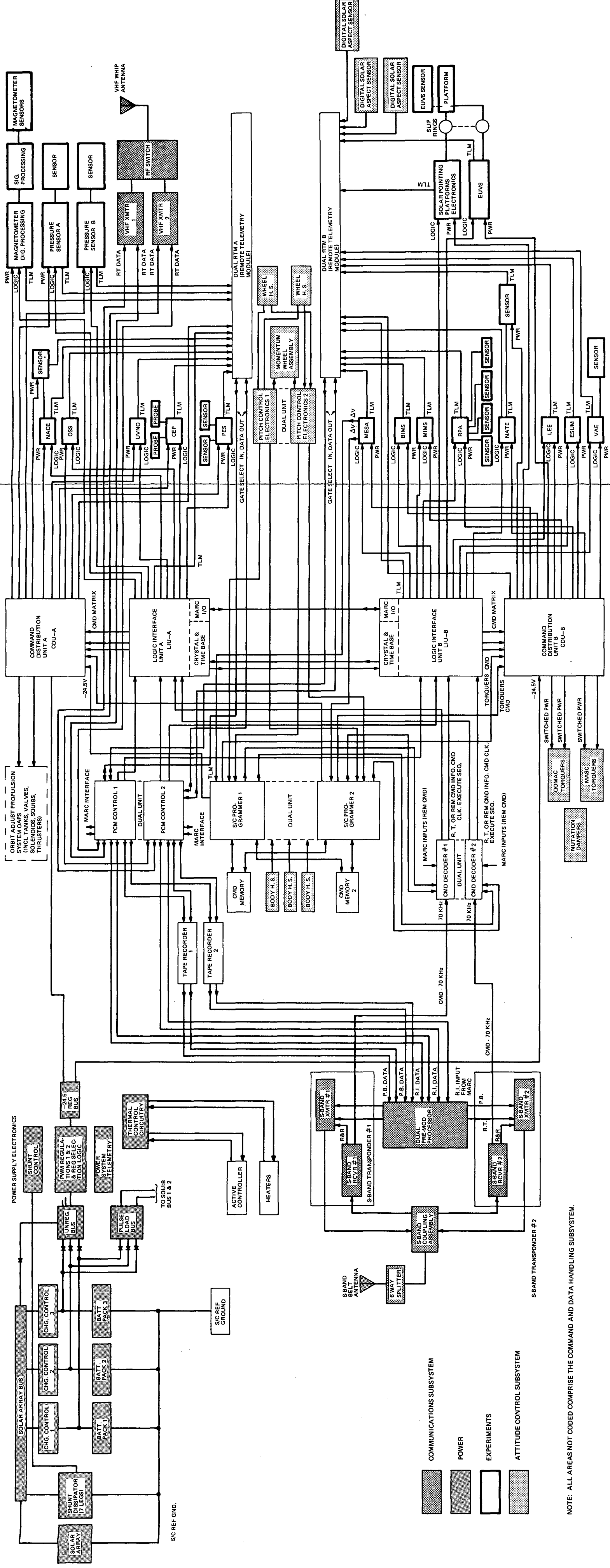
Figure II-2. Spacecraft Block Diagram

II-5/6
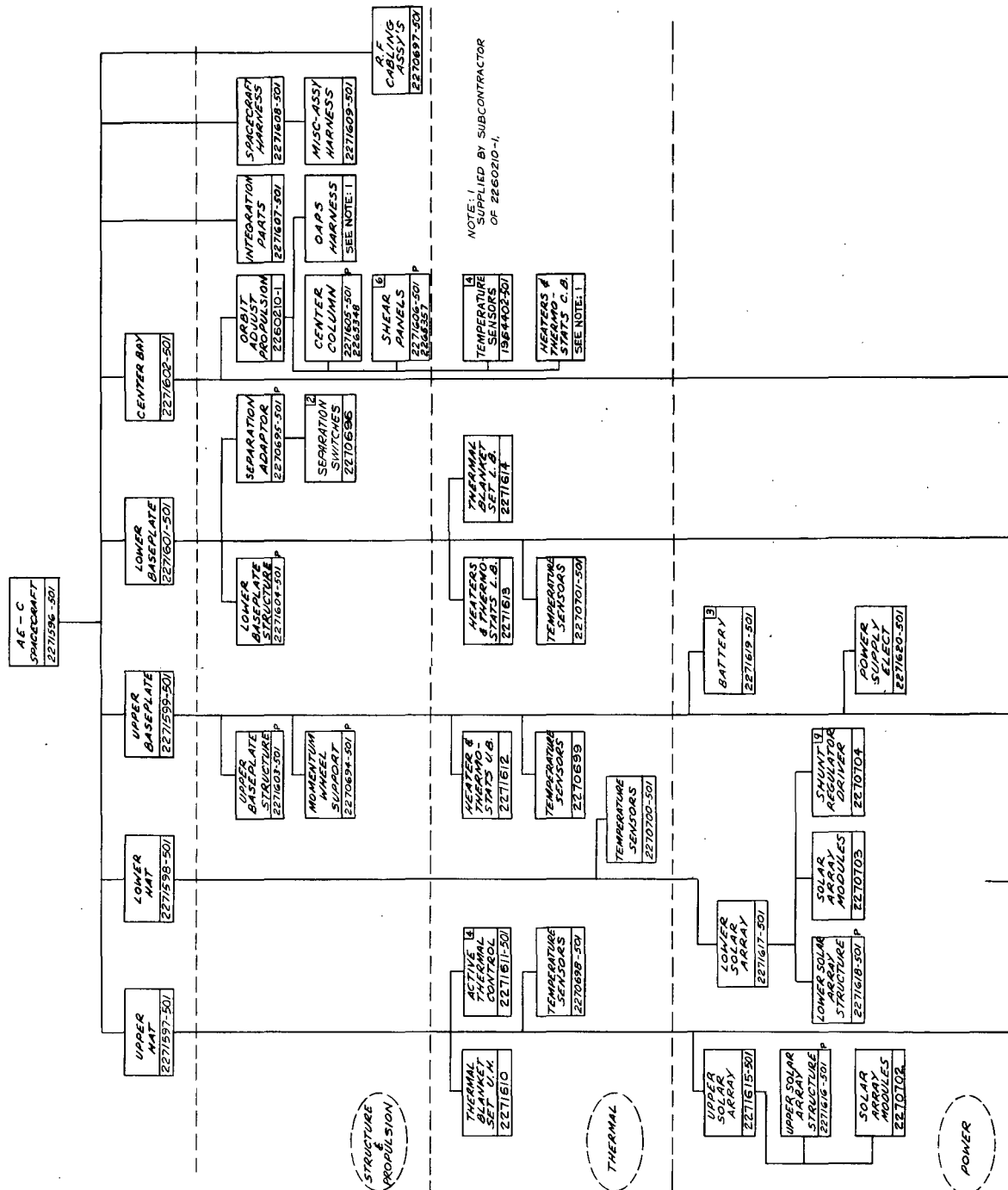
Figure II-3. Equipment Family Tree (Sheet 1 of 4)
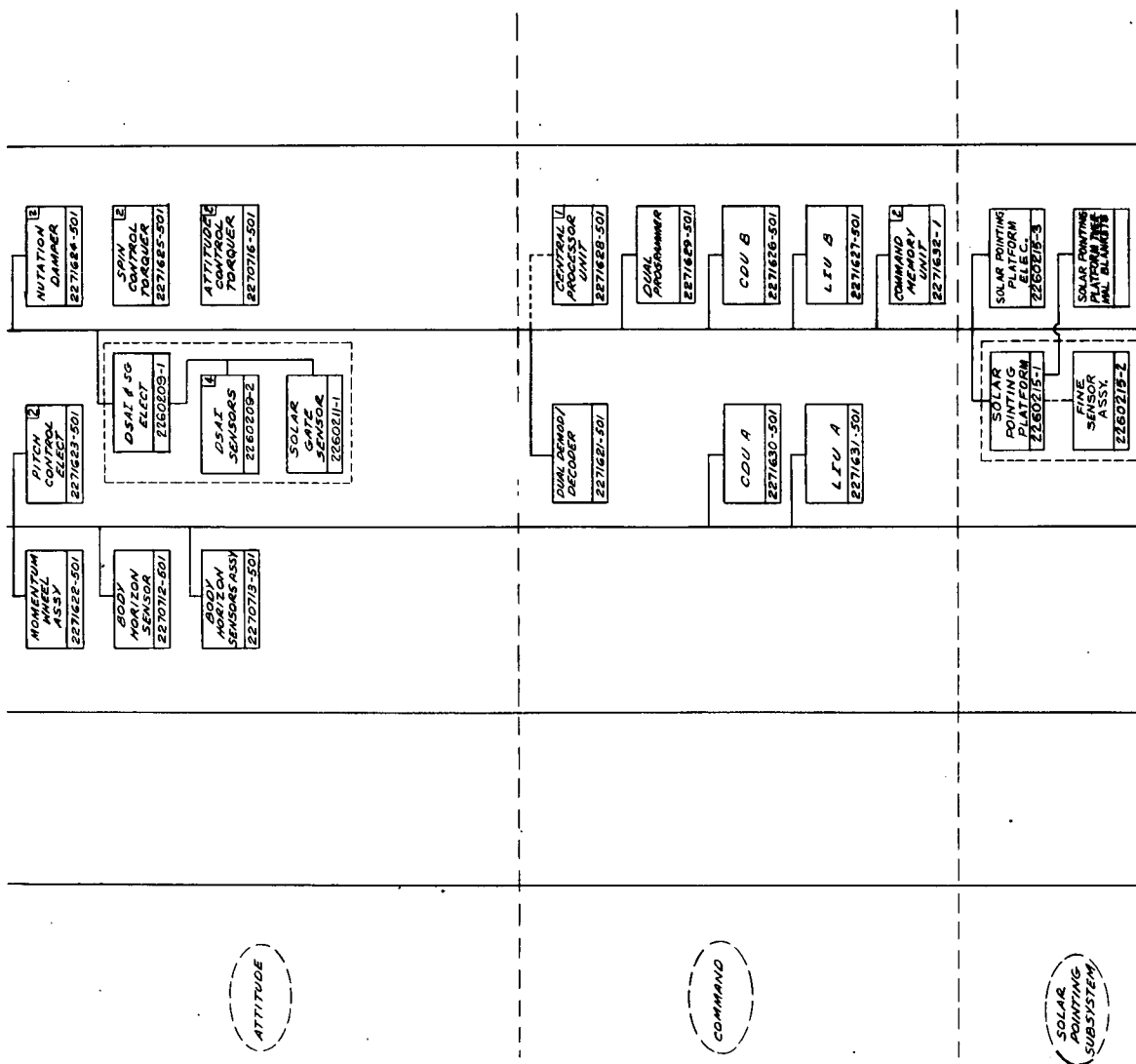
Figure II-3. Equipment Family Tree (Sheet 2 of 4)
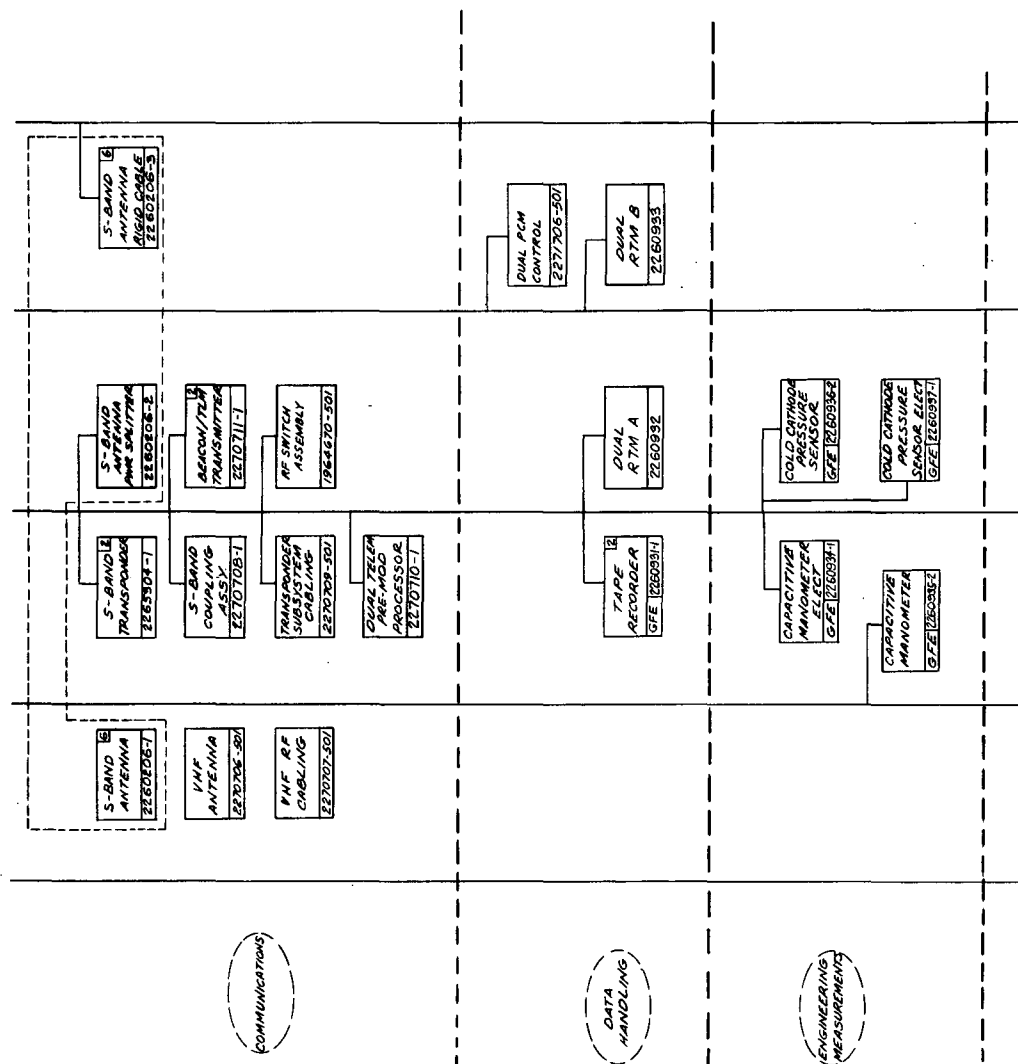
Figure II-3. Equipment Family Tree (Sheet 3 of 4)
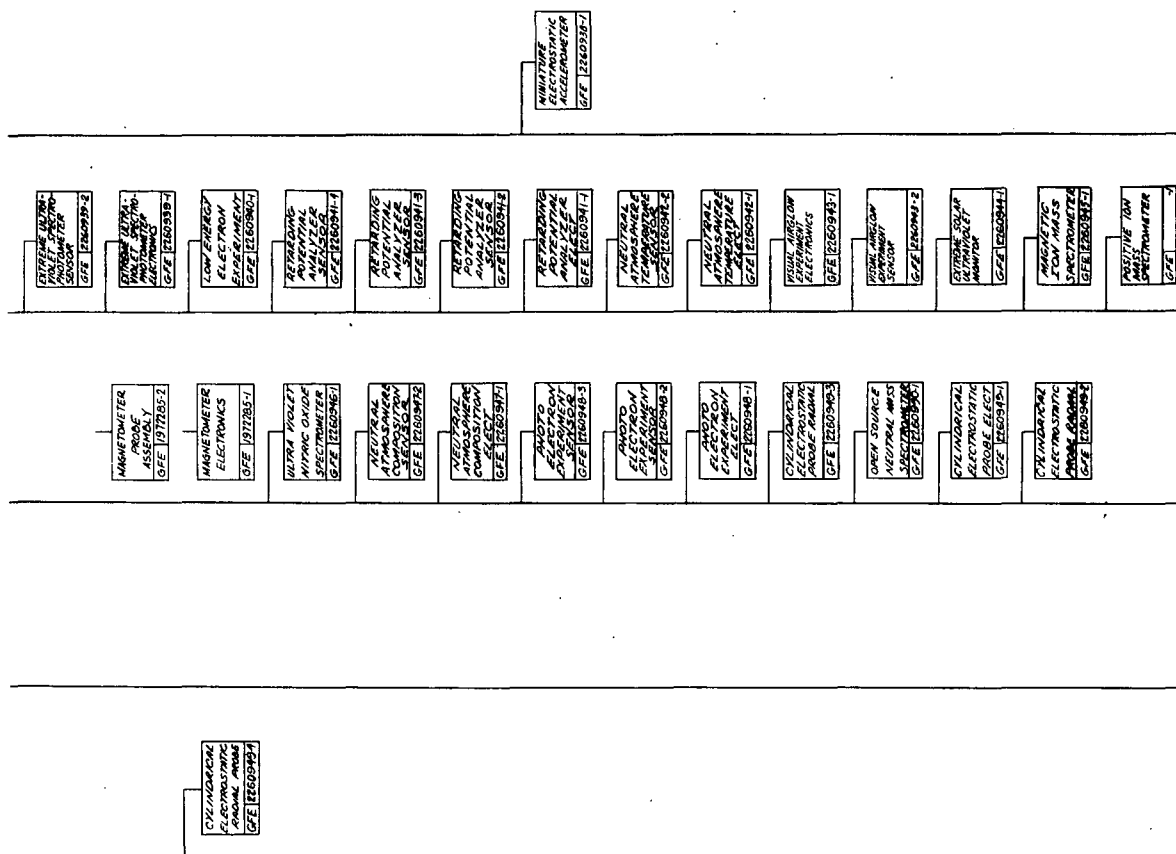
Figure II-3. Equipment Family Tree (Sheet 4 of 4)

propellant temperature above its freezing point under worst-case cold conditions. Similarly, baseplate heaters ensure that equipment temperatures are maintained within the desired range under quiescent conditions or when experiments are operated at low duty cycles for extended periods. Both sets of heaters are controlled by thermistor sensors with override by ground command.

Performance data, reflecting the addition of an active controller is given in Section IV of this report.

2.   Attitude Control

The AE spacecraft is a 3-axis stabilized dual-spin vehicle, controlled in pitch by means of momentum interchange between the spacecraft and an internally mounted wheel. Through momentum transfer between the wheel and the main body, pitch rotation can be accurately controlled at one revolution per orbit ('despun' mode) or any one of 20 selectable spin rates between 0.5 and 10 rpm. System momentum is nominally 1200 in-lbs-sec. Roll/yaw and momentum control is achieved by means of ground programmed magnetic torquing, through controlled interaction of internally generated magnetic dipoles with the earth's magnetic field. Nutation damping is provided by a silicone fluid filled loop oriented such that its axis lies in the spacecraft xy plane.

The primary attitude sensors are thermistor-bolometer type horizon detectors housed within the momentum wheel assembly. Sensor signals are used on-board in closed loop fashion for pitch control and are telemetered to the ground for processing roll/yaw attitude. The subsystem also includes body mounted horizon and solar aspect sensors to provide supplementary attitude reference data. Two new features in the revised system include the provision of on-board real-time nadir reference information, required by certain experiments in spinning mode, and the means to select any one of 360 different pitch despun orientations by ground command. (Under routine experiment data-gathering operation, the spacecraft will be oriented with its +x axis in the forward facing direction.) Two possible further modifications, offering a simplification in the momentum control technique and a potential 2:1 improvement in attitude determination accuracy, are currently under study. These are discussed in Section III.

3.   Orbit Adjust Propulsion (OAPS)

The OAPS is a monopropellant hydrazine Shell 405 catalyst blowdown system providing a total deliverable impulse capability of 75,000 lb-seconds. The subsystem contains 370 lbs of propellant divided equally between six positive expulsion tanks. Redundant engines provide thrust over the range of approximately

4 lbs to 0.75 lbs depending on blowdown pressure. A third thruster is added for the "E" mission to facilitate yaw attitude maneuvers. Two revisions have been made during the study; namely, a change from a dual to a single stage blowdown configuration (permitting a significant simplification in the hardware) and a modification to the feed system, designed to improve subsystem failure mode characteristics.

4. Power Subsystem

In addition to the solar array, the power supply subsystem includes three six-ampere hour storage batteries, a shunt limiter, and a Power Supply Electronics unit housing, battery charge controllers, redundant PWM voltage regulators, protection circuits, and other associated components. The subsystem incorporates both regulated -24.5 volt, and unregulated supplies including a special high-current capacity bus for pyrotechnics, valves, etc., connected directly to the spacecraft batteries. No major revisions have resulted from the study. In the system as currently defined it is proposed to operate all spacecraft support equipment with the exception of the tape recorders from the unregulated supply, allowing the regulator to be deactivated except during experiment data-gathering and playback periods. To improve PSE reliability, regulator automatic switchover, originally proposed as a protection feature, has been discarded in favor of regulator shut-down. Experiment safety is in no way compromised by this change.

5. Communications Subsystem

The communications subsystem, as now defined, incorporates redundant VHF beacon/telemetry transmitters and redundant S-band transponders with the capability of providing simultaneous ranging, command reception, real time telemetry and playback telemetry. A VHF command link, originally required, has been deleted. As stated previously the subsystem will be fully compatible with the consolidated MSFN/STADAN network and in particular will provide the capability for both tone ranging via the GRARR stations and PRN code ranging via the MSFN stations.

The VHF transmitters (136 MHz frequency) have two modes of operation: a low power (1/4 watt output) mode, continuously powered to facilitate GRARR station acquisition, and a high-power (1 watt output) mode activated by command for real time telemetry transmission, at a data rate of 16,384 bits per second.

The S-band transponders can operate in receive mode only, in a transponding mode for ranging or in a transmit only mode (5 watts output) for telemetry. They include provisions for automatic transmitter turn-on upon receipt of an uplink

carrier. The output carrier can be coherently related to the uplink carrier or derived from a local frequency source. Receiver portions of both transponders are powered continuously, although, as a power saving feature, an alternate possibility of adding two supplementary low power S-band command receivers is presently under consideration. Some key system parameters are given in Table II-1.

6. Command

The command configuration as presently defined is substantially different from that originally proposed and described in the Phase B/C study report.

Experiment requirements identified during the study have shown the desirability of a greater degree of flexibility, in terms of remote programming capability, than originally envisaged. The command structure and modulation technique have been modified for compatibility with the new ground network combination. Some significant changes include:

- Conversion to a command modulation scheme compatible with MSFN standards (separate clock and data subcarrier)

- Conversion to a 1024 bps command bit rate

- Revision of the command word structure with expanded error-checking capability

- Inclusion of redundant magnetic memories providing for independent programming of individual experiments and increased flexibility for other spacecraft programming requirements. All commands can now be executed either real-time or remotely.

- Provision of both relay-driving and logic level pulse commands

- Addition of capability to distribute serial digital data words (up to 32 bits in length) for decoding within the experiments

- Addition of the capability to interface with all families of IC logic circuitry which operate between a positive supply and ground

This expanded capability is reflected in the equipment complement. The command related portion of the Command and Data Handling (CD&H) subsystem now comprises redundant demodulator-decoders, memories and programmers and piece-wise redundant command distribution and logic interface units. The Programmers provide memory interface control and certain special sequencing functions. Logic interface units (LIU's) furnish logic level interfaces, both command and timing, between individual spacecraft units and between the spacecraft and the experiments so that Command Distribution Unit (CDU) functions can now be restricted solely to commands at the non-logic level.

TABLE II-I. S-BAND LINK CHARACTERISTICS

Receve Frequency	2108 MHz
Transmit Frequency	2290 MHz
RF Power Output	5 watts
Command Bit Rate	1024 bps
Real Time Telemetry Bit Rate	16,384 bps
Playback Telemetry Bit Rate	131,072 bps

It is provisionally planned to incorporate an (additional) general processor in the system for off-line command decoding, telemetry formatting and adaptive control functions. For this reason, circuits designed to interface with a 16-bit word I/O bus will be included in both the command and data handling equipment.

Signal routing considerations, and the manner in which these impact the equipment packaging configuration are discussed further in Para II.4 below. Experiment command interfaces are described in Section III. Details of the command word structure, signal flow and all functional characteristics are discussed in Section IV-H.

7. Data Handling

The principal element in the data handling segment of the CD&H subsystem is the PCM Assembly which provides the means of gathering and formatting telemetry data into a single serial digital bit stream for direct transmission to the ground or for storage in the spacecraft tape recorders.

The PCM Assembly comprises redundant PCM controllers (PCMC) and piecewise redundant remote telemetry modules (RTM's), one on each baseplate. Under the control of the PCMC, analog, 8-bit digital and discrete (flag) telemetry data is multiplexed in the remote modules and transmitted serially to the PCMC, where the analog data is A to D converted and inserted into the digital data stream.

The telemetry main frame is 128 words in length (8 bits per word), and contains four principal subcommutator slots of either 64 channels or 128 channels each. At a bit rate of 16,384 bps, the main frame period is 1/16 second, the subcom either 4 or 8 seconds. Structure of the main frame for the 'C' mission is shown in Section III.

The digital recorders are single channel-2 track units each with 1.18×10^8 bit storage capacity equivalent to 120 minutes record time. Playback-to-record speed ratio is 8 to 1. The recorders are GFE.

A new feature added during the study is the capability to re-program the format of the main frame in orbit. For this purpose, redundant Read/Write memory modules are included in the PCM controller.

8. Solar Pointing Subsystem

The solar pointing subsystem (SPS), consisting of a two-axis gimballed platform and associated electronics, maintains sun-orientation of the EUVS experiment. The integrated assembly is housed in the spacecraft adapter section of the spacecraft. Gimbal drive servos, under the control of sun sensors, mounted on the experiment, can maintain pointing to within one minute of arc of the center of the sun, or, alternatively, provide offset pointing and raster scan modes of operation upon demand. Up to 40 slip rings are provided in the azimuth drive assembly to accommodate experiment electrical interfaces. This subsystem was originally treated as part of the experiment complement.

D. PACKAGING CONSIDERATIONS

Expansion of the spacecraft command capability and the need for extensive signal interfaces at the logic level require that special consideration be given to the distribution of equipment between the baseplates and the packaging approach adopted. Logic signals routed from baseplate to baseplate in large harness bundles can lead to potentially severe noise environment problems and of course, to weight and space penalties.

To minimize such risks special attention has been paid to signal routing in the packaging approach evolved for the AE spacecraft, particularly in the areas of command and telemetry. As an example with regard to the former, commands are transmitted serially from the demod/decoder in the form of 9-bit op-codes rather than in parallel line fashion. Code translation to a 2-out-of-32 format and fan-out occur in the LIU's, one of which is dedicated to each baseplate. The designations LIUA and LIUB refer to upper and lower baseplates respectively and each LIU recognizes only those commands addressed to function on its associated baseplate. Each is piecewise redundant. Fan-out from the CDU's is also accomplished locally and they are similarly dedicated and piecewise redundant.

An analogous approach is taken in the case of telemetry as noted earlier. Piecewise redundant RTM's (A&B) are dedicated to each baseplate such that all telemetry on any one baseplate is formatted and transmitted serially to either PCMC by the local module. Word enables, for telemetry readout are likewise distributed by the LIU's.

This approach greatly reduces the number of interface connections allowing complete flexibility in the location of the PCMC's and demod/decoder.

It simplifies the overall spacecraft harness configuration, alleviates possible inter-line signal interference and potentially eases the problems of equipment integration.

E. SYSTEM PERFORMANCE

A summary of some of the key system performance parameters and operational features of the AE spacecraft is given in Tables II-II through II-IV.

The temperatures quoted in Table II-II apply over the full range of sun angles (0° to 90°) encountered in the 63° inclined AE-C orbit and reflect the improved performance achieved with an active thermal controller.

Attitude control performance remains essentially as defined at the outset of the study and meets specified requirements under both low perigee and nominal conditions. Of note is the addition of the "Nadir Pulse" feature, which furnishes experiments with a local vertical attitude reference in the spinning mode.

The OAPS net deliverable impulse of 75,000 lbs/sec provides in excess of 2000 ft/sec ΔV capability for apogee restoration and other orbit adjust maneuvers. Analysis shows that ΔV burns of up to 24 ft/sec can be accomplished without excessive attitude disturbance.

The command and data handling characteristics reflect the flexibility now provided by this subsystem. Up to 64 kilobits time-tag memory storage capacity has been provisionally selected which will meet experiment programming requirements for at least four orbits duration with the associated facility of modifying modal states during record operations as required. As shown in Table II-IV, the memory allows independent turn-on and turn-off experiments with a granularity of a few seconds. Propulsion ΔV operations and other spacecraft support equipment related programming functions can similarly be accomplished with a higher degree of flexibility than afforded by the originally selected command approach.

Experiment duty-cycle capability as a function of sun angle is shown in Figure II-4. Curves show performance at both beginning of life and after 8 months in a near-polar orbit (representative, in terms of solar array degradation, of both the C & D missions). The curves represent the duty cycle limit imposed by solar array power capability; in the mid sun-angle range thermal performance may slightly restrict the utilization of maximum available power. Note that under worst-case sun angle conditions ($\gamma = 90°$), a duty cycle of 15.5% at 8 months is achievable based on an experiment total power requirement of 115 watts. This is equivalent to 17.5% referenced to the original experiment requirement of 100 watts.

TABLE II-II. SYSTEM PERFORMANCE SUMMARY

Life Time	>12 months
Projected Area	2400 in^2
Weight	1282 lbs
Thermal Performance	
Upper Baseplate	0°C to 20°C
Lower Baseplate	5°C to 35°C
Attitude Control Performance	
Roll/Yaw	<2° rms @ 120 km
	(5° max during orbit adjust operations)
Pitch (despun)	<2° rms
Pitch (spinning)	±1% of commanded rate
Nadir Pulse	±2°
Propulsion	
Propellant Capacity	370 lbs
Deliverable Impulse	75000 lbs sec (min.)
ΔV per burn capability	24 ft/sec (within ±5° roll limit)
Command and Data Handling	
Memory Capacity	2 x 32 kilobits
Major Mode Comands Available	496
Record Capability	120 minutes per recorder
Experiment Power	
BOL	115 watts @ 20%
8 month-near polar	115 watts @ 15.5%
Experiments	
Weight	184 lbs
Power	115 watts
Mounting Area	1335 sq inches

C

TABLE II-III. LOW PERIGEE PERFORMANCE

Item	Baseline Performance
Roll Angle Error at 120 km	
First Perigee Peak Error	2.3 degrees
Continuous Contacts	1.5 degrees
Momentum Change/Orbit	1.4%
Lost Contact Performance	
Minimum Component Temperature	-5 °C
No Contact after Orbit Adjust, ± 3-degree Roll Limit (Automatic Roll Control)	Maintained for 12 orbits
Thermal Altitude Limits*	
Spinning Perigee in Sun	114 km (100% margin at 120 km)
Despun Perigee in Sun	129 km
Despun Perigee in Eclipse	121 km
*Spacecraft capability. Experiment thermal considerations may limit lowest perigee.	

TABLE II-IV. OPERATIONAL FEATURES

Experiment Programming	Up to 72-hours delay time with 4 sec granularity. On-time selectable to 4 second granularity.
	Pulse or data-loading commands
Science and Status Telemetry Readout	S-Band/VHF/real time 16384 bits/sec.
	S-Band Playback 131072 bits/sec.
Command	S-Band 1024 bits/sec.
Orbit Determination	S-Band Range and Range Rate Tracking
Orbit Adjustment	Up to 24 ft/sec with < 1 ft/sec granularity (thrust range 4.1 lbf to 0.75 lbf)
Attitude Control	Mode change (despin/spinning) by direct momentum transfer. Roll/yaw control by magnetic torquing.
Attitude Determination	Horizon/Solar Sensor data: ground processing.
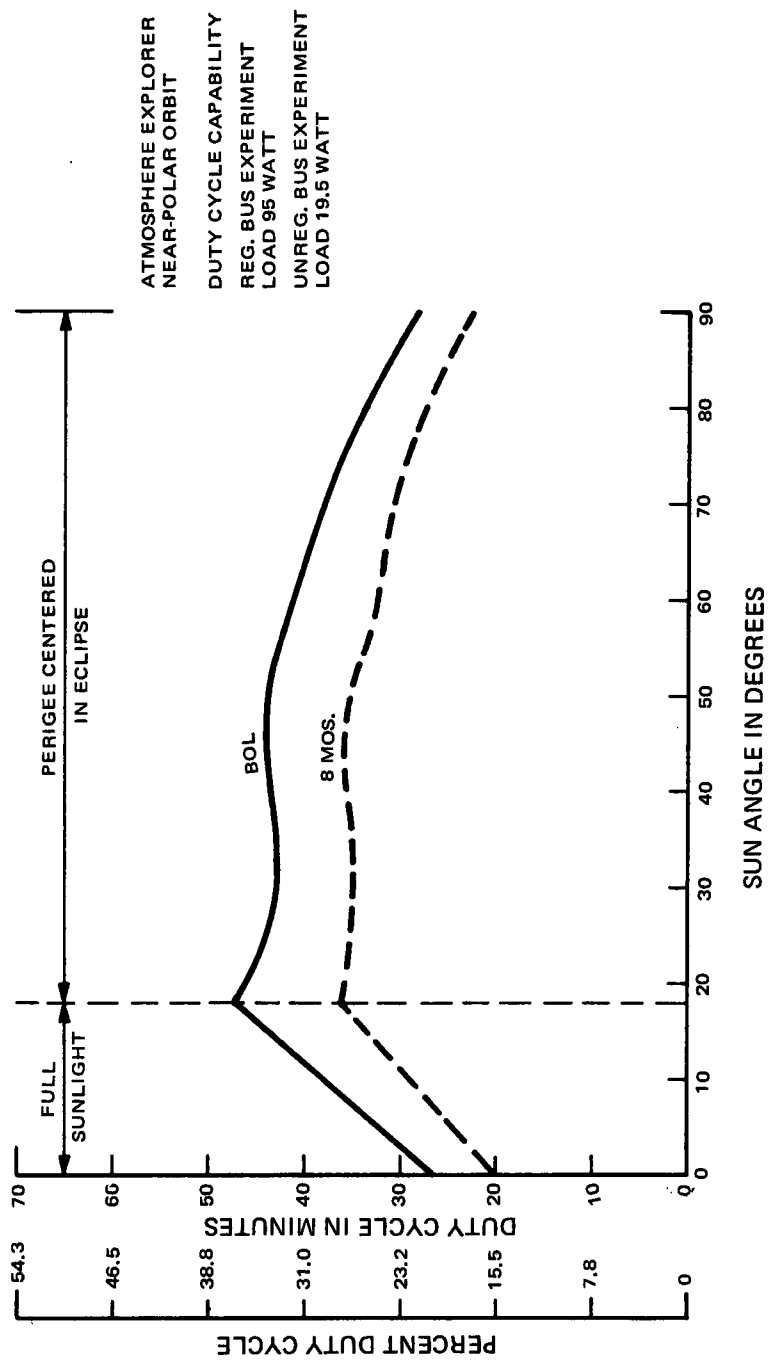
Figure II-4.   Experiment Duty Cycle vs Sun Angle

SECTION III
EXPERIMENT AND GFE MEASUREMENTS ACCOMMODATION

In this section of the final report, the overall accommodation of the experiments and GFE engineering measurement instruments within the spacecraft is discussed with emphasis on the mechanical and electrical experiment/spacecraft interface characteristics and the environment under which the experiments are required to operate.

Tables are included, summarizing experiment weight, size and power requirements, the command lists, and the allocation of channels in the main and subcom telemetry frames.

In the areas of detailed accommodation study the baseplate layout for the AE-C spacecraft is described including the specific arrangement of the experiments in the forward facing area. The reasons for the location of each experiment are discussed, highlighting the influence of mission objectives, and considerations of balance, thermal and magnetic environment on the mounting arrangement for the experiment complement. Areas requiring special attention, such as placement of the Extreme Ultra Violet Spectrometer and accommodation of experiments with special dimensional requirements (e.g. the NATE experiment) are addressed in a little more detail.

The discussion of experiment electrical accommodation provides a description of the command interfaces with the AE spacecraft, and the approach adopted for data handling and status telemetry. Power subsystem interfaces, grounding philosophy and the anticipated EMI environment are also addressed. The summary report on the status of the electrical accommodation studies is concluded with a detailed description of the interface circuits between the experiments and the spacecraft command and data handling subsystems.

Discussion of the spacecraft environment covers the present status of studies which have been carried out to characterize the anticipated experiment magnetic, pressure, contamination, thermal and mechanical noise environments.

With regard to magnetic characteristics of the spacecraft, maps have been prepared showing the predicted field intensity in the vicinity of experiment apertures due to the combined effect of the spacecraft torquers and magnetic material within the experiments themselves. While methods of further reducing the levels will continue to be investigated, these preliminary analyses show that field strengths are in general well within specification.

The question of the spacecraft internal pressure is one of general environmental concern since the Atmosphere Explorer spacecraft will be descending to a low (120 km) perigee on occasion throughout the various missions. Studies have been conducted, briefly reported here, as to the pressures that may be expected within the spacecraft during the low perigee excursions, and the approaches being considered to reduce these pressures.

A spacecraft subsystem of interest regarding its impact on the experiment environment is the Orbital Adjust Propulsion Subsystem (OAPS) which utilizes hydrazine as the propellant. The possible environmental effects resulting from the operations of the OAPS thrusters in space is discussed.

Low-level vibration effects have been investigated due to their possible detrimental effect on the accuracy of drag data measured by the sensitive accelerometers that constitute the MESA (Miniature Electrostatic Accelerometer) experiment. These units are susceptible to mechanical noise and the value of the experiment will be decreased if adequate filtering to attenuate noise cannot be accomplished. The steps being taken to analyze the potential problem are outlined.

Finally the spacecraft thermal environment, and its impact on the interfaces with individual experiments is addressed. Of particular importance in this regard are the thermal interfaces with the EUVS and ESUM experiments and the behavior of experiment grids and other exposed elements under the effects of aerodynamic heating.

This section concludes with a report of the testing that has been performed on the COS/MOS series of devices identified for possible application to the AE system.

Full details of all mechanical, electrical and environmental interfaces are given in the General Interface Specification PS-2260216 and the associated experimental unique documentation.

A. OVERALL ACCOMMODATION

The experiment and engineering measurement instrument complements for the AE-C, D, E missions are listed in Table III-I. Note that all experiments are included in the C-mission. It is the most complex in this respect and unless otherwise stated, subsequent discussion will focus on this case.

The major characteristics of the experiments and GFE engineering measurement units (i.e., the pressure sensors) comprising the complement for the AE-C mission are summarized in Tables III-II through III-VIII. Details of any specific accommodation problems or areas of interest are discussed in later paragraphs.

The principal mechanical parameters of the experiments as defined at the date of submission of this report are given in Table III-II. All have been accommodated successfully within a 53.5" diameter spacecraft envelope. Layout drawings in Paragraph III.2 and the overall weight summary given in Section IV are based on the characteristics listed.

It should be noted that several experiments are using release mechanisms or blow off caps of various kinds, and that some measurements necessitate mechanical motions within the instruments. Those using blow off caps or similar mechanisms are shown in Table III-III, while experiments requiring moving parts within the instruments are listed in Table III-IV.

Power requirements are given in Table III-V. The duty cycle capability shown earlier in Section II is based on these estimates.

The list of commands that have been identified for each of the experiments and the GFE sensors are shown in Table III-VI.

The telemetry main frame requirements are presented in Table III-VII and Table III-VIII gives the subcom assignments for each experiment.

TABLE III-I. ATMOSPHERE EXPLORER EXPERIMENTS

Investigator	Experiments	AE-C	AE-D	AE-E
L. Brace	Cylindrical Electrostatic Probe Experiment (CEPE)	x	x	x
K. Champion	Atmospheric Density Accelerometer (MESA)	x	x	x
J. Doering	Photoelectron Spectrometer (PES)	x	x	x
W. Hanson	Retarding Potential Analyzer (RPA)	x	x	x
D. Heath	Extreme Solar Ultraviolet Monitor (ESUM)	x	x	x
H. Hinteregger	Extreme Ultraviolet Spectro-photometer (EUVS)	x	x	x
A. Nier	Open-Source Neutral Mass Spectrometer (OSS)	x	x	x
D. Pelz	Neutral Atmosphere Composition Experiment (NACE)	x	x	x
N. Spencer	Neutral Atmosphere Temperature Experiment (NATE)	x	x	x
J. Hoffman	Magnetic Ion Mass Spectrometer (MIMS)	x	x	
H. Brinton	Bennet Ion Mass Spectrometer (BIMS)	x		x
C. Barth	Ultraviolet Nitric Oxide Spectrometer (UVNO)	x	x	
R. Hoffman	Low Energy Electron Experiment (LEE)	x	x	
P. Hays	Visual Airglow Experiment (VAE)	x	x	x
J. Armstrong*	Magnetometer		x	x

*This experiment was added at the time of preparation of this report. Interface data is not included herein.

TABLE III-II. MECHANICAL PARAMETERS

Experiment	No. of Units	Weight (lbs)	Footprint (in^2) (each unit)
RPA	3 Sensors 1 Electronics	Front Unit 3.0 lb Rear Units 1.6 lb each 4.8	16.0 each 42.5
MIMS	1	10.0	105
BIMS	1	7.6	67
PES	Electronics 2 Sensors	4 3 each	9 22 each
MESA	1	16	(Center Well)
OSS	1	15	55
NACE	Sensor Electronics	10 6	45 46
NATE	Sensor Electronics	10 5.2	45 46
PSA	Sensor Electronics	2.5 3.5	8 35
PSB	Sensor Electronics	3.0 3.2	12 20
ESUM	1	18.08	81
EUVS	Sensor Electronics	18 6	(Center Well) 36
UVNO	1	15.5	130
VAE	Sensor Electronics	12	115 19
CEP	2 Sensors 1 Electronics	0.75 3.3	(Outside) 48
LEE	1	9.5	160

TABLE III-III. RELEASE MECHANISM REQUIREMENTS

ESUM	Squib actuated blow off cover
VAE	Biphenyl actuated blow off cover.
CEP	One biphenyl, one squib actuated release
OSS	Squib actuated blow off vacuum cover
NACE	Squib actuated blow off vacuum cover
NATE	Squib actuated blow off vacuum cover
PSA	Squib actuates blow off vacuum seal

TABLE III-IV. MOVABLE PART REQUIREMENT

ESUM	A rotating filter wheel
EUVS	Moving gratings;
VAE	Rotating filter wheel
NACE	Movable shutter used to cover aperture
NATE	Part of the instrument undergoes "dithering" or back and forth oscillation.

TABLE III-V. POWER REQUIREMENTS

Experiment	Nominal Power (watts)	Peak Power (watts)
RPA	6.0	6.0
MIMS	7.0	7.0
BIMS	2.0	2.0
PES	2.5	3.0
MESA	19.5 (Unreg.)	23.4
OSS	8.0	12.5
NACE	16.0	16.0
NATE	16.0	18.0
PSA	1.5	1.5
PSB	2.0	3.5
ESUM	2.25	2.25
EUVS	12	12
UVNO	8.2	8.2
VAE	7	9
CEP	2	2
LEE	2.5	2.5

TABLE III-VI. COMMAND REQUIREMENTS

Experiment	Power	Ordnance	Major Mode			Minor Mode Bits
			Logic	Relay	Minor	
RPA	2	0	0	10	1	16
MIMS	2	0	0	0	1	18
BIMS	2	0	2	0	1	24
PES	2	0	1	6	1	12
MESA	6	0	0	18	0	0
OSS	4	2	3	0	1	21
NACE	2	2	0	4	2	30
NATE	2	2	0	2	2	23
PSA	2	1	0	0	0	0
PSB	4	0	0	0	0	0
ESUM	2	4	7	3	1	12
EUVS	4	0	25	0	3	78
UVNO	2	0	1	0	1	8
VAE	4	4	3	0	2	15
CEP	6	2	0	13	0	0
LEE	2	0	2	2*	1	32

* 4 for AE-D

1 SYNC	2 SYNC	3 SYNC	4　　　5 CMD VERIF		6 RPA A	7 UVNO D	8 UVNO D
9 CEP A	10 BIMS A	11 EUVS D	12 EUVS D	13 EUVS D	14 EUVS D	15 RPA A	16 BIMS A
17 S/C	18 S/C	19 MIMS A	20 EUVS D	21 NACE D	22 NACE D	23 BIMS A	24 RPA A
25 CEP A	26 MIMS A	27 NATE D	28 NATE D	29 UVNO D	30 NATE D	31 NATE	32 RPA A
33 RPA A	34 ESUM D	35 ESUM D	36 BIMS A	37 SUB COM COUNTER	38 PES D	39 PES D	40 PES D
41 CEP A	42 RPA A	43 LEE D	44 LEE D	45 LEE D	46 VAE D	47 VAE D	48 VAE D
49 BIMS A	50 UVNO D	51 RPA A	52 RPA A	53 NACE D	54 NACE D	55 ESUM D	56 BIMS D
57 CEP A	58 MIMS A	59 NATE D	60 NATE D	61 RPA A	62 BIMS A	63 OSS D	64 OSS D
65 SUB COM	66 SUB COM	67 SUB COM	68 SUB COM	69 PSA	70 RPA A	71 HOT WIRE A	72 UVNO D
73 CEP A	74 MIMS A	75 BIMS A	76 OSS D	77 OSS D	78 OSS D	79 RPA A	80 BIMS D
81 S/C	82 S/C	83 MIMS A	84 MIMS A	85 NACE D	86 NACE D	87 BIMS A	88 RPA A
89 CEP A	90 MIMS A	91 NATE D	92 NATE D	93 UVNO D	94 OSS A	95 NACE A	96 RPA A
97 RPA A	98 ESUM D	99 ESUM D	100 BIMS A	101 PSB	102 PES D	103 PES D	104 PES D
105 CEP A	106 RPA A	107 MAG D	108 MAG D	109 MAG D	110 VAE D	111 VAE D	112 VAE D
113 BIMS A	114 UVNO D	115 RPA A	116 NACE A	117 NACE D	118 NACE D	119 MESA D	120 MESA D
121 CEP A	122 MIMS A	123 NATE D	124 NATE D	125 RPA A	126 BIMS A	127 RPA D	128 LEE A

TABLE III-VIII. SUBCOM REQUIREMENTS

Experiment	Subcom Analog Words		Subcom Digital Words		Relay Flag Bits
	4 sec	8 sec	4 sec	8 sec	
RPA	25	0	6	2	4
MIMS	0	10	2	0	4
BIMS	5	6	4	4	0
PES	0	6	2	0	4
MESA	6	3	0	0	12
OSS	0	13	4	0	0
NACE	0	9	0	5	0
NATE	0	10	0	4	0
PSA	0	4	0	0	0
PSB	0	5	0	0	0
ESUM	0	9	0	4	0
EUVS	0	4	0	3	0
UVNO	0	7	0	1	0
VAE	2	8	0	3	0
CEP	0	6	0	0	6*
LEE	0	5**	0	5	0

*Each bit to be sampled at 4 sec. intervals.

** 6 for AE-D

B.   MECHANICAL ACCOMMODATION

1.   Experiment Layout

During the Interface Definition Study, an experiment layout was derived for the "C", "D", and "E" experiment complements. The "C" spacecraft will contain all of the experiments presently defined for AE; hence, resolution of the experiment layout configuration for the "C" spacecraft represents the most difficult design requirement.

The "C" experiment complement is shown in Figure III-1. The experiments require approximately 1,335 square inches of baseplate mounting area, and occupy 10,242 cubic inches of volume. Half of the experiments are mounted at or near the forward, or +x side of the spacecraft (NACE, NATE, PES, OSS, MIMS, BIMS, RPA). Others are located to provide a view along the zenith or nadir (VAE, LEE) or exposure to the sun (EUVS, ESUM). The MESA experiment is mounted within the spacecraft, with a defined location with respect to the spacecraft co-ordinate system. The UVNO is oriented to point rearward, along the -x axis, and the CEP requires two probes located external to the spacecraft oriented parallel and perpendicular to the spacecraft spin axis.

With exception of the MESA and the new Magnetometer experiment, all units require access to the external surrounds of the spacecraft in order to accomplish the desired measurements. Generally, external access is provided by allowing the experiment sensing element to pass through the spacecraft outer shell (solar array). The spacecraft solar array is not configured as a load path for the experiments, the main load path from the individual experiments to the space-craft is via the spacecraft baseplate mounting surface. Experiments are thus positioned on the spacecraft baseplates adjacent to the spacecraft solar array. Cutouts are provided to allow portions of the experiments to project beyond the solar array. (Details of the solar array apertures design are shown in Figure IV-1, Section IV-A.)

The composite solar array cutout configuration is shown in Figure III-2. The spacecraft side area available for solar cell installation is approximately 6,796 square inches (exclusive of the S-band antenna). Of this amount, 546 square inches is unavailable due to experiment array cutouts, and 334 square inches is lost to provide ground planes for the RPA, MIMS, and BIMS experiments. The total unavailable area is equivalent to 8 additional 2 x 2 solar cell series strings.

A number of experiments require a 2π clear field of view at the entrance aperture of the instrument. In order to meet this requirement, the entrance apertures must project beyond all external spacecraft protuberances. Experiments with a 2π field of view requirement located on the forward facing portion of the space-craft are configured to place all of the instrument entrance apertures in the

same plane beyond the S-band antenna. The antenna projects 0.75 inches beyond the front forward flat of the spacecraft, requiring a similar projection for the experiments.

The experiments on the upper baseplate (OSS, NACE) are located with the plane of their apertures tangent to the S-band antenna outside surface. The experiments mounted on the lower baseplate (RPA, MIMS, BIMS) are located with their aperture planes coincident, and approximately 0.21 inches within the S-band antenna outer diameter. The antenna appears in the extreme edge of the field-of-view in these cases. This compromise location was selected to minimize the structural support associated with projecting a full 0.75 inches beyond the spacecraft shell.

2. Special Experiment Accommodation Considerations

Several of the experiments, by virtue of their complexity or special requirements, have specific accommodation needs unique to the instrument. The spacecraft design has accommodated these needs, without major spacecraft design impacts.

a. NACE - The NACE is designed to use a quadrapole tube developed for past applications. The tube length and orientation is such that it exceeds the headroom available for components between the baseplate and the solar array. In order to accommodate the instrument, a hole will be provided in the spacecraft baseplate mounting surface, allowing a portion of the instrument to extend into the propulsion bay section of the spacecraft. The NACE location on the spacecraft has been chosen to provide the desired scientific location, within the constraints of the available volume between the propulsion tanks.

b. UVNO - The UVNO location has been chosen to maximize the length of the sun shade attached to the instrument. The outboard end of the sun shade is configured as a removable section, to allow illumination of an aperture slot on the spacecraft solar array for the UVNO projection. The removable section will be installed on the UVNO after the array installation on the spacecraft.

c. LEE - The LEE experiment has 19 individual detectors, each with a removable section. The removable sections will be attached after the spacecraft solar array is installed on the spacecraft, thereby eliminating multiple slots for the detector projections through the array.

d. MIMS/BIMS/RPA - The ground plane requirements for each of these experiments has been satisfied by a single ground plate 16 inches in diameter, centered at the approximate center of the instrument cluster (see Figure III-3).
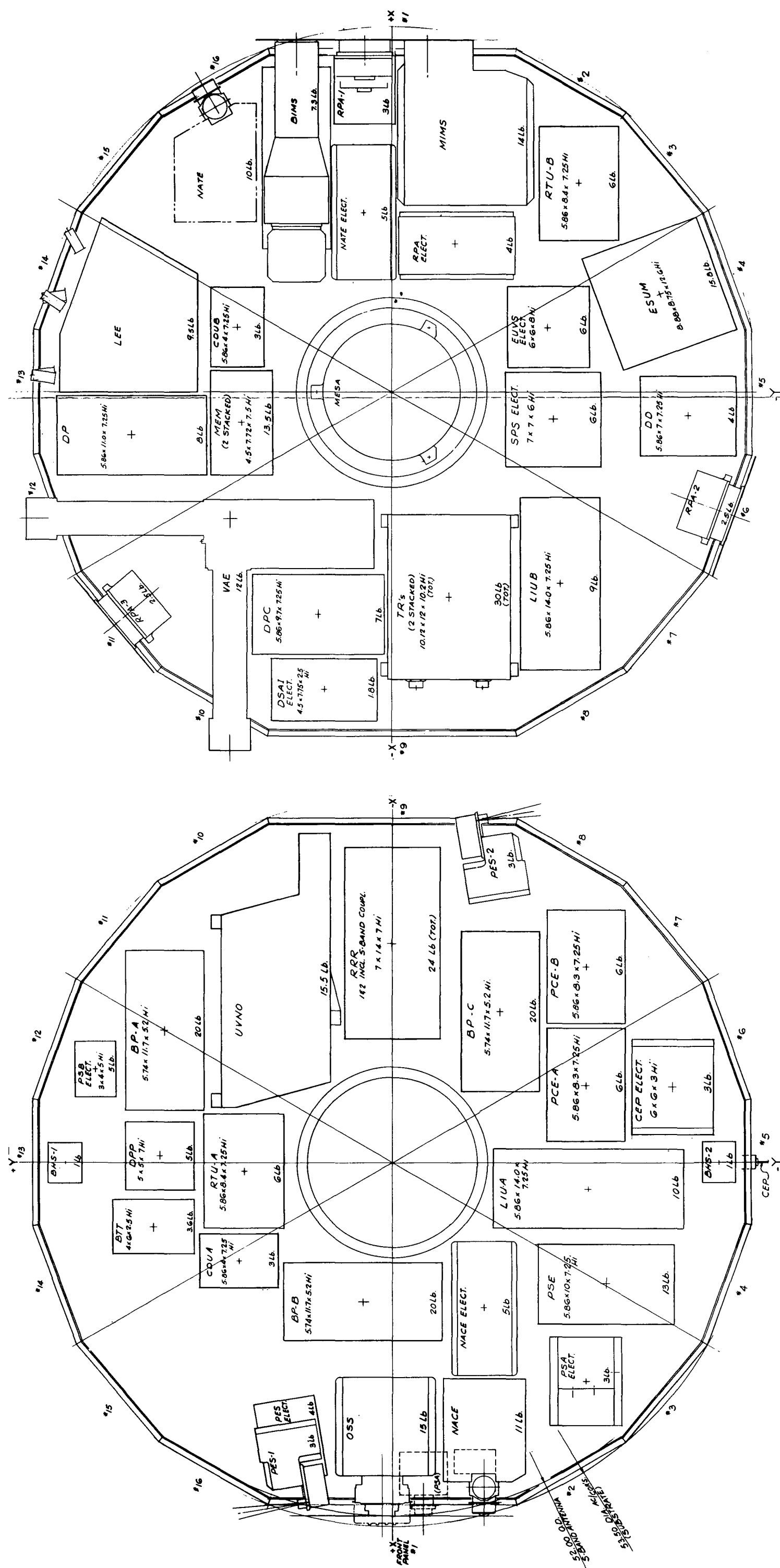
Figure III-1. Experiment Layout

III-13/14
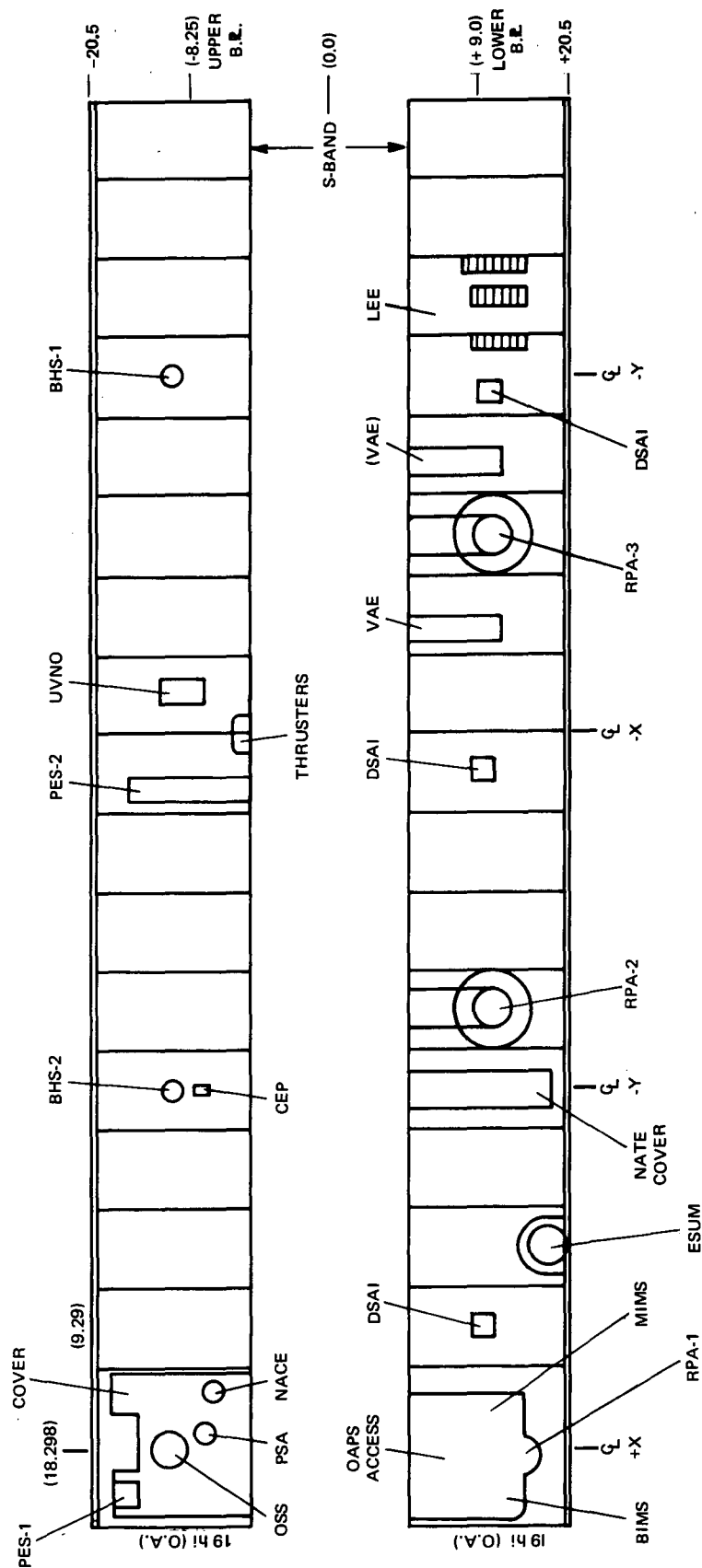
Figure III-2. Solar Array Cutout Configuration

The ground plate encompasses the ground plane area requirements of the individual experiments and will remain at spacecraft potential at all times. It will contain clearance holes to allow one forward portion of the MIMS, RPA and BIMS experiment to view through the plate surface. The forward portion of these experiments can be biased individually through experiment programming without changing the potential of the main ground plane.

The ground plane will be of solid aluminum, gold plated on the external surfaces. Since the plate will be at high temperatures in the sunlit portion of the orbit (approximately 275° C), its attachment to the spacecraft will be designed to minimize the thermal coupling.

     e.   BIMS/MIMS Vent – The BIMS and MIMS experiments contain venting provisions to lower the pressure internal to the instruments during low perigee passages. The vents are configured to allow passage of particles from the internal portion of the instruments to the low pressure region at the +z end of the spacecraft.

The BIMS vent is configured as a right angle tube, passing from the internal portion of the experiment through the array +z surface. The vent portion is constructed of a low-thermally-conducting material to minimize the effects of solar heating of the vent on the internal spacecraft temperatures.

The MIMS vent is configured as a rectangular tube, providing venting from the forward section of the MIMS to the +z end of the spacecraft. The vent tube is located outside the spacecraft, behind the ground plane described in section III-D. The external vent tube configuration eliminates the requirement to provide an additional cutout in the spacecraft solar array.

     f.   ESUM – The ESUM experiment requires a viewing elevation angle of 25 degrees, necessitating an array cutout in the corner at the junction of the side array and +z end array of the spacecraft. The instrument will contain a shield to reduce the thermal flux through the array cutout. The shield will contact the spacecraft array substrate, forming a seal with a foam type gasket at the edges of the array cutout. The foam seal will allow the instrument to be in contact with the array without forming a parallel load path or a thermal leak.

     g.   EUVS – The EUVS experiment is contained within the spacecraft booster adapter, mounted to a 2 axis gimballed platform (the SPS). The platform compensates for spacecraft rotation and orients the EUVS in elevation to maintain the instrument continuously pointed at the solar disk.

The spacecraft mechanical interface will be designed to provide an environment conducive to EUVS launch survival and orbital operation.

LOWER BASE PLATE
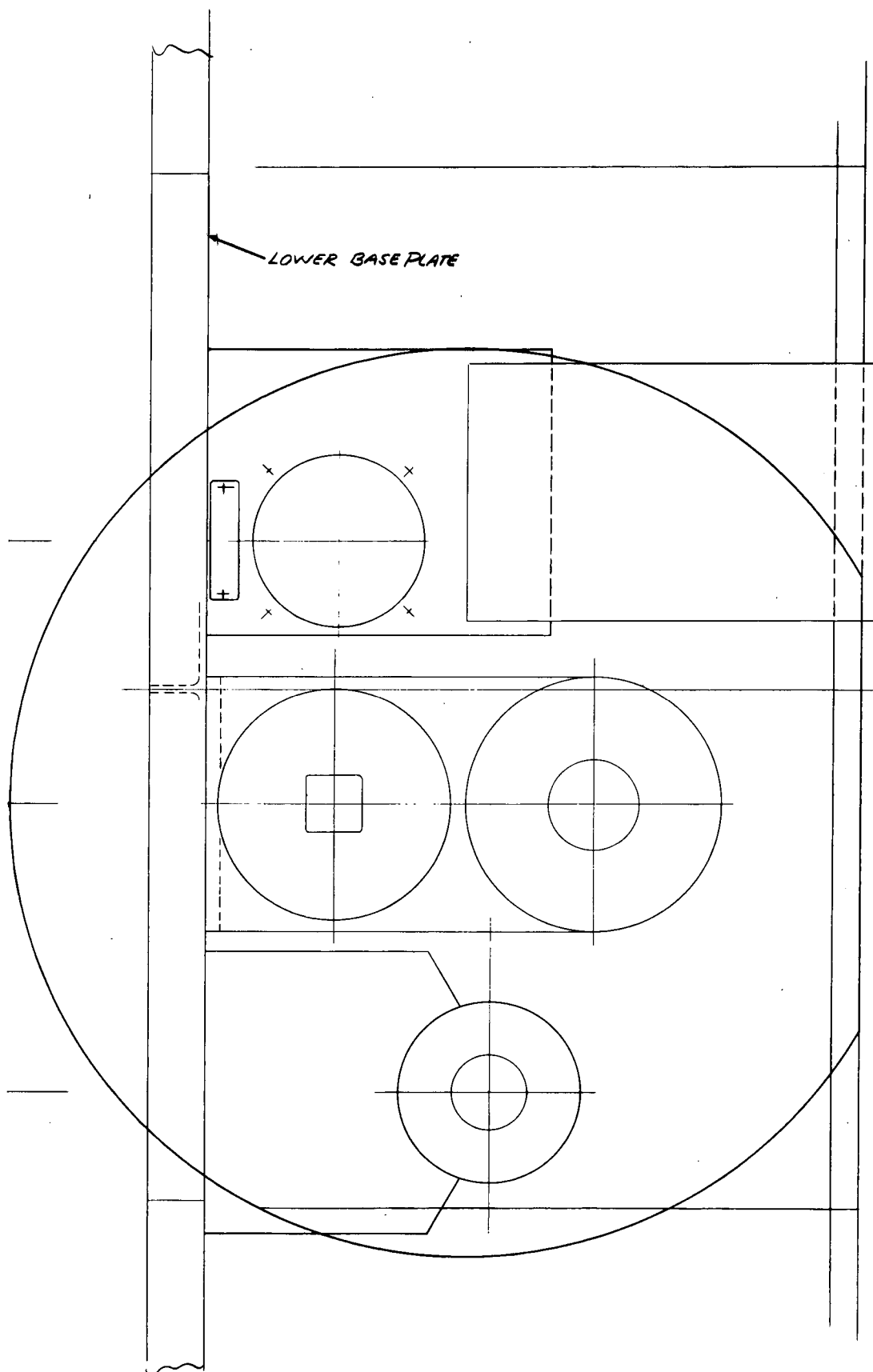
Figure III-3. Ground Plane Configuration

In order to reduce the vibration environment seen by the EUVS during test and launch phases, a snubbing device is desired to lower the vibration transmissibility through the gimbals to the EUVS experiment. The snubbing device, presently under study, will modify the cantilever condition of the EUVS and gimbal drive supported from the gimbal azimuth bearings. A removable load path is being considered between the gimbal yoke and the spacecraft booster adapter. The snubber will limit the response amplitude of the combined EUVS/ gimbal system, consequently reducing the vibration environment seen by the EUVS. The snubbing mechanism may also maintain the azimuth and elevation motion of the gimbal in a locked position during launch, in order to increase the envelope available for the EUVS within the constraints imposed by the booster separation springs.

Two snubber design approaches are being evaluated. One approach will utilize a soft compliant stop which will limit the yoke deflection at its fundamental frequency. The stop will be removed upon command via a pyrotechnic or electromechanical device after completion of the launch phase. A second approach uses a mechanical pin or "hard" load path between the yoke and the adapter, also removed on command by a pyrotechnic or electromechanical actuator. The final design approach will be chosen after an analysis of the design complexity and snubber performance is completed in January, 1972.

   h.   Capacitance Manometer - The capacitance manometer (PSB) sensing element is located on the -z end of the spacecraft, on the spacecraft radiator, or cold plate. The installation is designed to minimize thermal input to the cold plate due to solar or aerodynamic heating effects on the PSB, or due to leakage from the PSB heaters. An insulating washer and minimal contact area will restrict the heat input to the cold plate to approximately 1 watt.

C.   EXPERIMENT ELECTRICAL ACCOMMODATION

The electrical capabilities of the spacecraft and specific interface characteristics are based on the findings of the Interface Definition Study. To assure satisfactory spacecraft/experiment interface control, the Atmosphere Explorer Experiment General Interface Specification (PS-2260216) was generated. In the following paragraphs, the electrical interface requirements established during the study and reflected in this general specification are discussed.

Specific areas addressed in the electrical section of the specification are:

Power sources and protection

Grounding configuration

Connector types and pin allocation philosophy

Command information

Sync Signals

Telemetry Interface

EMI Environment

Ordnance Operation

Digital Signal Interface Circuitry.

1.   Power Sources and Protection

The power sources available to the experiments are a -24.5 Vdc regulated (±2% at experiment input) bus, an unregulated (-26 to -38.5 Vdc) bus and an an unregulated pulse load bus (-26 to -32 Vdc). With the exception of MESA, all of the experiments will draw their primary power from the regulated bus.

As corona poses a potential problem in many of the experiments due to the high voltage supplies required in their design, current limiting in the main power input of each experiment is a requirement. This permits the experiment to be operated subsequent to such a fault without blowing the fuse committed to the unit. Five-amp fusing for the main power inputs has been selected, which is well above the worst case current limit values, the fuse thus serves to protect against a short in the current limit circuitry. Fusing for input powers not drawn from the main power input (such as heaters, etc.) will be sized according to the particular case and derating factors applied consistent with the load currents drawn.

All of the experiments develop their internal operating voltages via dc/dc converters which permits separation of power and signal grounds within the experiment (see also Grounding Configuration). This approach to voltage generation minimizes adverse effects of electrical noise within the equipment.

2. Grounding Configuration

The grounding configuration of the spacecraft and experiments consists five required grounds and a sixth, optional, ground. These are:

›Power Ground

Signal Ground

Shield Ground

Chassis Ground

Pulse Load Ground

Command Ground (optional)

Separation of the grounds into the above categories is done to establish a configuration which will minimize electrical noise coupling within the experiments and the spacecraft equipment. In certain cases, separation between the signal ground and chassis ground cannot be achieved due to the nature of the experiments and in these cases waivers to the requirement may be granted. Isolation between the power ground and signal ground is assured in all of the experiments by utilizing dc/dc converters for internal voltage development. With this approach, dc offsets due to current flow in the signal grounds and coupled noise generated by the various dc/dc converters in operation are minimized.

3. Connector Types and Pin Allocation

A common set of connector types has been identified for use in interfacing the experiments to the spacecraft harness. For such connectors, the distribution of signals of the connectors and the spare pin requirements have been established. Selection of connector types for intra-experiment harnessing is left as an option to the experiment. However, flight harnessing between physically remote elements of an experiment will be built by RCA to ensure that spacecraft layout-dictated harness routing constraints are satisfied.

4. Command Information

Principal Spacecraft command and data handling capabilities are summarized in Table III-IX. Command information in the system takes three forms:

Power Commands

Major Mode Commands

Minor Mode Commands.

Power commands are defined as switched power levels which are presented to the experiment interfaces. In the presence of the power command, the receiving unit will enter the mode of operation as defined by its internal logic.

The format of the non-power commands has been selected based on the volume of command information required by the experiments, as determined during the study.

TABLE III-IX. C&DH CAPABILITIES

COMMAND	
Major Mode Commands	Supplied as either Relay Driving Pulses or Logic Level Pulses. (496 available)
Minor Mode Commands	32 bit serial data stream. A given experiment may use as many bits as required and/or as many commands of this type as are required.
TELEMETRY	
Main Frame	128 words
Subcom Frames	4, either 64 or 128 words long. (Also, one 4-word subcom for MESA)
Word Length	8 bits
Real Time Data Rate	16,384 bps (16 main frames/sec) 64 word subcom complete every 4 seconds 128 word subcom complete every 8 seconds
Format	Fixed or dynamic main frame
Analog TLM	either 0 to +5.12 Vdc or 0 to -5.12 Vdc A/D converted to 8 bit words

Major mode commands are uniquely defined pulses of a fixed duration which can be delivered either as pulses capable of driving relays or as logic level interfaces for use where the command information is to be stored in a flip-flop within the experiment.

Minor mode commands consist of a major mode command (load command) and a serial burst of command information 32 bits in length. The minor mode command information is designed for storage in a register in the experiment. Included in the command information delivered to the experiments is a command clock at the command bit rate (1024 bps). Thirty-four pulses of this command clock will be generated whenever any major mode command (including the load commands for the minor mode commands) is generated. The command clock will be delivered in a specific phase relationship to the 32 bits of the minor mode command.

5. Sync Signals

The spacecraft will provide all required sync signals to the experiments for the purpose of synchronizing the experiment to both the telemetry system and the pitch position of the spacecraft body. Included in the sync category are all continuous clock frequencies required, both for telemetry interfaces and for general operation of the experiments. Clock frequencies and sync signals not related to the body spin rate are all derived with binary relationships to the 16,384 bps telemetry rate. The spin rate related sync signals, phase referenced to the local vertical, are supplied to those experiments requiring nadir-related pitch position information in real time.

6. Telemetry Interfaces

The system will accommodate either digital or analog telemetry from the experiments. To accept digital information, the spacecraft generates and distributes digital word enable signals for the purpose of interrogating the source unit for the telemetry. Upon reception, the unit serially reads out the appropriate 8 bit digital word during the presence of the word enable. The read-out is accomplished by the basic clock signal distributed to all experiments (16,384 bps), such that a known phase relationship exists between the gathered digital telemetry and the operation of the data handling equipment.

To minimize interfaces between the spacecraft and an experiment all 8 bit words destined for the PCM main frame are multiplexed onto redundant outputs within the experiment. 8 bit words destined for the subcoms are similarly treated. Word enables are delivered to the experiment on separate lines for different words so that reprogramming of the main frame structure may be accomplished without additional logic being required within the experiments.

Analog telemetry is not required to be commutated within the experiments. The system will A/D convert all analog output data into 8 bit words and will insert the converted information into the serial output telemetry bit stream. The system is capable of operating with either 0 to +5.12 Vdc or 0 to -5.12 Vdc signals but will not satisfactorily convert signals whose output range crosses zero. All experiment analog telemetry is in the positive voltage range. If required, word enable signals for analog telemetry points can be delivered to the experiments.

The spacecraft will assemble discreet telemetry points (digital flag bits) into 8 bit words. Thus, if the experiments have digital bits of information left over after assembling 8 bit telemetry words internally, the spacecraft will perform the function, combining the discreets from various units into suitable 8 bit groups.

7. EMI Environment

Included in the General Interface Specification is a definition of the EMI environment in which experiments must perform and the tests required to demonstrate satisfactory operation under these conditions. The areas covered include:

Conducted Emission

Conducted Susceptibility

Radiated Emission

Radiated Susceptibility.

The environment is based on MIL-STD 461 as modified to reflect an estimated worst case environment for the AE spacecraft. Within the constraints of these limits, testing is defined per MIL-STD 462.

8. Ordnance Operation

The C&DH subsystem will provide the command and power switching required to operate all experiment ordnance devices. Included in the spacecraft is the "fanout" and isolation circuitry to operate redundant ordnance devices, from fully redundant circuitry. All ordnance devices on the AE spacecraft are Class B devices as defined in the ETR and WTR range safety manuals.

9. Digital Signal Interface Circuitry

A separate topic addressed during the study was an investigation of design approaches to the digital signal interfaces between the experiments and the spacecraft which permit standardization of these interfaces to the greatest practicable degree. Trade-off analyses showed that the standardization objective could best be met by providing, in the source circuits, a ground as the active signal level and an open circuit as the inactive signal level. In this approach the source circuit is connected to a receiving circuit in the load unit where a pull up resistor, returned to the load unit's logic supply voltage, is located. By so doing, the need for the generation of active interface voltages in each redundant source unit, for the different families of IC logic used in the experiments, is eliminated.

This technique is the same as that traditionally used in the design of logic interfaces with the following exceptions:

1. The pull-up resistor is moved from the source unit to the load unit.

2. The source unit does not generate a voltage for the interface.

3. The same design can be used independent of the logic families of IC's and their operating voltages in either the source or the load unit. (The only restriction being that the load unit operate its logic between some positive voltage and ground.)

This interface approach is used for all logic level digital interfaces between the AE spacecraft and the experiments (both input and output). To ensure satisfactory control of the digital interfaces, RCA designed both source and receiving circuits for the interfaces and provided a complete worst-case analysis including an evaluation of the worst-case noise environment in which the logic interfaces would be required to operate.

These circuits, which are also included in the general interface specification are shown in Figures III-4 through III-8.

Figure III-4. LPTTL Digital Input Buffer
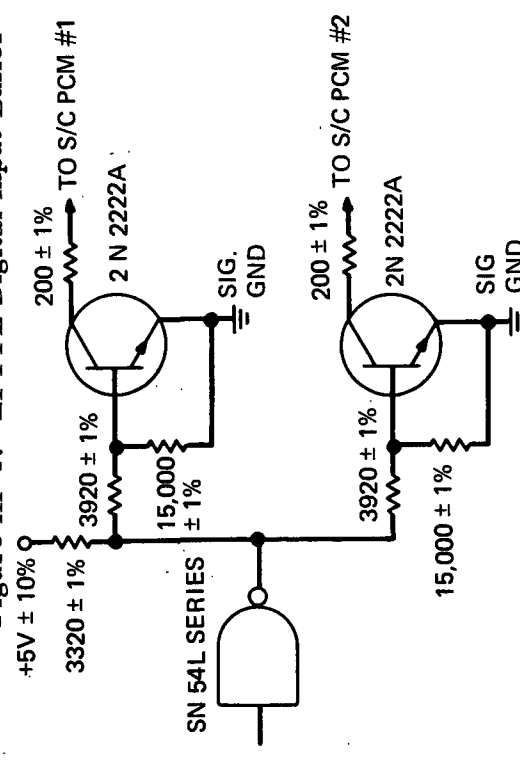
a) Output Buffer if Supplied from Non-Redundant Gate in Experiment

Figure III-5. LPTTL Digital Output Buffers

b) Output Buffer if Supplied from Redundant Gates in Experiment

Figure III-5. LPTTL Digital Output Buffers

Figure III-6. CMOS Digital Input Buffer
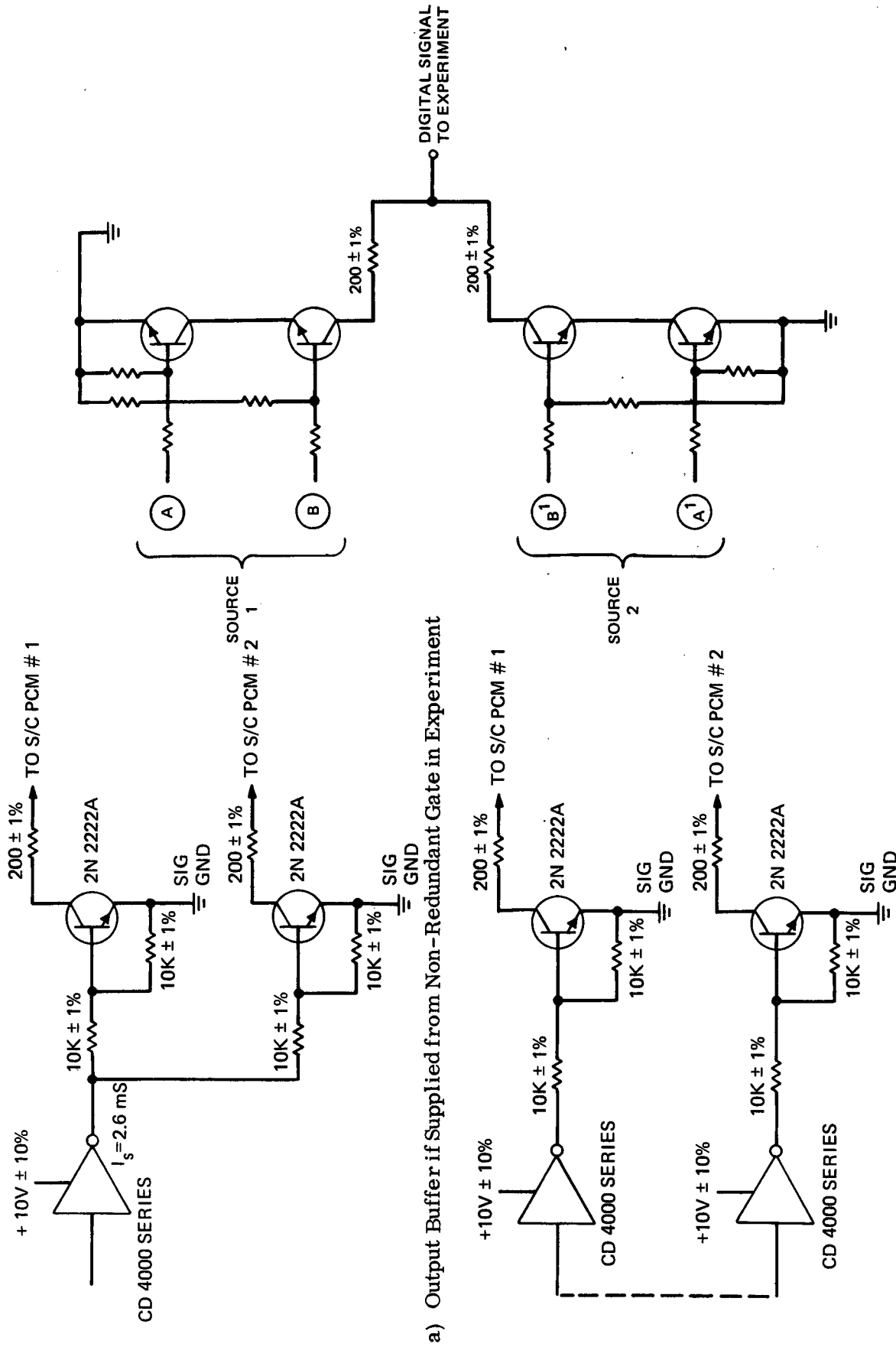
Figure III-8. Spacecraft Digital Signal Source Circuit

a) Output Buffer if Supplied from Non-Redundant Gate in Experiment

b) Output Buffer if Supplied from Redundant Gate in Experiment

Figure III-7. CMOS Digital Output Buffer

D. ENVIRONMENTAL ACCOMMODATION

Details of the environmental interfaces between the experiments and the spacecraft are called out in Section 3.6 of the General Interface Specification RCA PS -2260216.

Some specific environmental considerations and the analyses which were conducted in support of the preparation of the specification are briefly discussed here.

1. Magnetic Environment

While care will be taken to minimize internally generated magnetic fields within the spacecraft, special provisions have not been made in the design of Atmosphere Explorer to achieve a very high degree of magnetic cleanliness since such is not a requirement.

Spacecraft fields are due primarily to the magnetic torquers used to maintain the attitude and momentum of the spacecraft and magnetic components within the experiments themselves. It has been determined that it is possible to maintain the desired degree of control over the attitude and the momentum with use of the magnetic torquers restricted to times remote from perigee, since perigee is of most scientific interest in the missions. Hence the environment under quiescent conditions is of principal interest.

Estimates of local magnetic intensities have been made with the torquers both 'on' 'and' 'off' in combinations which give rise to the worst case conditions. In the latter case (for which residual magnetism of 2% of the 'on' value is estimated), the contribution of the major instrument magnetic sources, namely OSS and the Ion Gauge pressure sensor, were included. The orientation of the torquers within the spacecraft is shown in Figure III-9 with dimensional details given in Table III-1 of Appendix III-D. Data was obtained using a program also described in Appendix III-D. The results are presented in two forms:

- Tables of magnetic field magnitudes at each experiment aperture for various conditions.

- Plots of the magnetic field magnitude at spacecraft cross sections through the experiment bays, for various conditions.

For data applicable to the torquer residuals, the following experiment magnets were included, since in this case they become significant.
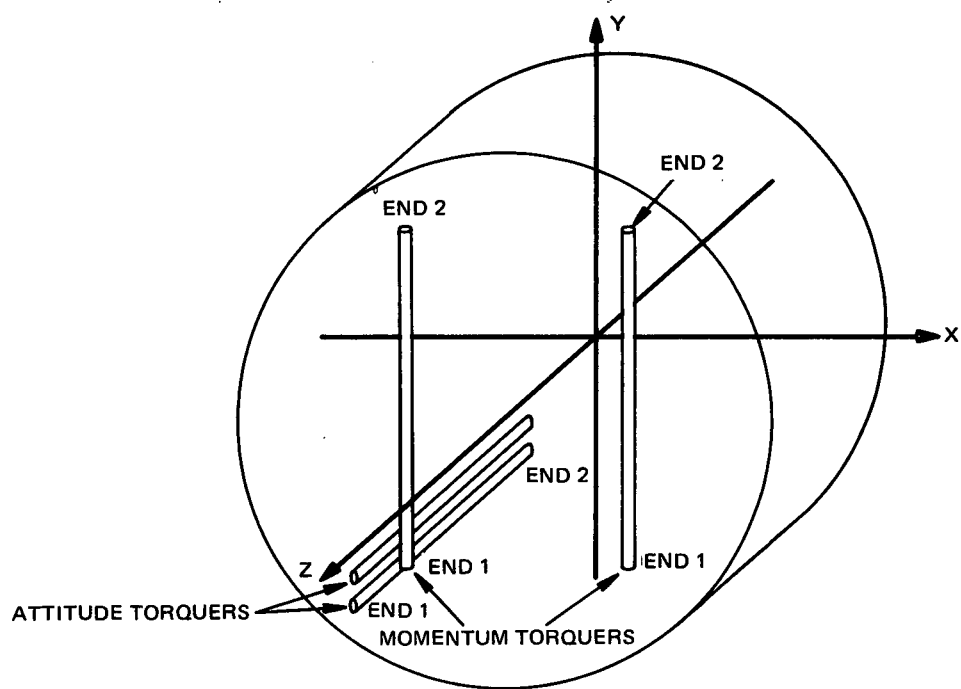
Figure III-9. a. Near-Polar Orbit Configuration
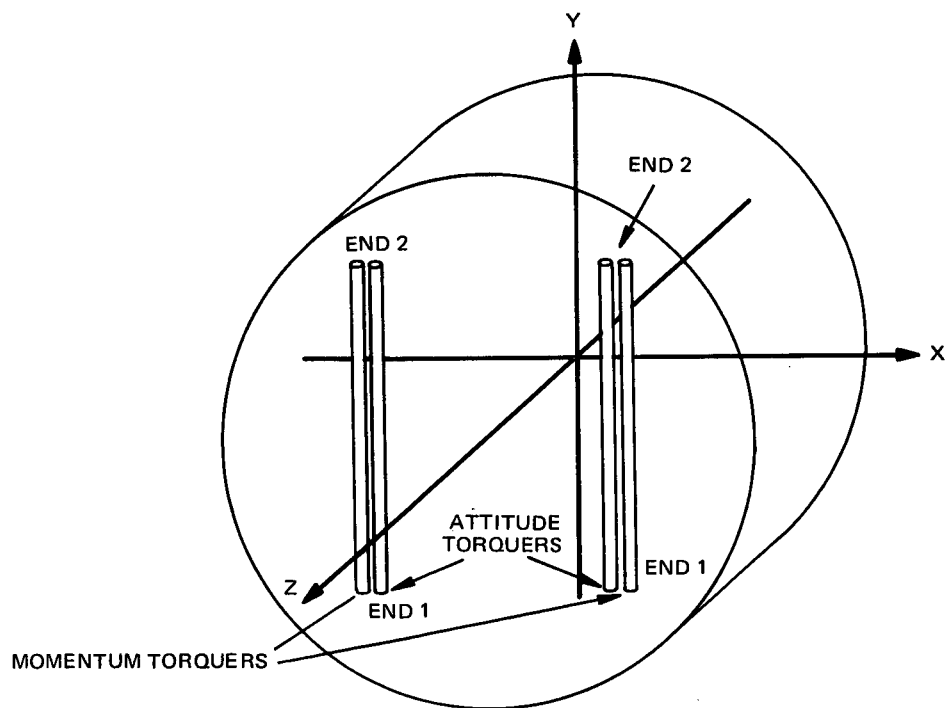
Figure III-9. b. Near-Equatorial Orbit Configuration

Instrument	Axis	Magnitude	Location (cm)					
			North Pole			South Pole		
			X	Y	Z	X	Y	Z
OSS	x	170 pole-cm	40.6,	1.25,	-31.1	66.0,	1.25,	-31.1
	y	4540 pole-cm	50.0,	-7.6	-31.1	50.0,	8.9,	-31.1
	z	45 pole-cm	50.0	1.25,	-21.0	50.0	1.25,	-41.5
PSA	x	3300 pole-cm	63.4,	-3.2,	-15.2	68.6,	-3.2,	-15.2

Table III-X presents the magnetic field intensities, for the near-polar missions and Table III-XI for the near equatorial mission. Values in the tables are the calculated intensity at the locations of the appropriate experiment apertures. The cases listed in the tables ('A' 'B' etc.) are for various torquer dipole sign combinations which are defined in detail in Tables II & III of Appendix III-D.

Figures III-10 and III-11 are magnetic field plots in the spacecraft x-y plane through the experiment bays for the various cases identified.

The conditions selected are not comprehensive but do represent worst case situations. Further work is being carried out in an attempt to devise better shielding for those experiments which contain significant magnetic sources.

With regard to the experiments themselves, most are insensitive to magnetic fields below ~1 gauss. Table III-X shows acceptable environments for most experiments (torquers off). A few which are sensitive are: PES, NACE, NATE, and to a lesser degree RPA & CEP. The nature of the susceptibilities is as follows.

CEP/RPA   These experiments measure bulk electrons, and as such can be affected by the presence of magnetic fields, which deflect the electrons in the vicinity of the sensor, resulting in erroneous readings.

NACE/NATE   These experiments employ an electron beam to produce the necessary ionization in the stream of neutral gas. Magnetic fields can cause a deflection of this beam to produce a proportionally incorrect amount of ionization.

PES   This experiment is designed to measure the trajectories (angles of arrival) of electrons external to the spacecraft. These trajectories are susceptible to variations in the magnetic field.

At the time of this report, reduction in the PSA dipole through shielding is being effected and should provide acceptable fields for the above.

TABLE III-X. NEAR-POLAR MISSIONS (AE-C, D) - MAGNETIC FIELD
INTENSITY AT EXPERIMENT APERTURES

Expt.	Torquers ON		Torquer Residuals Only		Residuals Plus Expt. Fields				Expt. Fields Only
	A	B	C	D	E	F	G	H	I
VAE	1.24	1.10	0.025	0.022	0.029	0.025	0.019	0.021	0.006
LEE	0.18	0.42	0.004	0.008	0.006	0.013	0.005	0.008	0.006
BIMS	0.14	0.15	0.003	0.003	0.024	0.023	0.019	0.018	0.021
NACE	0.17	0.16	0.003	0.003	1.31	1.31	1.31	1.31	1.31
NATE	0.88	0.71	0.018	0.014	0.017	0.015	0.021	0.025	0.01
MIMS	0.19	0.16	0.005	0.003	0.054	0.053	0.051	0.050	0.049
ESUM	0.60	0.36	0.012	0.007	0.017	0.017	0.016	0.021	0.015
OSS	0.16	0.17	0.003	0.003	1.23	1.23	1.43	1.43	1.32
RPA1	0.17	0.16	0.003	0.003	0.032	0.031	0.028	0.027	0.029
RPA2	1.80	1.53	0.036	0.031	0.035	0.031	0.032	0.038	0.069
RPA3	0.28	0.36	0.006	0.007	0.008	0.009	0.007	0.003	0.028
PES1	0.14	0.14	0.003	0.003	0.381	0.381	0.380	0.379	0.38
PES2	1.92	1.93	0.038	0.039	0.034	0.035	0.043	0.043	0.005
CEPA	0.52	0.53	0.010	0.011	0.011	0.011	0.018	0.018	0.011
CEPR	0.31	0.28	0.006	0.006	0.008	0.007	0.011	0.012	0.009
MESA	1.16	1.16	0.023	0.023	0.034	0.033	0.044	0.043	0.031
UNVO	0.94	0.99	0.019	0.020	0.014	0.015	0.027	0.026	0.009
EUVS	1.41	1.27	0.028	0.025	0.032	0.029	0.025	0.027	0.009

NOTE: Values in gauss

These results are applicable to both AE-C and AE-D.

TABLE III-XI. EQUATORIAL MISSION (AE-E) - MAGNETIC FIELD INTENSITY
AT EXPERIMENT APERTURES

Expt	Torquers ON	Torquer Residuals Only	Residuals Plus Expt Fields	
	A1	B1	C1	D1
VAE	1.49	0.03	0.035	0.025
BIMS	0.73	0.015	0.027	0.027
NACE	0.34	0.007	1.31	1.31
NATE	1.66	0.033	0.029	0.04
ESUM	4.40	0.088	0.086	0.092
OSS	0.26	0.005	1.35	1.32
RPA1	0.67	0.013	0.039	0.031
RPA2	3.68	0.074	0.071	0.077
RPA3	2.17	0.043	0.045	0.042
PES1	0.22	0.004	0.38	0.38
PES2	0.22	0.004	0.008	0.004
CEPA	0.11	0.002	0.012	0.010
CEPR	0.40	0.008	0.012	0.010
MESA	0.80	0.016	0.044	0.024
EUVS	1.68	0.034	0.040	0.029

NOTE: Values in gauss
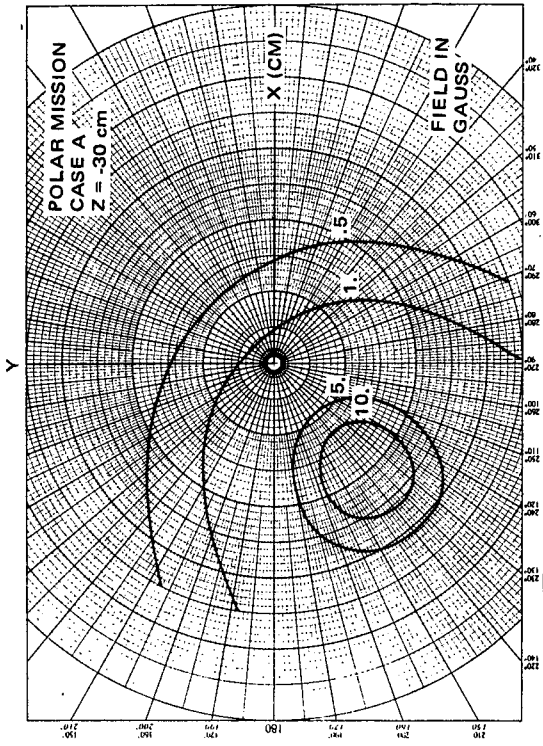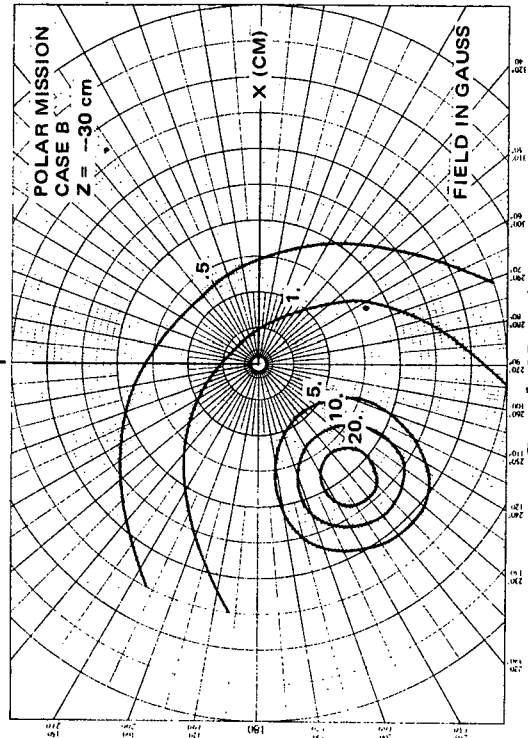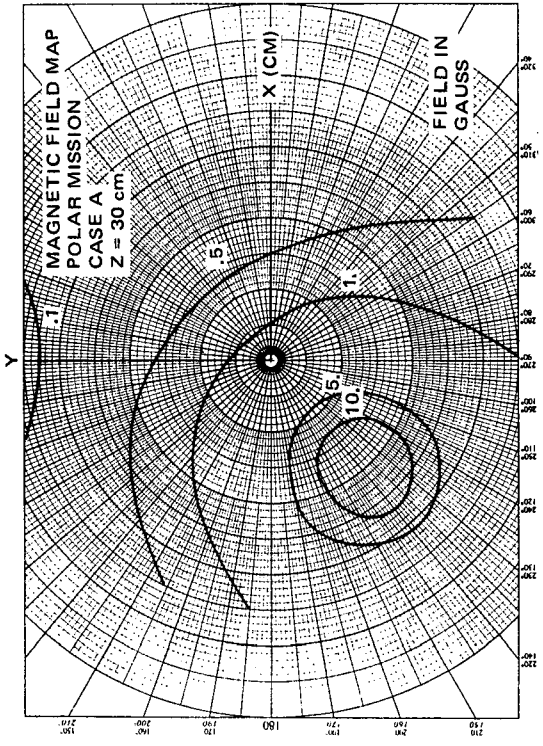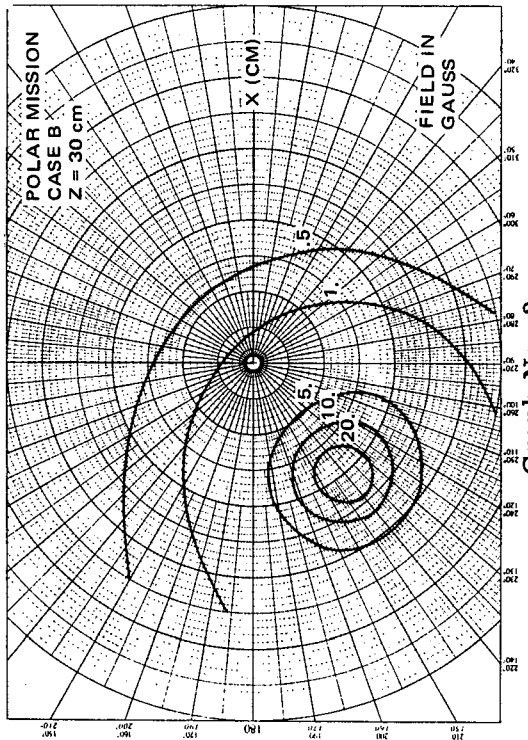
Figure III-10. Magnetic Field Maps: Polar Mission
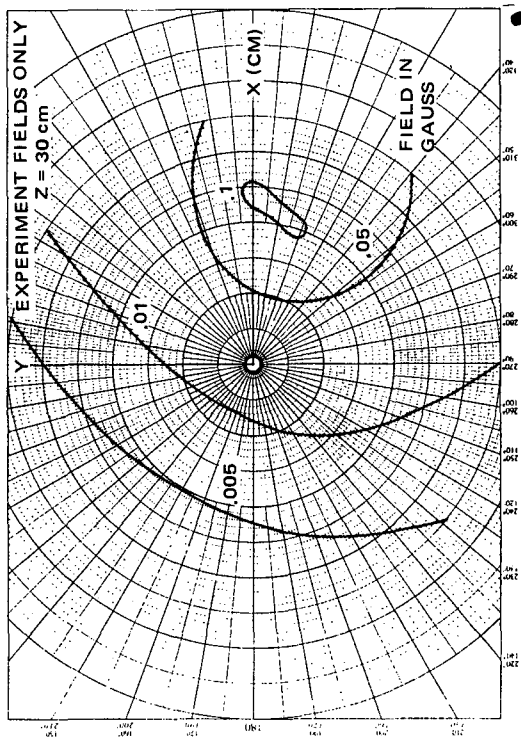
Graph No. 6
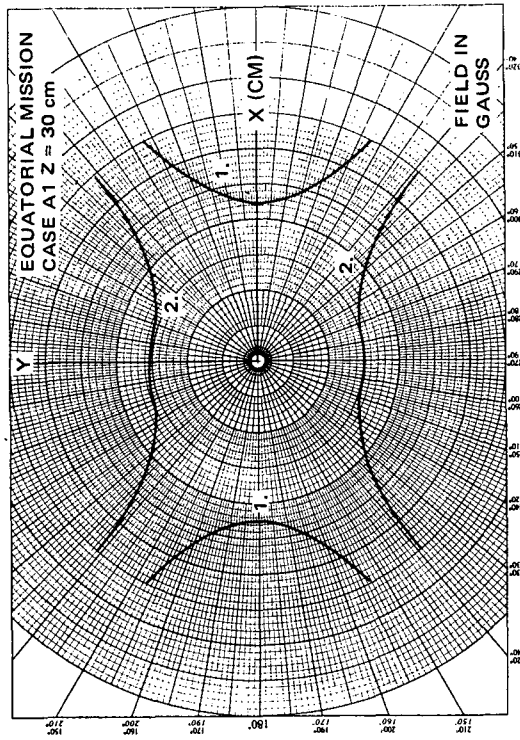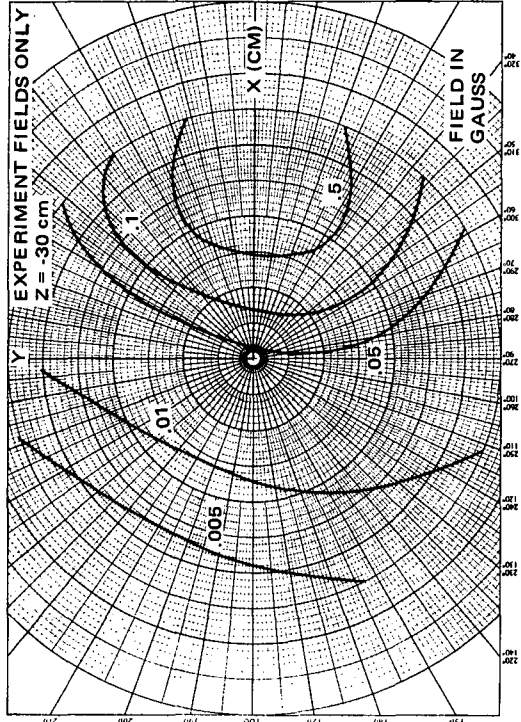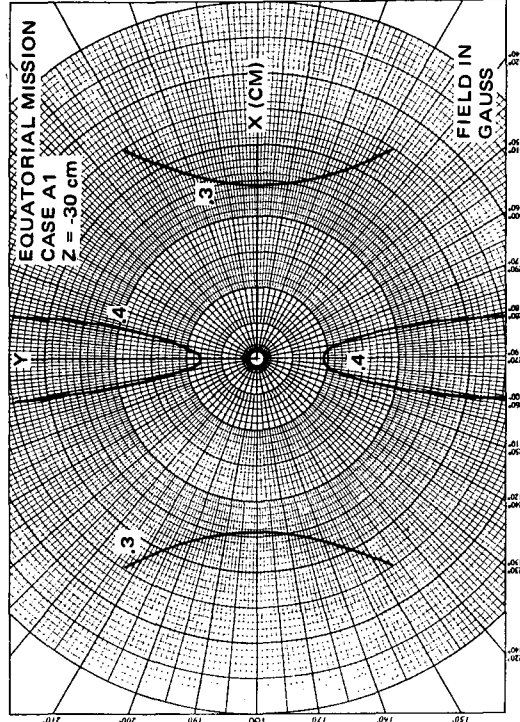
Graph No. 5

Graph No. 8

Graph No. 7

Figure III-11. Magnetic Field Maps: Experiment Field and Equatorial Mission

2.   Internal Pressure

Since the Atmosphere Explorer Spacecraft will be probing low altitude regions, the interior of the spacecraft will become pressurized during perigee excursions. A study of this phenomenom, published as Design Note DN-537-2.9 (AE) indicated that, based on the information on experiment aperture designs available at the present stage of spacecraft design, a peak internal pressure at 120 km altitude of 8×10^{-4} Torr is possible. The significant parameter in the governing equation for the process is Ai/Ao, or the ratio of the area through which the ram pressure can gain access to the interior of the spacecraft to the total leakage area available, both modified by transmission coefficients. Design studies are continuing to minimize this ratio and further reduce pressure using a sealing technique around experiment apertures, and thus decrease the predicted peak pressures. The calculations performed also indicated a pressurization time constant of less than one second, indicating that any attempt to "smooth out" perigee pressure excursions would not be effective.

3.   Propulsion

The AE Orbit Adjust Propulsion Subsystem is a monopropellant hydrazine system. The design note referenced above (DN-537-2.9 (AE)) also considers the environmental effects of thruster firing at low perigee. Essentially the predictions are based upon the theory that a boundary layer of hydrazine exhaust products can migrate from the engine, around the spacecraft. At some point this migration will revert to free molecular flow, at which time it is possible, via collisions with ambient molecules in the free stream, for some of this hydrazine derived contaminant to be directed back towards the spacecraft. Calculations presented in the design note indicate a contaminant flux of the order of 10^{14} particles/cm^2/sec into an experiment located 90° around the spacecraft from the thruster. The same theory indicates that of the order of 10^{13} particles/cm^2/sec would flow towards a forward facing experiment.

Two experiments considered highly susceptible to such contamination, NACE and NATE, have since modified their design to include shutters over the experiment apertures which will be closed during thruster firing.

4.   Mechanical Noise

The MESA experiment is sensitive to mechanical excitations on the spacecraft during the period that the instrument is collecting acceleration data. The AE spacecraft contains moving masses which can potentially contaminate the MESA data. In order to assess the potential effect, a study was conducted on the impact of acceleration noise on the MESA experiment. In parallel, a determination of the measurement and analysis techniques which may be utilized to define the expected noise environment on the spacecraft was made. By the

combination of the results of two tasks, i.e., a) the identification of the types and magnitudes of environmental excitations for which data contamination would result and b) the identification of the methods to be used to determine if the excitations exist on the spacecraft, an overall plan was established to verify the compatibility of the interface between the MESA experiment and the spacecraft. The MESA sensitivity study characterizes the tolerance of the experiment to random impulse and sinusoidal excitations in the sensitive and cross axis directions of the MESA experiment. The data will be used to assess the acceptibility of the excitations which are measured or predicted for the spacecraft.

A measurement technique was identified which can be used to measure spacecraft vibration excitation levels in the magnitude and frequency range of interest. The technique employs spectral analysis of vibration data measured with piezo electric accelerometers, and supplemented by analytical prediction of noise spectra. Measurements can be made of excitations in the 10^{-5} g range, at frequencies of the order of 5 Hz or less.

Acceleration levels due to momentum wheel operation at 150 rpm were measured on another RCA spacecraft. (RCA DN 538-5.1 (AE), 9/7/71). Comparison of the measured vibration levels with the MESA tolerances reported in the study indicates that the MESA can operate satisfactorily within that particular random and impulse noise environment. If the actual random and impulse environment on the AE spacecraft is no more severe than that characterized in the measurements, the MESA is compatible with that portion of the excitation environment.

This study and a determination of acceptable solutions is continuing in concert with NASA.

5.   Experiment thermal environment and interface considerations

The AE scientific experiment complement will be exposed to both the spacecraft internal thermal environment and external thermal factors, including:

- Direct solar radiation

- Albedo

- Earth emitted radiation

- Aerodynamic heating flux

The experiment internal power dissipation and internal and external thermal design will interact with that of the other spacecraft equipment and structural components to produce a total operating temperature profile which will be maintained within specified ranges for the various components. In order to achieve an optimum overall thermal design, certain thermal interface requirements will be imposed on the experiments.

a. BASEPLATE MOUNTED EXPERIMENTS

The distribution of these experiments is indicated in Table III-XII. In order to minimize the temperature gradients across the baseplate and between the experiments and surrounds, the radiative and conductive properties of the experiment packages will be controlled, including the following items:

- Experiment package external surface finishes exposed to the spacecraft internal environment.

- Characteristics of the joint between experiment mounting flange and baseplate.

- Conductance between dissipating elements in experiment packages and their external case and mounting flange.

These interface requirements are detailed in the various interface specifications.

The net heat transfer between the experiment ports and external environment from worst case hot to worst case cold conditions are to be controlled to minimize the effect on the spacecraft operating temperature range. The port thermal effects are determined by the following:

- Apertures (characterized as black surfaces) including crack area allowance around ports

- Surfaces required to be electrically conductive (High α_s/ϵ , low ϵ)

- Other surfaces for which thermal finishes are selectable.

Based on latest experiment design data, the magnitudes of these areas are shown in Table III-XII. In addition to the conductive area on the ports themselves, as shown in this table, certain experiments will require relatively large ground planes which can possibly be thermally decoupled from the ports by means of isolating bushings or standoffs to minimize the thermal effect on the spacecraft internals.

A preliminary study was made of the effect of several possible finishes for the aperture housings and non-conducting surfaces, including black, white, gold aluminum finishes. It appears that a black finish will give the best

TABLE III-XII. AREAS OF EXTERNAL PORTS OF BASEPLATE MOUNTED EXPERIMENTS

Experiment	Baseplate	Areas (In^2)			
		Total Exposed to Ext Env	Aperture $\epsilon = 1$	Non Aperture	
				Available For Thermal Control	Not Available For Control $\epsilon < 0.1$
BIMS	L	17.0	3.1	7.7	6.2
LEE	L	24.6	10.7	13.9	-
MIMS	L	50.7	0.9	43.6	6.2
NACE	U	5.5	0.6	2.5	2.4
NATE	L	3.6	0.6	0.6	2.4
OSS	U	40.1	0.4	38.0	1.7
PES	U	18.4	0.1	18.3	-
PSA	U	8.9	0.4	8.5	-
RPA (SENS HD)	L	45.6	2.9	27.5	15.2
RPA (DRIFT HD)	L	23.4	2.1	10.3	11.0
UVNO	L	46.2	3.1	3.1	-
VAE	L	42.4	8.1	34.3	-
Total	—	286.4	33.0	208.3	45.1

hot-to-cold heat transfer conditions since these surfaces are generally cylindrical and approximately perpendicular to the array. They will receive full sun at the worst case cold sun angle (0°) and are partially shadowed during spacecraft rotation at the worst case hot sun angle (45°). A final determination of the optimum finish will be made when the experiment designs and locations in the spacecraft are sufficiently firm.

Two of the baseplate mounted experiments (BIMS and MIMS, both on the lower baseplate) will require vents to the external environment to the bottom spacecraft surface. The solar absorption and IR emittance characteristics of these openings are essentially equivalent to that of a black surface. This will require careful control of the vent material internal and external finishes, so that vent heat gains and losses for worst case hot to cold conditions will not have an adverse effect on the baseplate-equipment complex operating temperature range. Suitable thermal design schemes for these vents are presently under study.

b.   OTHER EXPERIMENTS

Experiments not mounted directly on either baseplate include:

Symbol	Location
CEP-2	Top external
EUVS/SPS	Booster adapter well
MESA	Inside center column
PSB	Top external
ESUM	Junction of side and bottom arrays.

Cylindrical Electrostatic Probe (CEP). The CEP contains a resistance heater near the tip which heats this section to a temperature of 500°C during the short period of operation. An investigation was made to determine the effect of radiation from the probe during operation on the CO_2 band horizon sensor located in the MWA. It was determined that the horizon sensor response to this radiation is below the sensor threshold, with the probe in the desired location. The thermal input from the probe to the spacecraft top during the period of heater operation will have no significant effect on the temperature profile (for details see DN-515-5.0 (AE)).

Extreme Ultra Violet Spectrometer (EUVS). The thermal interface between the SPS/EUVS installation and the spacecraft internal and external environment will be controlled to maintain the temperature of this equipment within the required limits and minimize its effect on the temperature range of the space-craft internal components. Open area of the well exposed to the external environment would allow a large heat gain from solar radiation at the worst case hot orbit sun angle (45°) and a large heat loss at sun angles close to the 90° maximum value. A shield installed between the EUVS unit and the booster adapter would reduce the magnitude of solar heat gains and losses to acceptable values. This shield would rotate with the SPS. Features of a preliminary thermal design concept, presently being examined in more detail by RCA, for this installation are shown in Figure III-12.

Atmosphere Density Accelerometer (MESA). The MESA experiment will be radiatively and conductively coupled to the center column. These couplings will be sufficiently large so that the operating temperature range of the MESA will be near the average of the upper and lower baseplate-equipment complexes.
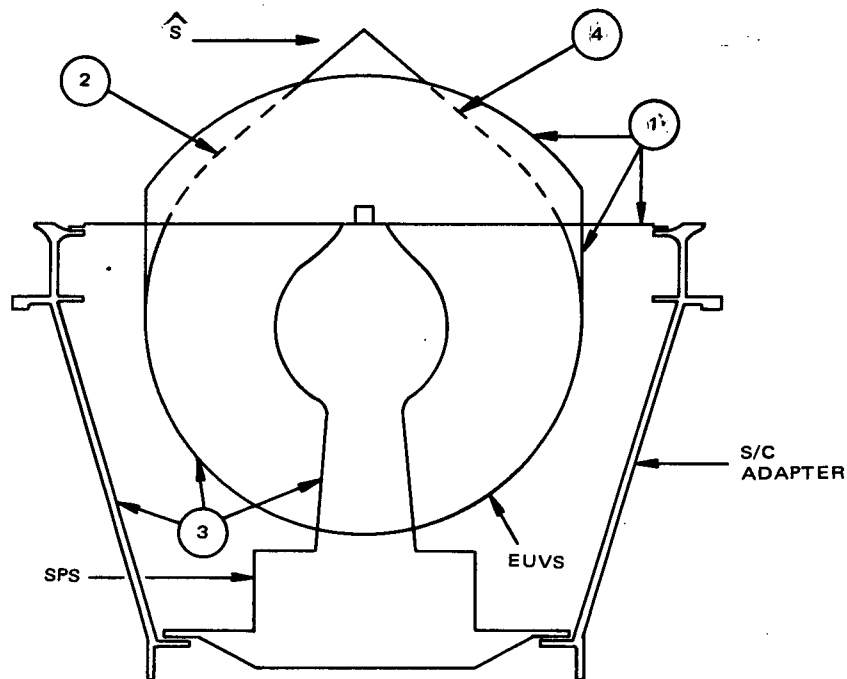
Figure III-12. Preliminary Thermal Design Concept for
EUVS/SPS Installation

LEGEND

(1) Lighweight thermal shield between unit and adapter with
low α_s/ϵ finish on shield external surfaces to minimize effect
of solar radiation variation over the sun angle range and low ϵ
finish on shield internal surface to limit value of radiative
coupling from shield to EUVS/SPS and adapter.

(2) Low α_s/ϵ high ϵ radiator on EUVS external surface. EUVS
rotation with sun angle would expose this radiator to the external
environment at worst case hot conditions and cover it at worst
case cold. The size of this radiator would be set to give optimum
temperature conditions.

(3) High ϵ finish on EUVS/SPS and adapter internal surfaces to pro-
vide large coupling from the experiment to the adapter.

(4) Low ϵ finish on all surfaces of EUVS exposed to external environ-
ment except the radiator.

Capacitance Manometer (PSB). The external surfaces of the PSB experiment will be subject to aerodynamic heating during perigee passage and direct solar radiation at the higher sun angles. Since it is mounted on the top surface which serves as the principal external radiator for the spacecraft internal components, it is desirable to prevent transfer of any significant amount of the external thermal energy received to this radiator. To accomplish this, isolating mounts for the PSB will be provided. A low ε finish on the external surfaces is also desirable to limit radiative heat exchange with the top surface.

Extreme Ultra Violet Solar Photometer. The ESUM experiment will view the external environment through an opening located at the junction of the bottom and side solar arrays about 45° from the +x toward the -y direction. The unit will be supported by a bracket mounted on the lower baseplate, which passes through the insulating blanket. The orbit average solar radiation incident on this opening will vary with orbit sun angle. In order to minimize the effect of this varying solar radiation on the baseplate operating temperature range, it is desired to limit the heat gain or loss between this experiment and the lower baseplate to 1 watt. This can be accomplished by:

- Preventive of direct impingement of solar radiation on the lower baseplate by suitable bracket design.

- Radiative decoupling of bracket from baseplate through the use of a low emittance finish.

- Conductive decoupling of bracket from baseplate by means of non-metallic isolating bushings.

c. ORBITAL TEMPERATURES OF THIN WIRES AND PLATES IN EXPERIMENT PORTS

A study was conducted at the request of NASA/GSFC to determine the orbital temperatures of thin wires and plates under simulated thermal conditions in the experiment ports for various perigee altitudes and positions relative to the projection of the sun direction in the orbit plane.

Details of the results of this study are covered in DN-540-4.6 (AE). The basic parameters of the study were as follows:

- Materials and thicknesses

Wire	Tungsten	0.001 to 0.1 inch
Plate	Aluminum	0.001 to 0.1 inch

  (No external finish on wires or plates)

- Orbit parameters

  Apogee altitude   3800 km

  Perigee Altitudes   150 and 120 km

  Angle between line of apsides and sun line -   -100° to 100°

- Operating mode

  120 km   -   4 rpm

  150 km   -   1 RPO from end of eclipse to 10 minutes after perigee; otherwise, 4 rpm.

Table III-XIII presents a summary of maximum orbit temperatures determined in the study and position of the line of apsides at which these temperatures occur.

TABLE III-XIII. SUMMARY OF RESULTS OF PARAMETRIC STUDY OF TEMPERATURES OF WIRES AND PLATES IN AE EXPERIMENT PORTS

Perigee Altitude (kM)	Operating Mode During Perigee Passage	Angle Between Perigee & Sun Line for Max. Temp.				Maximum Temperature °C			
		Wire (in)		Plate (in)		Wire (in)		Plate (in)	
		0.001	0.1	0.001	0.1	0.001	0.1	0.001	0.1
120	4 RPM	0	-80	0	-80	404	163	561	191
150	1 RPO	80	0	85	0	263	128	418	178

E. COS/MOS RADIATION TEST PROGRAM - PHASE I

During the Interface Definition study, special tests were conducted on the RCA Complementary MOS Integrated Circuit Series (COS/MOS) to characterize the performance subsequent to radiation exposure.

A complete report[1] of the test program conducted to date, was submitted to NASA on 7 October 1971. The significant highlights of this report, and the conclusions and recommendations are summarized here.

1. Impact on AE Subsystem Design

The radiation doses for components within electronics boxes on the AE spacecraft will vary from below 10^4 rads (sheltered locations, near-polar missions) to about 2×10^5 rads (more exposed locations, near-equatorial missions). While borderline cases must be analyzed carefully, there will be many instances under the above conditions when no design problem at all will be encountered in the use of CMOS devices. For example, even after a dose of 2×10^5 rads, the CD 4004 counters tested still counted at the full specified top speed and with no switching current increase. At 10^6 rads, the counters still operated, only at reduced speeds.

Table III-XIV gives instances of two locations on the worst case mission - within a more exposed electronics box, and within a more sheltered package. The table summarizes the results of the above tests, as translated into the effects to be expected on circuit performance in these locations. It can be seen that very little occurs in the more sheltered location. Even in the more exposed locations, the CMOS device can be used on AE with proper derating techniques. It should also be noted that effects are reduced when the device is in the unpowered mode.

2. Conclusions

The results of these tests suggest that RCA CMOS CD 4000A devices using single oxide gate insulators are eminently satisfactory for use in space - providing the total dose experienced is less than 2×10^5 rads. Obviously, circuit designers must take into account the consequences of the exposure, but these effects are mild enough to accept along with other changes in performance of solid state devices (e.g., $\Delta Vs \cong 1.5$ volts, single inverter $< 50 \mu A$). Changes such as these can be accomodated by simple derating schemes similar to those used now for bipolar transitors. Also, changes in transition times will have to be taken into account (the original transition times may double) but these are only of importance in unusually fast circuits.

---

[1]RAP 71-G Space Radiation Qualification of COS/MOS Integrated Circuits - Oct. 6, 1971 - A.G. Holmes-Siedle and W.A. Schreiner

TABLE III-XIV. EFFECTS OF RADIATION ON CMOS SUBSYSTEMS IN WORST-CASE AE MISSION[1,2]

Subsystem Parameter	Sheltered Location 4×10^4 rads	More Exposed Location 2×10^5 rads
Noise Immunity (V_{NIL})	Slight (loss of 0.6V)	Significant (loss of 1.5V)
Noise Immunity (V_{NIH})	Improved (gain of 0.6V)	Improved (gain of 1.2V)
Standby Power (P_D)	Negligible	Significant (approx. 50μA) per gate
Switching Power	Negligible	Negligible
Speed (fcL)	Negligible	Significant (30% increase in rise time of output)
Load Driving Capability (I_D)	Negligible	Slight (8% drop in n-channel gain)

NOTES:

1. Orbit Apogee   2040 nmi
        Perigee   80 nmi
        Inclination   18°

2. Power supply during irradiation is 10V; device bias condition is worst-case, namely duty cycle near 100% in "1" state

The most significant and pleasing feature of the test program is the radical improvement of the behavior of all P-channel devices in the "new" series by comparison with the "old" series (about a factor of 20 in ΔV_T). This was expected, and is due to the change in gate oxide from "sandwich" to "ultra-clean single" type. This device improvement leads to system improvements such as that seen in the CD 4004A counter circuit, which still operated at 10^6 rads which is equivalent to over three years in the 18° orbit and over fifteen years in the near-polar case.

Figure III-13 represents an estimated worst case shift of the switching threshold of a CD 4000A series inverter as a function of radiation dose and operating bias during exposure. It assumes that the inverter is held in "1" state during the entire dose. It was obtained by a simple average of P and N 4007A transistor threshold shifts measured during the test program.
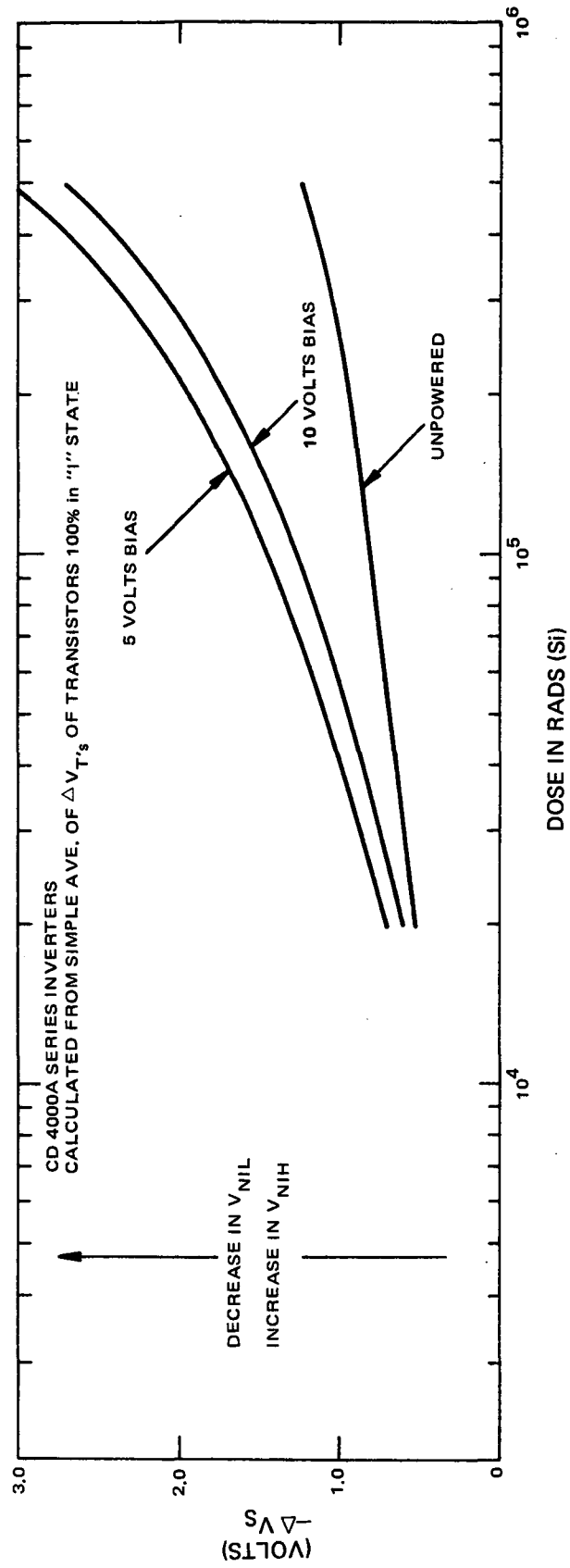
Figure III-13. Worst Case Switching Threshold Shift ($-\Delta$ 1/S)

At 2×10^5 rads exposure, the threshold shift observed on the 5 volt applied bias devices was approximately 2.0 volts, which results in a 0.5 volt nominal noise immunity.

However, for the 10 volt applied bias devices, a threshold shift of approximately 1.7 volts was observed. This shift corresponds to a nominal 3.3 volt noise immunity.

A preferential bias voltage near 10 volts seems evident.

For logic gates, the general effect of the P channel improvement is the reduced shift in logic switching threshold voltage, V_S. The change in the N channel devices is, unfortunately, not so pronounced, although a new feature is that some N channel devices reverse themselves in ΔV_T at high radiation doses (due to interface state generation). This causes switching voltage, V_S, to move back towards its original position at high radiation doses. However by its nature, this effect also reduces the "drive" in the "1" state and gives little relief in the power drain problem.

Specific findings of interest on the device level are:

- that, although use of the new, single gate oxide in the new devices is generally advantageous, a greater dominance of radiation-induced interface states makes the behavior of the new devices more difficult to model. For example V_T and V_s shifts actually reverse in some cases contrary to expectations. Also the benefits of a "powered down" state will be less than expected.

- Type-to-type variation is relatively small, although the CD 4007A test devices were generally more sensitive than the other more widely-used gates. As expected, no basic difference in radiation response was found between the devices which had been through a hi-rel burn-in procedure and the non-screened "commercial" devices.

- The voltage dependence plots, as on previous occasions, have proved to be an important diagnostic tool in assessing radiation resistance in MOS systems.

- The "biased off" state for both P and N channel devices shows excellent correspondence with the "unpowered" state. This simplifies modelling of V_T changes, since some difference might have been expected.

In summary it can be said that, for the AE project, the prospects for use of CD 4000A devices look very favorable provided a reliable device response prediction scheme can be developed for "derating" (producing parameter degradation

drawings for) all members of the series and a "screen" is developed to ensure that the gate oxide quality does not change. For circuits very sensitive to change in V_S or increased power drain, it should be possible to find sheltered locations within the spacecraft to meet their requirements. Recommendation for work on the device response predictions ("Phase II") have been made to NASA[1], while recommendations for clarifying effects seen in the present tests are made below.

3. Recommendations:

It would be of value to investigate questions of device behavior raised by the Phase I results which were of unexpected complexity. Answers to items (1) and (2) are strictly necessary if optimum derating schemes are required.

- Investigate unexpected peaking of V_I dependence at about 5 volts, by further tests.

- In order to determine the worst-case deviation from the simple mathematical model for charge buildup, the limits of the lot-to-lot variance of interface-state effects must be further established and these limits used to construct a corrected model.

For proper engineering tradeoffs of specific cases, it is often desirable to analyze subsystem responses under radiation, and to include the known bias duty cycles for each device. For such design studies, the unexpected 50% duty cycle test results will have to be understood and extended to other values of duty cycle.

---

[1]RCA and NASA are jointly reviewing the Phase II Program, to determine if further tests are necessary.

SECTION IV
SUBSYSTEM STUDIES

In this section of the report, changes to the spacecraft support subsystems which have been made as a consequence of the accommodation studies are described. Also included are summaries of selected analyses carried out. The changes result directly in some cases from specific experiment requirements identified during the Interface Definition Study, in others from revised system requirements established by NASA or, thirdly, as a consequence of further design iteration by RCA. The revisions represent the system arrived at upon conclusion of the study phase.

A. STRUCTURE

1. General

As a result of the Interface Definition Study effort, some modification has been made to the AE spacecraft structure to accommodate the requirements of the experiment complement. In summary, the spacecraft shape has been revised to provide extended flat panels perpendicular to the x-axis, the spacecraft height has been increased, and the solar array aperture cutouts have been redesigned to optimize the interfaces between the experiments and the spacecraft.

2. Structural Modifications

a. CONFIGURATION

The spacecraft configuration as described in the Phase B/C report comprised an eighteen-sided polyhedron 53.5 inches in outside diameter, and 41.0 inches in height. The design provided the capability for four experiments to be mounted on the forward face of the spacecraft with their axes parallel to the +x-axis and facing into the velocity vector when in the despun mode.

The experiment complement for the AE-C spacecraft includes six instruments to be located in the forward facing portion of the spacecraft (See Figure III-1, Section III-B). For best accommodation, an extended mounting area, placing the units side by side with their viewing axes parallel to the +x-axis has been provided. The experiment sensors generally have a limited capability to project beyond the spacecraft shell and, as the lateral distance from the spacecraft +x-axis to an experiment axis increases, the experiment cannot in general be located far enough forward of an axi-symmetric shell to achieve a 2π clear field of view.

To best meet experiment viewing requirements, the two panels either side of the +x-axis have been merged into a single panel; as a result, the experiment projections required for a 2π clear field of view have been reduced, and thermal control and solar cell shadow concerns of external projections minimized. This extended flat panel on the forward facing portion of the spacecraft (+x-axis) has been duplicated on the rear facing portion (-x-axis) in order to provide a symmetrical viewing aspect for the Photoelectron Spectrophotometer (PES).

To provide the flats, the baseplate shape and rib pattern will be modified from the original eighteen sided configuration. Design and manufacturing techniques are unaffected by the change.

Similarly, the solar array substrate design and manufacturing techniques are unaffected. The large forward and rear panels will be made of single pieces, bonded in place as are the other side panels. The panel joint miter angles will be redesigned to properly merge the large panels into the smaller side panels, and the substrate assembly tooling will provide the references needed for proper substrate assembly bonding.

b.   BASEPLATE CUTOUTS

Due to the length of the sensor portions of the NACE experiment, a portion of these instruments will pass through the spacecraft baseplate into the center propulsion section of the spacecraft. A cutout will be provided in the baseplate at the periphery in the required area. The cutout size is approximately 3.0 inches along the baseplate chord and 2.0 inches along the baseplate radius. The baseplate rib pattern will be modified and reinforced locally to provide baseplate structural integrety in the cutout zone.

c.   SPACECRAFT HEIGHT

In order to provide sufficient experiment power with the experiment apertures now defined for AE-C, a spacecraft height increase of 3.8 inches above the 41 inches of the Phase B/C Study has been selected. The height modification allows between 45 and 50* solar cell strings of 2 X 4 cm cells to be mounted to the sides of the spacecraft compared to the 53 of the Phase B/C study configuration. The height increase is accomplished by adding 1.9 inches to both the lower and upper array substrates. Internally, the growth allows increased head-room for electronic components on both baseplates, and an increased envelope within the central column along the z-axis. The increased envelope will be used to accommodate growth in the overall Solar Pointing Platform height to meet final experiment slip ring and weight requirements.

---

*Not finalized due to further anticipated changes in experiment interfaces.
Performance data in Attachment B is based on 48 circuits.

d.   SOLAR ARRAY SUBSTRATE MODIFICATIONS

The solar array substrate has been modified to provide increased aperture cutouts for the defined AE-C experiment complement. A single large cutout on the forward panel encompassing all the experiment cutout requirements, is provided. That portion of the cover plate on the experiment side of the baseplate mounting surface will be attached to the spacecraft baseplate prior to installation of the solar array. (See Figure IV-1). All sealing between the experiments and the cover plate will be accomplished before solar array installation. After the array is installed, structural ties between the cutout cover plate and the array will be made.

The cutout area between the baseplates will be used for access to test plugs and connectors (see Figure IV-2) and the cover plate will be installed at a later time when the spacecraft is "buttoned up" for launch. The cover plate modification simplifies the array installation procedure and provides better protection against experiment damage during spacecraft handling procedures.

The spacecraft solar array has been modified to include a hole on the +z-end to allow the vent portion of the BIMS experiment to pass through the substrate. Local reinforcement will be used on the substrate as required in the area of the cutout.

Mounting hard points will be installed on the cold (-z) end of the spacecraft for the sensor portion of the Capacitance Manometer pressure sensor. Detailed design of the thermal interface will include features to minimize the thermal coupling between the sensor and the spacecraft cold plate radiating surface.

Mounting cavities for the bi-metallic elements of the active thermal controller will also be provided in the spacecraft cold plate radiating surface. Details of the active controller and substrate installation are given in DN-505-4.5 (AE).

3.   Spacecraft Mechanical Characteristics Summary

a.   SPACECRAFT WEIGHT

The spacecraft weight for the defined AE system with the experiments selected for the AE-C mission is summarized in Table IV-I. A summary of spacecraft characteristics is given in Table IV-II.

SOLAR
ARRAY
CUTOUT

SPACECRAFT
TEST PLUGS

EXPERIMENT
CUTOUT
COVER PLATES
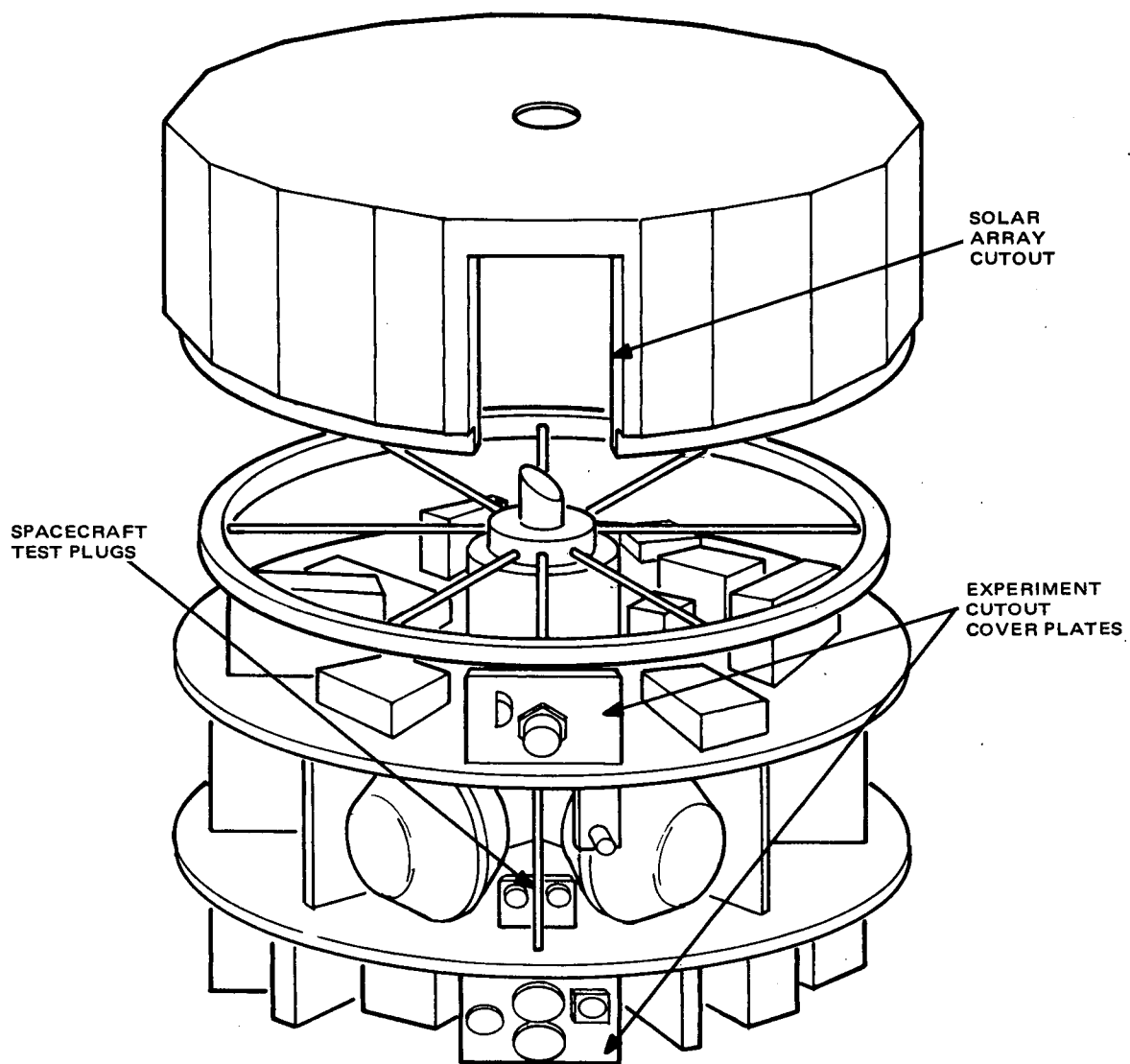
Figure IV-1. Solar Array Cutout Configuration

EXPERIMENT
CUTOUT
COVER PLATE

S-BAND
ANTENNA

TEST PLUG
COVER PLATES
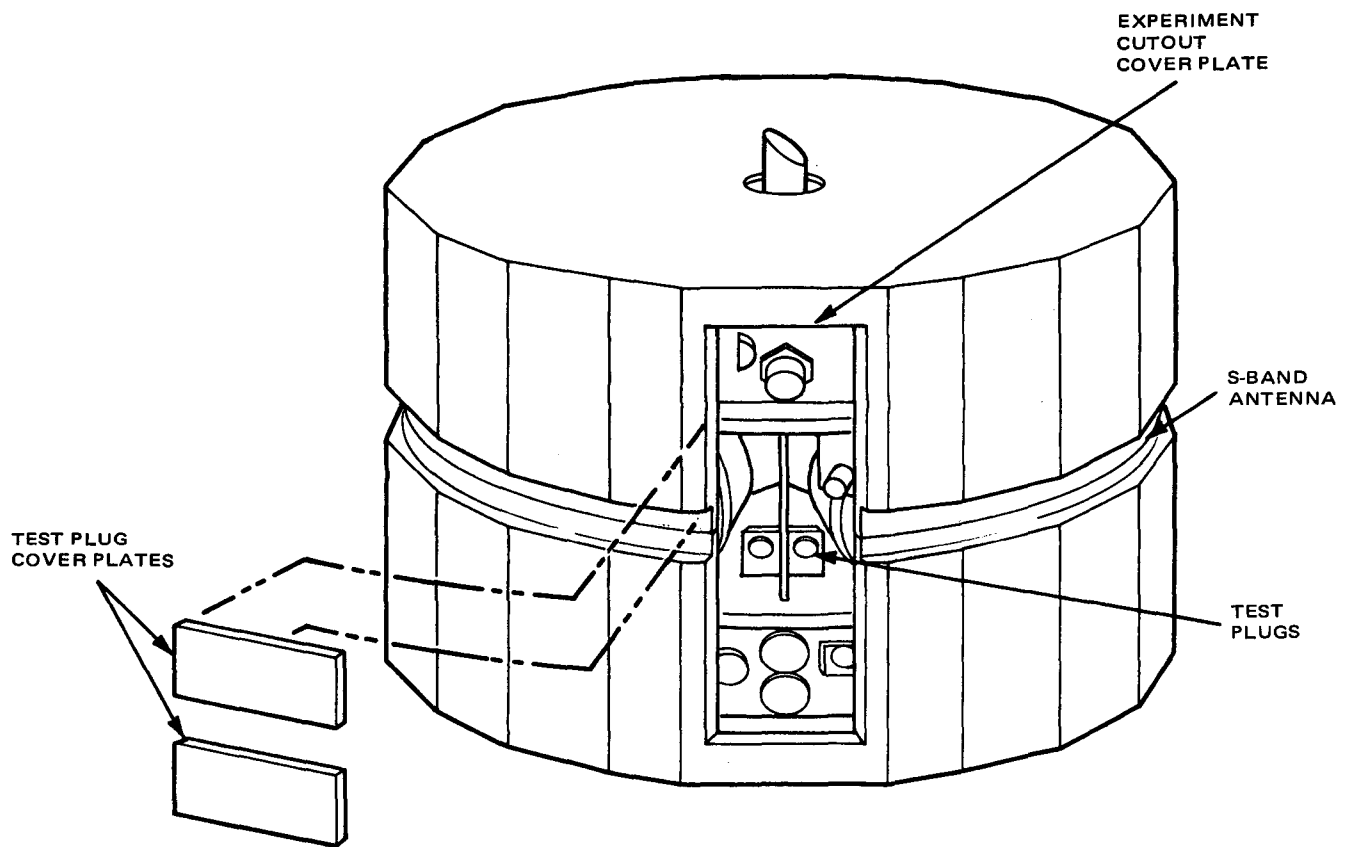
TEST
PLUGS

Figure IV-2. Test Plug Access After Array Installation

TABLE IV-1. SPACECRAFT WEIGHT ESTIMATE

ITEM	Weight (lbs)
Structure Subsystem	
Baseplates and Brackets	54.4
Central Column and Adapters	20.0
Upper Array Substrate	17.7
Lower Array Substrate	17.7
	110.0
Attitude Control Subsystem	
Momentum Wheel Assembly	48.0
Pitch Control Electronics A	7.0
Pitch Control Electronics B	7.0
Nutation Damper	4.0
Attitude Torquers	6.4
Momentum Torquers	1.6
DSAI Electronics and Sensors	5.0
Solar Gate Sensor	0.1
Magnetometer	1.5
Body Horizon Sensors	3.0
	84.0
Data Handling Subsystem	
Dual PCM Controller	7.0
RTM A	6.0
RTM B	6.0
Tape Recorders (2)	26.0
	45.0
Command and Control Subsystem	
Dual Programmer	8.0
Memory (2)	14.0
Logic Interface Unit A	10.0
Logic Interface Unit B	9.0
Command Distribution Unit A	4.0
Command Distribution Unit B	4.0
Dual Demodulator/Decoder	4.0
	53.0
Orbit Adjust Propulsion Subsystem	
Propellant Tanks	105.0
Thrusters	1.2
Valves, Piping and Misc.	26.0
	132.2

TABLE IV-1. SPACECRAFT WEIGHT ESTIMATE (Continued)

ITEM	Weight (lbs)
Power Subsystem	
Solar Array (exclusive of substrate)	46.0
Power Supply Electronics	13.0
Shunt Dissipators	3.0
Batteries (3)	60.0
	122.0
Communications and Ranging	
VHF Antenna	2.4
VHF Antenna Network	2.2
Beacon/Telemetry Transmitter	3.6
Range/Rate Transponder (2)	20.0
S-Band Coupling Assembly	4.0
Dual Pre-Modulation Processor	5.0
S-Band Antenna	5.0
S-Band Power Splitter	1.0
VHF RF Switch	0.4
	43.6
Engineering Measurement Subsystem	
Cold Cathode Pressure Sensor	2.5
Cold Cathode Pressure Sensor Elect	3.5
Capacitance Nanometer	3.0
Capacitance Nanometer Elect	3.2
	12.2
Solar Pointing Subsystem	
Solar Pointing Platform	25.0
Solar Pointing Electronics	6.0
	31.0
Support Equipment	
Harness	40.0
Hardware	10.0
Balance Weights	20.0
Baseplate Heaters	6.0
Thermal Blankets	10.0
Active Thermal Controllers	5.0
Temperature Sensors	0.5
	91.5

TABLE IV-1. SPACECRAFT WEIGHT ESTIMATE (Continued)

ITEM	Weight (lbs)
Total Spacecraft	724.5
Total Experiments	184.0
Propellant	370.0
Pressurant	3.4
Total	1282.0
Experiments	
CEP	4.0
BIMS	7.6
PES	10.0
RPA	11.0
MIMS	10.0
LEE	9.5
MESA	16.0
OSS	15.0
NACE	16.0
NATE	15.2
UVNO	15.5
VAE	12.0
ESUM	18.1
EUVS	24.0
Total	184.0

TABLE IV-II. SPACECRAFT CHARACTERISTICS

Characteristics	Dimensions
Total Weight	
AE-C	1282 lbs
AE-D	1275 lbs
AE-E	1251 lbs
Spacecraft Size	53.5 in. Diameter
	44.8 in. Height
Spacecraft Projected Area	2374 in.^{2}
Spacecraft Base Area	1000 in.^{2}
Spacecraft Spin Axis Inertia (AE-C)	1166 in-lb-sec^2

B. THERMAL DESIGN

The thermal design and analysis effort during the IDS was concentrated in the following areas:

- Parametric trade-off studies of temperature control capabilities of both active and passive temperature control methods for the AE spacecraft.

- Preliminary definition of a suitable active control unit.

- Definition of internal and external thermal interface requirements for the scientific experiment packages.

- Analysis of orbital temperature profiles for thin wires and plates under simulated conditions.

The results of the first two items of this work are summarized in the following paragraphs; the last two items are discussed in Section III.D.6.

1. Active vs Passive Control Study

To evaluate the impact of sun angle range and baseplate power distribution on spacecraft thermal design, an orbit average temperature study was performed during the study using a multi-node model, with the upper and lower BP equipment complexes treated as two lumped nodes. The variable parameters used in this study were:

- coupling from upper baseplate-equipment complex to top (-Z) surface (variable with an active controller)

- power distribution between baseplates

- experiment duty cycle

The results of the tradeoff study were used to compare the performance of an active and a passive design approach. Details of the analysis are given in Appendix IV. B.

In the design evolved during the Phase B/C study the nominal maximum continuous duty cycle was 30% and the minimum available at the worst case cold sun angle (0°) was 19% (end of 8 months) based on a total experiment power dissipation of 100 watts during the record cycle. Since latest available experiment power dissipation data indicates a total experiment power requirement of 95 watts regulated load and 19.5 watts unregulated load at nominal power, these duty cycles will be correspondingly modified.

The temperature data obtained from the parametric study provided performance curves as presented in the appendix from which worst case hot to cold temperature ranges could be determined for both active and passive control systems. Table IV-IV summarizes the baseplate equipment orbit average temperature performance under the conditions given in Table IV-III, anticipated to be most nearly representative of the actual case when spacecraft layouts are finalized.

TABLE IV-III. CONDITIONS OF TEMPERATURE PERFORMANCE

● Baseplate power distribution – 60% upper, 40% lower
● Coupling from upper baseplate to top

Passive control	210 in^2
Active control – min	135 in^2
Active control – mix	355 in^2

A 10°C minimum margin is considered desirable for the preliminary analysis performed to allow for:

● Baseplate location temperature variation

● Orbital temperature variation

● Analytical errors (Differences between actual and calculated internal and external coupling)

● Variation in surface and material properties, and power dissipation from assumed values.

The available minimum temperature margins with passive control are considerably below the desired value. In order to attain 10° hot and cold margins with passive control it would be necessary to reduce the top coupling from 210 to 135 in^2 and cut back the duty cycle at worst case hot conditions to a very low value. With active control the required margin is available at the specified duty cycle (30%-100W) at worst case hot conditions and for the end-of-8 months available duty cycle (19%-100W) at worst case cold conditions.

2.   Active Controller Design

Details of the study covering requirements for an active temperature control system for AE are contained in DN-505-4.5 (AE).

The active control units for the AE spacecraft are not mounted externally because of aerodynamic considerations; rather they are mounted internally between the momentum wheel and the -z spacecraft surface. (See Figure IV-3.) This places dimensional and motion constraints on the controller design. However, since the main function of the control unit is control of the coupling between the
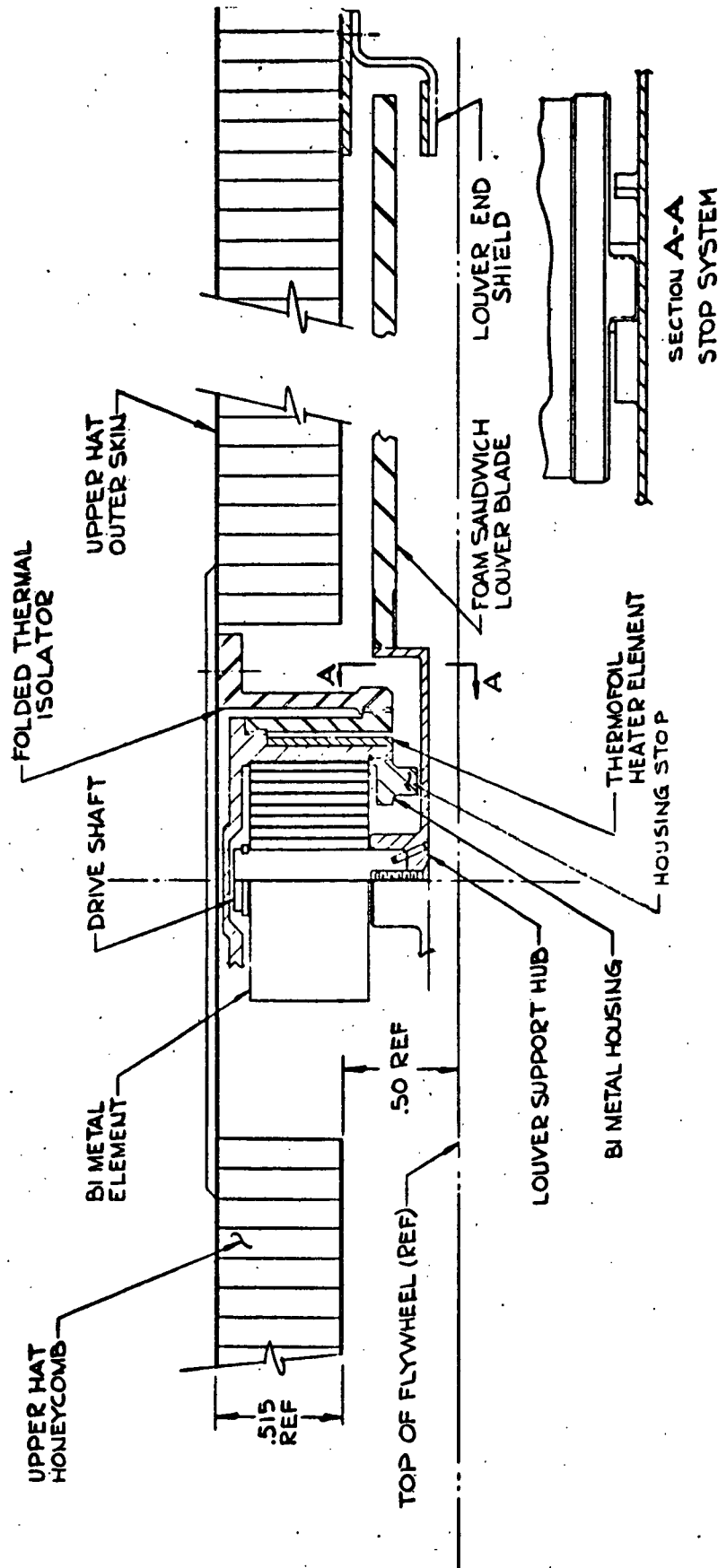
Figure IV-3. Detail of Active Thermal Control Louver Assembly

lower baseplate and top (-Z) surface, low profile rotary shutter units which can be installed between the momentum wheel and the top are considered to be the most satisfactory method of coupling control.

In order to obtain fully closed to open operation over a desired narrow temperature range an active (powered) controller drive system was selected. In the event of failure of the drive unit power supply, the units will have a degraded but failsafe operation capability by actuation through radiation from the baseplate to the unit. A summary of the design features of the proposed units is presented in Table IV-V.

TABLE IV-IV. ORBIT AVERAGE BASEPLATE TEMPERATURE PERFORMANCE

Baseplate Temperatures (^{o}C)

	Upper				Lower			
Control Mode	Required Range	Calculated Range	Margin		Required Range	Calculated Range	Margin	
			Hot	Cold			Hot	Cold
Passive	-5 to 30	-3 to 25	5	2	-5 to 40	8 to 38	2	13
Active	-5 to 30	5 to 12	18	10	-5 to 40	15 to 30	10	20

TABLE IV-V. ACTIVE CONTROL DESIGN FEATURES

No. of units	4
Type of unit	Rotary shutter which covers high emittance surface on S/C top when closed and exposes these surfaces when open.
Drive mechanism	Bimetallic torsion spring contained in a cylindrical housing with circumferential resistance heaters.
Heater power	0.25 watts/unit.
Heater actuation	Electronic bridge circuit with thermistor type temperature sensor on baseplate.
Operating bandwidth for heater actuation	0 to full heater power over 1°C temperature range on baseplate.
Operating bandwidth - power failure	Shutter fully closed to fully open over a 28°C temperature range on baseplate.j
Shutter size and material	20" diameter X 0.93" thick open cell polyurethane foam core with 1 mil Kapton film face sheets. 3" diameter aluminum hub.
Shutter rotation fully closed to open	45°

TABLE IV-V. ACTIVE CONTROL DESIGN FEATURES (Continued)

Shutter edge treatment	Gold finished end shield at circumference to provide mechanical constraint during S/C vibration and reduce heat transfer between edge and S/C.
Finishes	Shutter hub – Surface facing baseplate – high emittance. Surface facing top – vapor deposited gold on Kapton film. Drive housing –External – vapor deposited gold. Internal – high emittance.
Conductive coupling housing to S/C top	0.002 w/°C max./unit
Equivalent area x emittance of area covered by shutter	Closed 20 in²/unit Open 138 in²/unit
Fail safe features	Shutter normally closed with power off. Shutter will operate from baseplate radiation in the event of power supply failure.

C. ATTITUDE CONTROL

Only minor revisions to the attitude control subsystem have been made during the period of the Interface Definition Study and these mainly involve the recommended approach to packaging. With one exception, namely the provision of a nadir pulse reference, no basic changes have been made to the functions provided by the subsystem, its performance, or method of implementation. A complete description is given in the Phase B/C study report.

Two additional modifications are however presently under consideration. These are:

- A modification to the wheel horizon sensor processing electronics to improve sensor response and hence attitude determination accuracy. This improvement may permit a reduction in the digital solar aspect sensor complement.

- A revision to the momentum control approach whereby torquer commutation is accomplished via the body horizon sensors instead of magnetometers as in the current baseline.

These potential changes are discussed in more detail below, together with the proposed approach to nadir pulse provision. A decision regarding their implementation is anticipated prior to the AE spacecraft Preliminary Design Review.

Other topics discussed in this summary report include roll/yaw attitude determination, work accomplished on the three-axis dynamic simulation program and minor modifications to the overall subsystem block diagram.

1. Nadir Pulse Provision

Operational requirements for several experiments, identified during the interface definition study, have led to incorporation of a nadir reference to be generated during spacecraft operation in spin mode. The required nadir pulse can be provided utilizing either the body- or wheel-mounted horizon sensors. The selected approach is based on the use of the body-mounted sensors because of 1) improved accuracy, and 2) assured continuous experiment operation regardless of the operational status of the Momentum Wheel Assembly or the spin controller.

The geometry for generating a nadir reference utilizing a body mounted horizon sensor is shown in Figure IV-4a. From this it is seen that

$$\theta_i = W_B \, T_i \tag{1}$$

where

θ_i = angle between the earth sensor line-of-sight and the ith experiment

W_B = Spacecraft angular velocity

T_i = time for the body to rotate through θ_i

If the earth sensor is initially looking along nadir, T_i therefore represents that time later that the ith experiment will also be viewing along nadir. Considering this, T_i may be expressed as

$$T_i = \frac{te}{2} + \tau_i \qquad (2)$$

where t_e is the earth crossing time of the sensor and τ_i is that time after the sensor makes its earth/sky transition that the ith experiment will be at nadir. Combining equations 1 and 2 and solving for τ_i yields

$$\tau_i = \left(\frac{\theta_i}{2\pi}\right) T_B - \frac{t_e}{2} \qquad (3)$$

where T_B is the S/C spin period. Similarly, it may be shown that if the S/C is precessed 180 degrees during flight (as in Figure IV-4b), the time from the sensor earth/sky crossing until the ith experiment is at nadir is given by an identical expression. Therefore, the body mounted sensor nadir reference scheme has been configured to determine τ_i as in this case the implementation scheme is independent of spacecraft orientation.

A functional block diagram of the nadir reference scheme utilizing the body mounted sensor is shown in Figure IV-5. From the figure it is seen that the earth transition pulses from the horizon sensor are used to determine t_e and to trigger the "τ" counter. Logic circuits which receive t_e and T_B data are used to calculate τ_i and set a comparator to emit the desired nadir pulse as the τ counter passes the value of τ_i. When the value of τ_i has been reached, the comparitor is reset with the value of τ_{i+1}. After all of the nadir pulses in one revolution have been given, the counter is reset for the next revolution. The scheme, with a correction to equation 3 for the dynamic lag of the sensor, will provide the desired nadir reference to an accuracy of ±1.5 degrees.
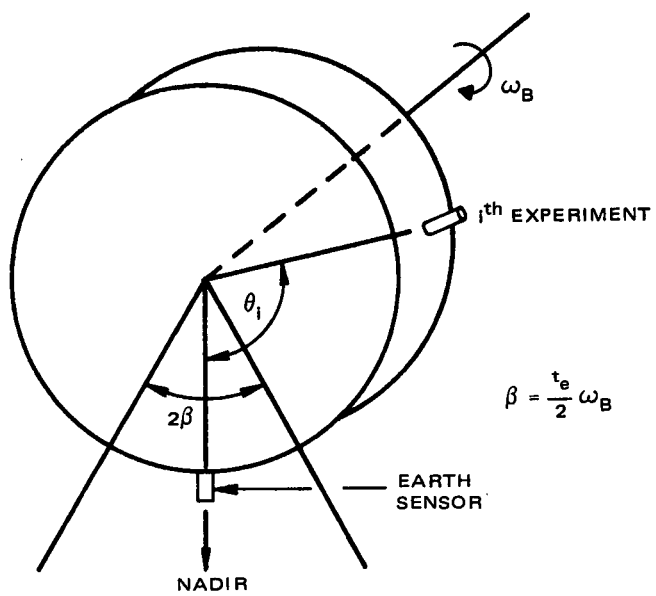
Normal Configuration
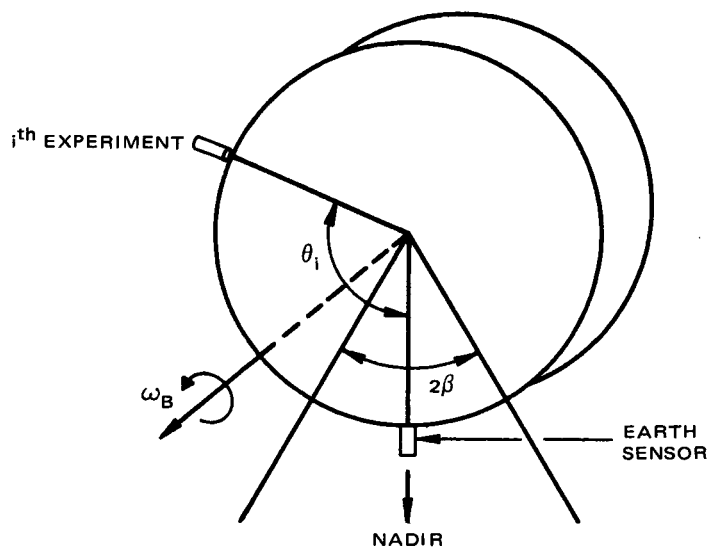
Inverted Configuration

Figure IV-4. Nadir Reference Geometry
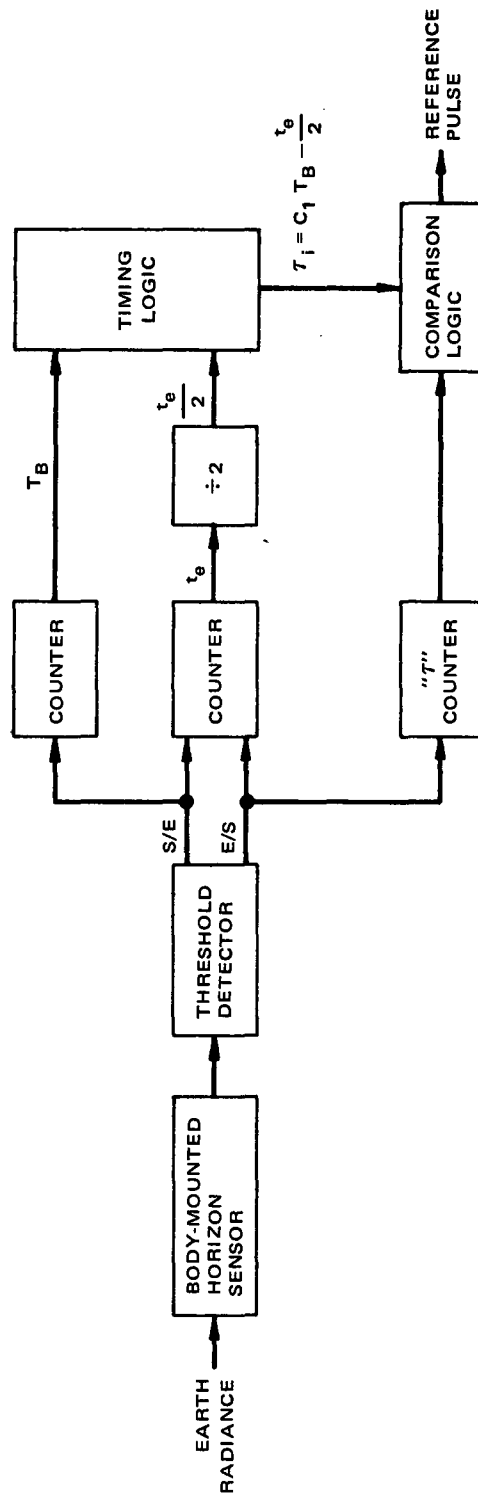
Figure IV-5. Nadir Reference Functional Diagram

2. Roll/Yaw Attitude Determination

The accuracy to which spacecraft roll/yaw attitude during perigee passage can be determined a posteriori from spacecraft horizon sensor data has been examined in detail in DN-515-5.0 (AE). Performance for both 120 and 150 km perigee altitudes was investigated. It was concluded that little benefit can be gained from recording roll error data during perigee passage since a better estimate of roll/yaw error can be obtained by interpolation between the errors measured prior and subsequent to perigee passage when the spacecraft is substantially free of disturbances. Using this approach, an accuracy of ±0.6 in roll/yaw altitude determination is predicted. If the improved sensor electronics discussed below is implemented, then performance will be further enhanced.

3. Pitch Accuracy with Improved Sensing Circuit

The accuracy in sensing pitch (and roll) attitude can be substantially improved by modifications suggested by NASA to the originally proposed AE scanning horizon sensor electronics (see Appendix IV.A). These modifications include signal peaking as previously employed on both the TIROS and NIMBUS programs and also dc restoration as used on NIMBUS. A block diagram of the processor transfer function is shown in Figure IV-6. The inclusion of these modifications in the sensor electronics can provide a better than two to one improvement in pitch sensing accuracy, i.e., from ±0.97° to better than ±0.4° 3σ. While the threshold to noise ratio is less than that of the originally proposed sensor, it is adequate for sensing in the CO_2 spectral band. Although the required circuitry is more complex, it does not appear that its implementation will require a significant increase in the number of circuits.

Hardware modification required to implement the approach shown in Figure IV-6 are currently under study and will be presented to NASA when this work is completed.

4. Multi-Rigid-Body Dynamic Simulation

A recently developed JPL general computer simulation for determining the attitude dynamics of a multi-rigid-body dynamic system has been adapted and modified for AE. It is particularly suited for this application because of the complex interaction between three control loops, i.e., the pitch control loop and the two independent control loops for the Solar Pointing Subsystem.
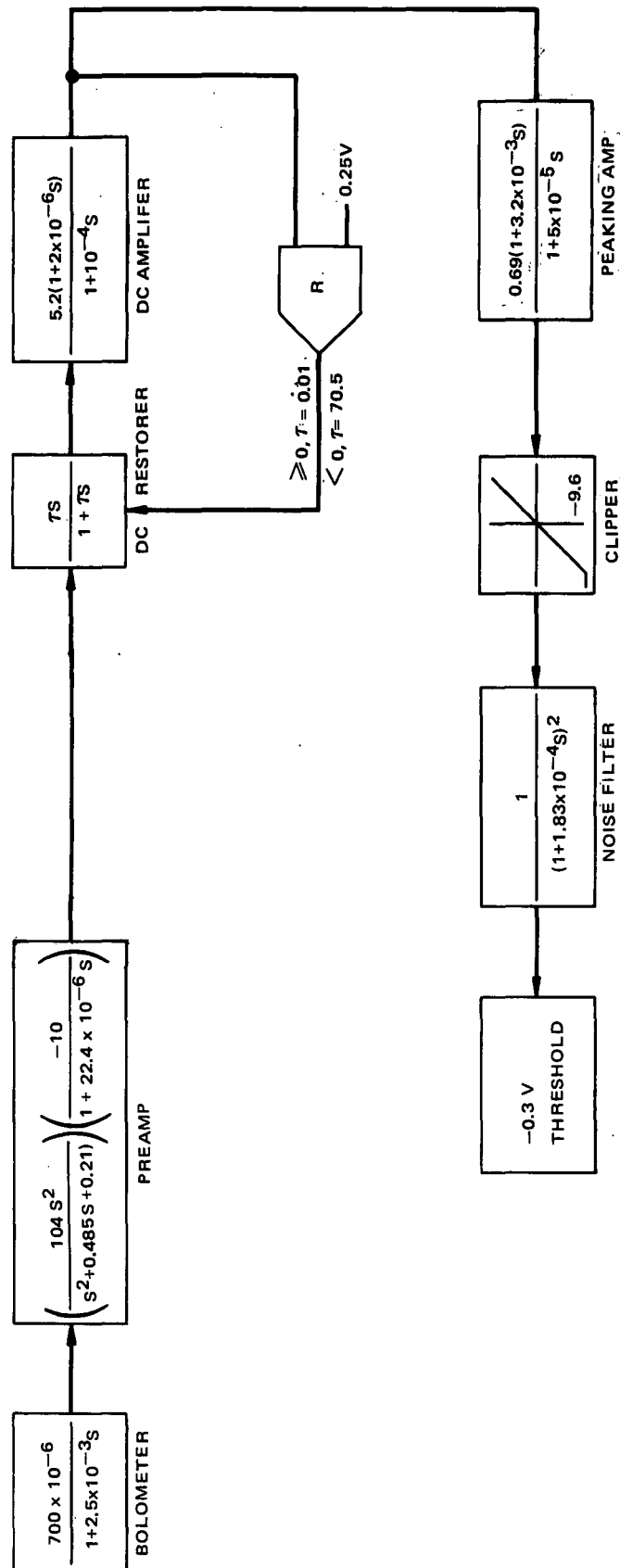
Figure IV-6. Revised Sensor Block Diagram

The simulator accommodates a system where moments of inertia and parameters change continuously. This computer program (for a detailed description see DN-575-5.0(AE)) provides the necessary means to study the dynamic interplay between these loops as well as the less significant effects of other experiments (such as NATE) and internal disturbances (tape recorders). The program has been debugged and is now operational. It will be utilized for design and performance studies when the characteristics of the solar pointing subsystem sensors have been tentatively established.

5. Revised Momentum Control Approach

A study is currently in progress to determine the feasibility of eliminating the requirement for the two magnetometers originally proposed for commutation of the spacecraft magnetic dipole, to provide momentum control in the spacecraft spin mode. Preliminary study results indicate that a satisfactory alternate approach to determination of the momentum control dipole polarity switching point can be achieved with the availability of the nadir pulse and ground-computed commands (referenced to time from the ascending mode) stored in the spacecraft programmer. Details of this approach will be reported upon study conclusion.

6. Revised Pitch Attitude Control Configuration

Figure IV-7 presents an updated block diagram of the pitch control loop. The diagram reflects proposed changes in the division of functions between the pitch control electronics (PCE) and spacecraft programmer.

The circuit elements comprising the spin controller, pitch offset register and earth sensor telemetry are now included in the PCE. This arrangement brings together all pitch loop related functions in a single (redundant) unit and simplifies the interfaces between the PCE and the spacecraft programmer. Note also that the sensor signal processor and threshold in each PCE is powered whether or not its associated pitch loop is powered. This permits simultaneous operation of both threshold circuits to provide roll telemetry and inputs to the programmer for auto-roll control. Another new feature is the inclusion of pitch offset telemetry.

The Momentum Wheel Assembly (MWA) characteristics are unchanged from those described in the Phase B/C study report.
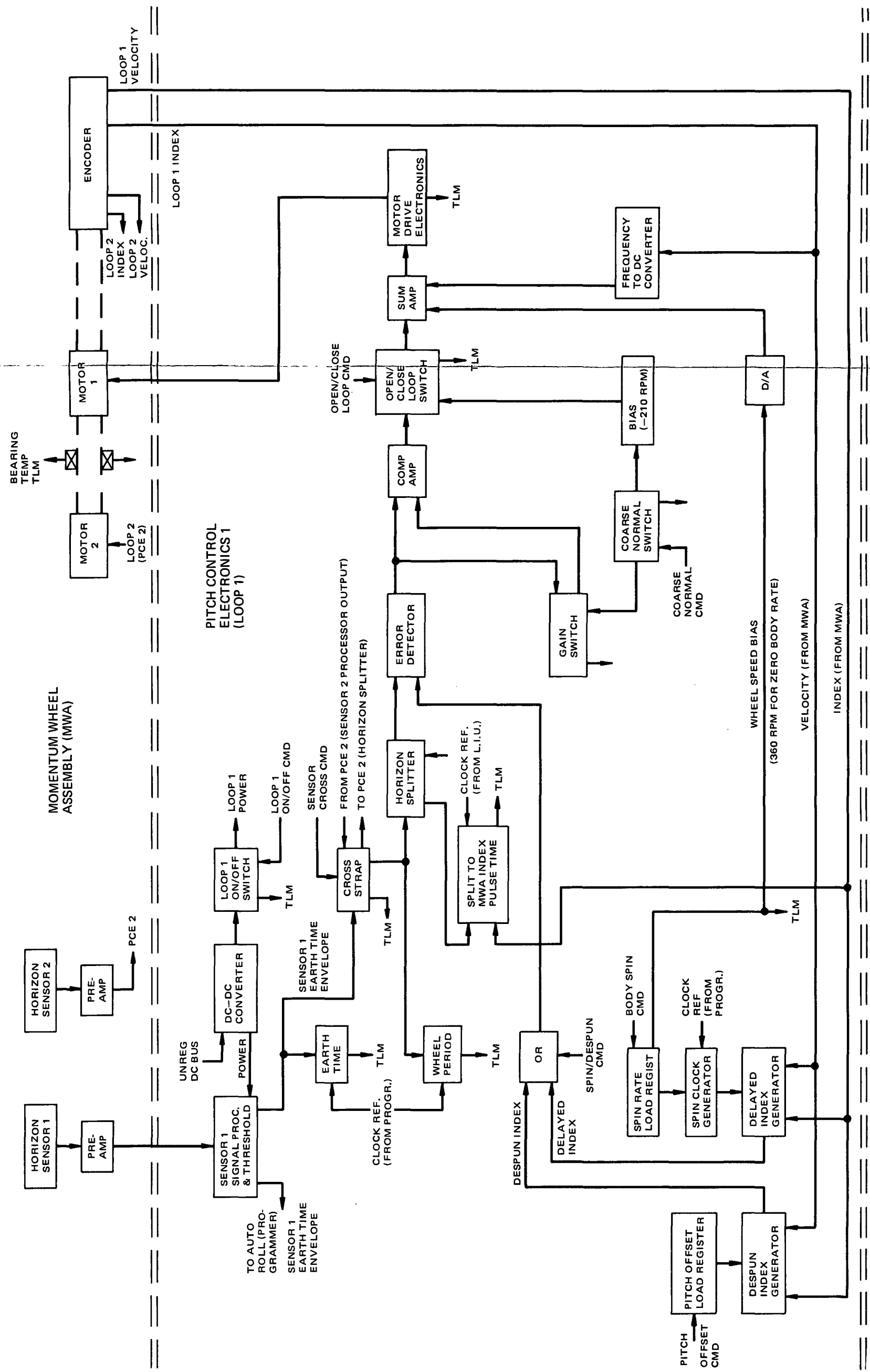
Figure IV-7. AE Pitch Loop Block Diagram

IV-23/24

D.   ORBIT ADJUST PROPULSION SYSTEM (OAPS)

1.   General

The AE spacecraft OAPS configuration is shown schematically in Figure IV-8 with pertinent specification performance parameters summarized in Table IV-VI. This subsystem has undergone considerable revision from the baseline of the Phase B/C study as a result of additional tradeoff studies relating to subsystem design complexity, failure mode characteristics and performance. Analyses made in support of the revision are discussed in the following paragraphs and in DN 595-6.0 (AE) included in Attachment C to this report.

The design, performance, fabrication, and test requirements for the OAPS are detailed in RCA Specification PS-226210 Revision C. The OAPS interface definition is contained in RCA Drawing 2265337 with the electrical schematic presented in RCA Drawing 2270676. A list of the key OAPS components required for the program are presented in Table IV-VII.

The OAPS is a single stage blowdown system with the propellant and pressurant contained in six identical tanks. Each tank contains a ring stabilized metallic diaphragm for positive expulsion. In the fully loaded propellant condition the diaphragms are partially reversed to provide the ullage volume to accommodate the required pressurant. The propellant/pressurant storage system is divided into two "half systems" with both the pressurant and propellant sides of the two sets of three tanks manifolded together. In normal operation each half system provides propellant to its associated thruster assembly. A propellant flow control valve is located at each tank outlet to permit selective propellant withdrawal for both x and y axis center of mass control and to provide tank isolation in the event of thruster valve failure.

A crossover line containing a normally closed squib valve connects the two systems. In the event of an engine failure in one of the half systems the valve can be activated to permit utilization of the remaining propellant through the good thruster. On the AE-E spacecraft a yaw thruster is located in the crossover line separated from one half system by the normally closed squib valve and from the other by a normally open squib valve. Under normal operation yaw thruster propellant is provided from the normally open side with failure mode operation capability from the normally closed side.

2.   Redundant Half-Systems

The OAPS was separated into two operationally independent half-systems in order to achieve at least a 50% impulse capability in the event of any single point failure at the part level. A summary of the primary alternate configurations considered in arriving at the revised baseline is contained in Section A of DN 595-6.0 (AE).
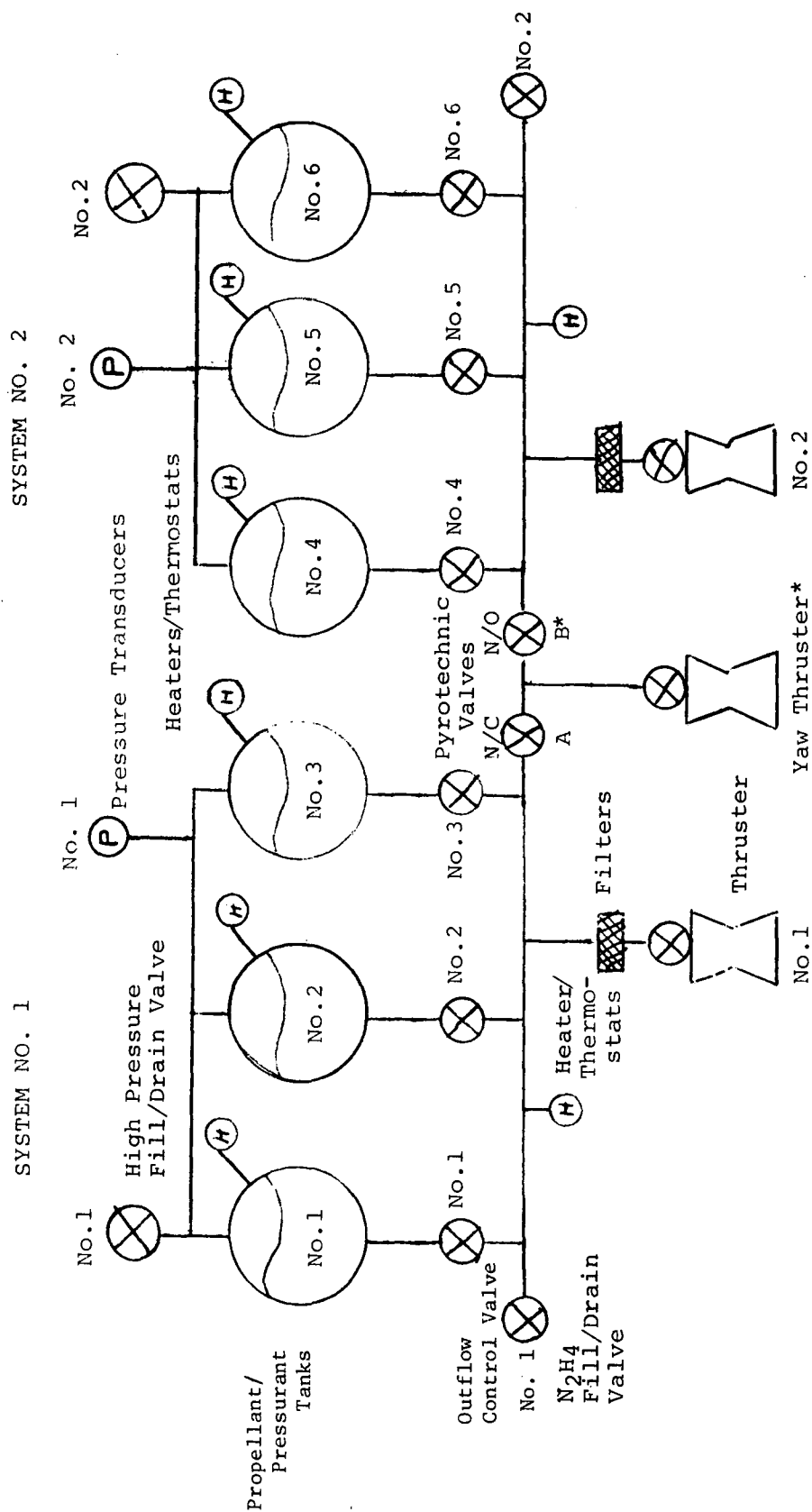
Figure IV-8. AE OAPS Schematic Diagram

TABLE IV-VI. SPECIFICATION PERFORMANCE SUMMARY

Propellant	Hydrazine MIL-P-26536C
OAPS Maximum Dry Weight	132 lbs
Propellant Weight	370 lbs
Minimum Delivered Total Impulse	75,000 lb-sec
Average Delivered Specific Impulse	210 sec
Minimum Impulse Bit	
Primary Mode (spacecraft despun)	100 lb-sec
Backup Mode (spacecraft spinning)	0.4 lb-sec
Thrust Level	4.1 to 0.75 lb$_f$
Thruster Operating Life	
Primary Mode	7 hours/80 Operational Starts
Backup (one thruster failed)	14 hours/160 Operational Starts Max.
Pressurant	Nitrogen MIL-P-27401B
Tank Pressure	
Maximum Operating @ 50° C	600 psia
Design Burst Pressure	1200 psia
Diaphram Reversal Life	
Qualification Value	3
Design Goal	5
OAPS Total Leakage, Design Goal	1×10^{-4} SCC GN$_2$/sec
Reliability	
1-year Operation	>0.95
Minimum Single Point Failure Impulse	50%

TABLE IV-VII. KEY HARDWARE REQUIREMENTS

COMPONENT	FLT "D" & PROTO FLT "C"	FLT " E"
Propellant Tank	6	6
Fill & Drain Valve	4	4
Pressure Transducer (Low Press)	2	2
Filter	2	2
Squib Valve/Squibs	1	2
Solenoid Valve (Tank Outflow)	6	6
Brackets Prop Tank	12	12
Brackets - Shipping	12	12
Thruster Assy	2	3
Thruster Valve	2	3
Heaters - Tank	6	6
Heaters - Line	6	6
Thermostats	7	7
Wiring Harness	1	1
Lines, Fittings, Access., Catalyst	A/R	A/R
Fittings Aeroquip	A/R	A/R
Clamps and Fasteners	A/R	A/R

As stated above, the selected configuration divides both the propellant and pressurant into two separate systems each containing its own thruster. Y and x axis c.m. control is achieved by placing a flow control valve at each tank outlet via the physical arrangement of each half system. Propellant withdrawal for each burn is preselected from the appropriate tank to maintain the c.m. within prescribed limits. Z-axis control is maintained by means of an appropriate division of ΔV operations between the two half-systems.

The yaw thruster arrangement illustrated in Figure IV-8 allows operation from one of the half-systems during normal operation and from the alternate half-system in the event of half-system failure. Squib valves, rather than solenoid latching valves, were chosen for the crossover to ensure a positive seal against reverse flow between systems.

3. Single-Stage Blowdown

As part of the study effort trade analyses were conducted to determine if the impulse performance loss associated with a single stage blowdown pressurization system would be offset by the lower cost and simplicity of this approach over the originally selected two stage pressurization system. Initial pressure levels of 450 and 600 psia and propellant loads of 350, 400 and 450 pounds were considered. Key performance results are summarized below for the fixed baseline tank volume of 2050 cubic inches.

Pressurization Technique	Initial Pressure psia	Propellant Weight, lb	Total Delivered Impulse, lb-sec
Original Baseline (2-stage)	450	400	82,000
Single Stage	450	347	69,500
Single Stage	600	370	75,000

The advantages of the single stage blowdown are a reduction in program cost and a decrease in complexity associated with the reduction in components.

To assess the impact of a decreased propellant load capability of the OAPS in terms of the AE spacecraft mission additional performance studies were conducted. These studies included the impact of different spacecraft total weights and frontal areas. Results of the tradeoffs are presented in DN 508-6.0 (AE).

Based on the overall study results it was concluded that the advantages in terms of cost reduction and design simplification warranted the approximate 12% reduction in total impulse performance. With concurrence of NASA-GSFC a single stage blowdown system with an initial tank pressure of 600 psia was selected as a new baseline configuration.

4. Thrust Chamber Assembly

Concurrently with the subsystem configuration studies discussed in Section IV.C above, a re-evaluation of monopropellant hydrazine thruster was conducted (see Section B of DN 595-6.0 (AE)).

This study showed that the TRW Intelsat III thruster originally selected during the Phase B/C study has the most favorable characteristics for the AE mission. Furthermore, with the decision to adopt a single stage blowdown pressurization system with an initial tank pressure of 600 psia, the beginning of life thrust level for the TRW engine increased to 4.1 pounds from the 3.3 pounds level appropriate to the originally selected two stage blowdown system.

Total impulse performance of the other engines considered namely the Hamilton Standard P95 and Rocket Research Intelsat IV, due to the lower range of inlet pressure over which they have been qualified, would be substantially lower than the selected engine in the AE case where gas ullage volume is limited.

5. Center-of-Mass Control

Spacecraft center-of-mass control will be maintained by selective withdrawal of the propellant from one tank at a time for each burn. By monitoring the spacecraft dynamics behavior between burns, actual center-of-mass location will be calculated and compared to the desired center-of-mass location. Based on this determination the appropriate tank will be selected for propellant withdrawal on the subsequent burn to cause the center-of-mass to shift toward the null point. This procedure will be repeated throughout the spacecraft life, with a general objective of maintaining the offset on the order of 0.1" in all axes. Figure IV-9 is a plot of the calculated center of mass shift over life for an alternating tank withdrawal control approach based on 24 ft/sec maneuvers. It represents a failure mode condition in that propellant is withdrawn from the two half systems sequentially. Nominal z axis shifts will be smaller than shown. Analyses describing the attitude control performance impact of center of mass errors are included in the Phase B/C Study Report.

The feasibility of simultaneous multi-tank propellant withdrawal has also been examined with a view of simplifying mission operations. With this technique all three tank outlet valves in either half system would be opened simultaneously during thruster operation. By balancing the outflow between tanks the center-of-mass shift can be minimized. Imbalance in flow will cause a center-of-mass shift toward the tank with the most remaining propellant. The primary contributor to the flow variation is the mismatch in reversal pressure of the metallic diaphragms. Test data on diaphragms similar to those to be used on AE indicates a mismatch in reversal pressure of 1 to 2 psi during the useful reversal range of the diaphragm.

The feed line pressure drop from the tank outlet to the common branch point of the propellant manifold is the only flow resistance that counteracts the effect of the diaphragm reversal pressure variation. By placing orifices at the tank outlets the effect can be reduced to maintain the center-of-mass drift to acceptable values. Figure IV-10 is a plot of the x axis shift as a function of percent expelled for three different orifice sizes assuming serial depletion of the half systems. Also shown are the maximum y axis and z axis shifts encountered during the withdrawal. Due to the cost performance impact of including orifices, no final decision on whether to implement this feature has yet been made.

6. Other Study Results

Additional tasks conducted during the period of the IDS study, which did not impact the proposed configuration were:

- Review of spherical bearing tank mounting support.

As NASA had expressed some concern about twist loads on the OAPS plumbing, RCA/TRW reviewed the proposed tank support and compared it with alternate approaches. On the basis of this trade study, no change is recommended. Details are furnished in Section C of DN 595-6.0 (AE).

- Determination of the impact of reducing the feed line pressure drop of the TRW engine.

The TRW engine is designed with a large pressure drop in the injector propellant feed tube (102 psia @ 4.1 pounds thrust). Consideration was given to the reduction of the restriction to permit an increase in OAPS impulse and in some cases reduce tankage weight, see Section D of DN 595-6.0 (AE). However, RCA does not feel that this change could be implemented without a re-qualification test of the engine. The cost and risk were considered greater than the potential performance gain. Furthermore, if the pressure drop were removed, a single stage pressurization system would no longer be a reasonable technical approach. The blowdown range would be excessive within the tankage envelope available on the AE spacecraft.
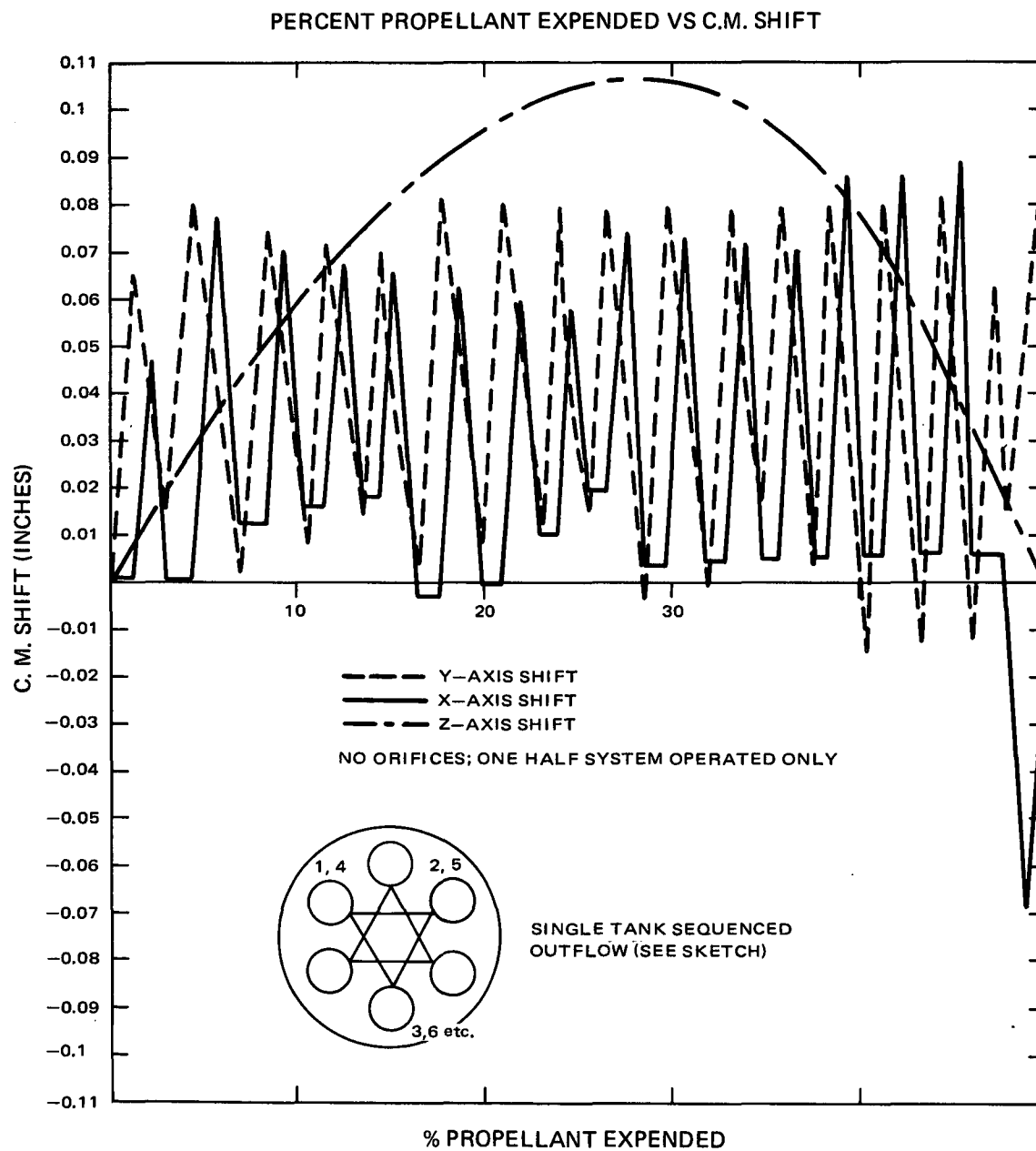
Figure IV-9. Percent Propellant Expended vs Center-of-Mass Shift
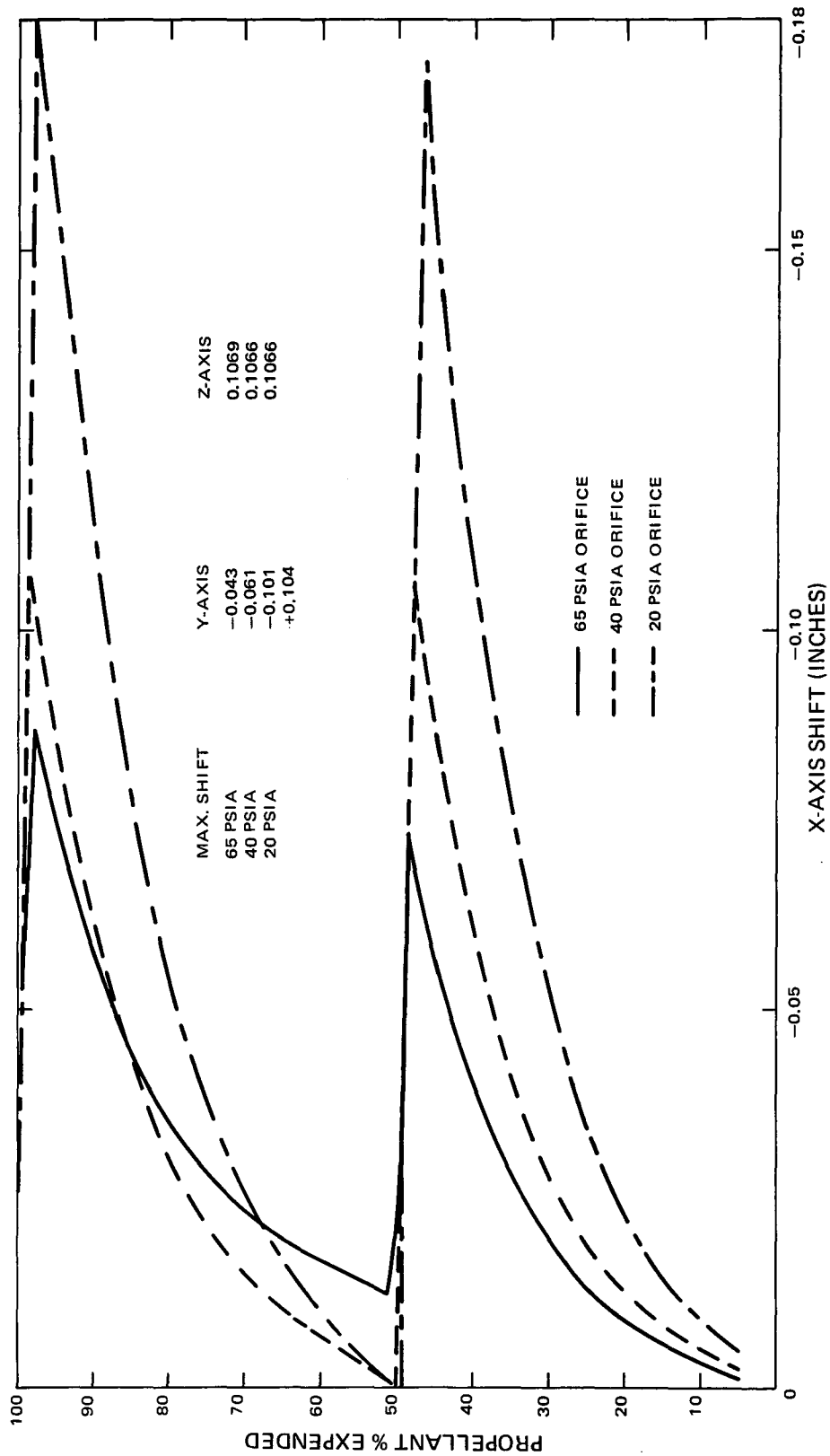
Figure IV-10. Three Tank Outflow Center-of-Mass Shift

●   Definition of the Arde diaphragm reversal life for both rim
and apex roll diaphragms as a function of the diaphragm per-
centage reversal.

The results of this study are presented in Figure IV-11. While the amount of
test data is limited, the metallic diaphragm appears to be capable of meeting
the AE requirements with either reversal mode. Since the rim roll represents
the better defined and lower cost approach it is retained as the recommended
diaphragm reversal mode.

a.   PREPARATION OF A SINGLE POINT FAILURE ANALYSIS FOR THE REVISED CONFIGURATION

A failure modes and effects analysis was conducted in conjunction with
the OAPS configuration studies discussed in Section IV-A. Table IV-VIII is a
summary of the results for the baseline configuration based on the information
presented in Section A of DN 595-6.0 (AE). The design retains a minimum 50
percent nominal impulse capability with x and y axis c.m. control in the event
of any single point failure at the component level.

b.   DEFINITION OF PROPELLANT AND PRESSURANT SERVICING PROCEDURES

Section E of DN 595-6.0 (AE) describes the OAPS propellant and pressurant
loading procedures for the two stage blowdown configuration.* While no longer
directly applicable to the current configuration it does serve to define the ma-
jority of steps in the procedures. The pressurant fill considerations are the
same as the low pressure fill procedure on the two stage system. The propel-
lant fill approach would remain unchanged. The propellant draining procedure
would be simplified for the single stage blowdown system due to the partially
cycled condition of the diaphragm in the fully loaded condition. Removal of fluid
would be accomplished by venting the gas side pressure to ambient and pressur-
izing the liquid side of the tank to be drained, to 3 to 5 psi above ambient pres-
sure, cycling the diaphragm to its initial position. The spacecraft would then be
tipped so that the propellant tank is oriented with its outlet at the low point, and
the liquid side allowed to blowdown expelling the propellant. Drain time will be
less than 2 hours. The system should be vacuum dried for 8 to 24 hours to com-
plete residual liquid removal.

---
*Work completed prior to configuration revision.
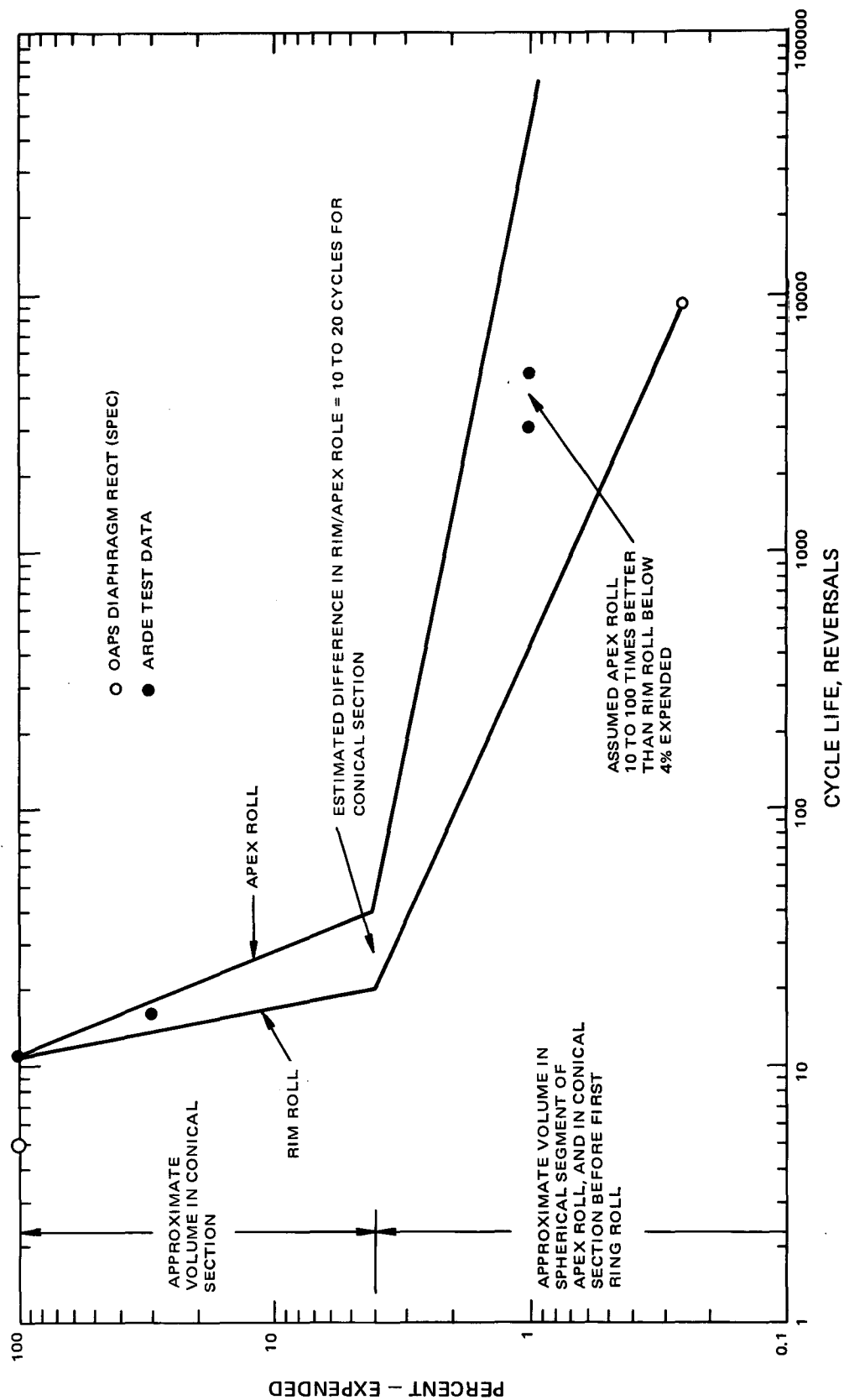
Figure IV-11. Estimated Reversals of Rim and Apex Roll Dimensions

TABLE IV-VIII. FMECA FOR KEY SINGLE POINT FAILURES

Component	Failure Mode	Corrective Action	Effect
Tank Outlet Valve	Fails Closed	Do not withdraw propellant from tank at 180° from failed tank.	Mission degraded due to loss of 1/3 (2 tanks) impulse. No loss of CM control.
	Fails Open	Use 180° opposite TOV* for CM balance; alternate engine firings between each half system.	Change in operational CM behavior. No net performance penalty
	Leakage	None	None
Rocket Engine	Valve fails closed or inactive catalyst.	Interconnect feed system and use opposite half system engine.	Possibly small impulse loss due to thruster performance degradation at end of life.
	Valve fails open or leakage	Isolate propellant from engine with tank outlet valves. Backup mode operation by using TOV for thruster flow control.	Degraded impulse predictability for failed half system. For AE-E must isolate yaw thruster from failed side.
N.O. Squib Valve (Only an AE-E)	Accidental Closing	Open NC squib & feed yaw thruster from other half system. Provide for yaw thruster propellant requirements in half system usage schedule.	None
NC Squib Valve	Accidental opening	None	Propellant from either side can be used in either thruster. No performance penalty.
Diaphragm	Rupture	Keep failed tank outlet valve closed. Do not withdraw propellant from tank at 180° from failed tank.	Change in operational CM behavior. Possible loss of up to 1/3 of propellant.
Tankage/Plumbing	Gas leakage	Use remaining half system.	Loss of up to 50% of impulse.
	Liquid leakage upstream of TOV	Do not cycle TOV, deplete propellant from 180° opposed tank.	Temporary loss of CM, control & loss of up to 1/6 of impulse. Probable contamination of S/C by propellant.
	Liquid leakage downstream TOV	Use opposite half system.	Loss of up to 50% of impulse. Possible contamination of S/C by propellant.

*Tank Outlet Valve

E.   POWER SUBSYSTEM

No major differences exist between the spacecraft power distribution configuration as defined at the outset of the study and described in Attachment A, and that resulting from the experiment accommodation studies. The overall subsystem block diagram is shown in Figure IV-12; unit load estimates are given in Table IV-IX.

The solar array layout will not be finalized until all experiment aperture requirements are defined. Provisional layout studies indicate that between 45 and 50 2 x 4 cm cell strings can be accommodated on the sides of the array within an overall spacecraft height of 45 inches. Performance estimates given in this report (Section II) are based on a 48 string layout.

The original configuration, described in the Phase B/C Study Report, provided three electrical busses; an unregulated supply, a series-regulated -24.5V supply, and a pulse width modulated (PWM) regulated +28V bus for experiment loads. Subsequent to completion of Phase B/C, the subsystem was revised to delete the +28V bus and furnish experiment power instead from the regulated -24.5V supply. The series regulator was replaced with a PWM regulator, which due to its higher efficiency, provided a better thermal environment and somewhat improved experiment duty cycle capability.

As stated above no further significant modifications at the system level have been made during the current study. Certain spacecraft regulated loads have been transferred to the unregulated supply in order to require activation of the regulated supply only to experiment data-taking and data-playback periods. While this change does not affect the net efficiency of the subsystem, it does provide a means of removing power from any experiment in the event of a power relay failed-closed condition.

Other changes of a more minor nature (mainly in the area of fault protection) are discussed below. Power subsystem performance estimates in terms of achievable experiment duty cycle are discussed in Section II.

1.   Regulated Bus Fault Protection

A change has been made in the approach to protection of the -24.5V regulated bus from an out-of-tolerance condition. In the originally proposed design, a regulated bus comparator continuously monitored the -24.5V bus and, if a voltage outside the -26.0 ± 0.5 to -23.0 ± 0.5V range was observed, the comparator acted to disconnect the on-line regulator and connect the standby regulator.

This approach has been revised for the following reasons:

- A failure in a subsystem other than the regulator (such as the regulated bus comparator) may result in an unstable mode of operation in which the comparator alternates endlessly from one regulator to the other.

- The condition described immediately above may be corrected, but at the expense of increased circuit complexity.

- There are no critical loads drawing power from the -24.5 spacecraft bus; temporary interruption of the regulator - supplied power is not objectionable from the viewpoint of mission survival.

A preferable approach now proposed is to disconnect the on-line regulator in the presence of a fault, and keep the standby regulator in reserve until it is connected on-line by ground command. The on-line regulator is switched out if an out-of-tolerance condition is detected on the bus, even if caused by the presence of current limiting. An additional ground command has been included which will take both regulators "Off Line". This is primarily a back-up command to disconnect all experiment power.

2. PWM Regulator Current Limit Modification

The current limit threshold on the PWM regulator has been increased from 9 to 16 amperes. This change was necessary because the maximum anticipated fuse size on the regulated bus has been increased to 5 amperes (reference General Interface Specification, PS-2260216). The regulator therefore must be designed to clear any fused fault occuring in the 5 amp fused line while supplying the remaining regulated load in a reasonable length of time.

3. Shunt Regulator Modification

The number of power dissipating sections in the shunt regulator has been changed from seven (7) to nine (9). This change was made as a result of a trade-off study made to minimize the power dissipation in the transistor section. This was required to maintain the junction to case temperature differential within the desired limit. The trade-off is given in detail in AE design note DN-381-6.2 titled "AE Shunt Limiter Resistance Wire Trade-Off Study".

4. Battery Charge Select

The battery charge controllers are the only means by which each battery can be safely charged in an efficient manner while isolating the batteries from the unregulated bus. If a failure occurs in a charge controller such that the battery is no longer isolated from the solar array bus, the battery will
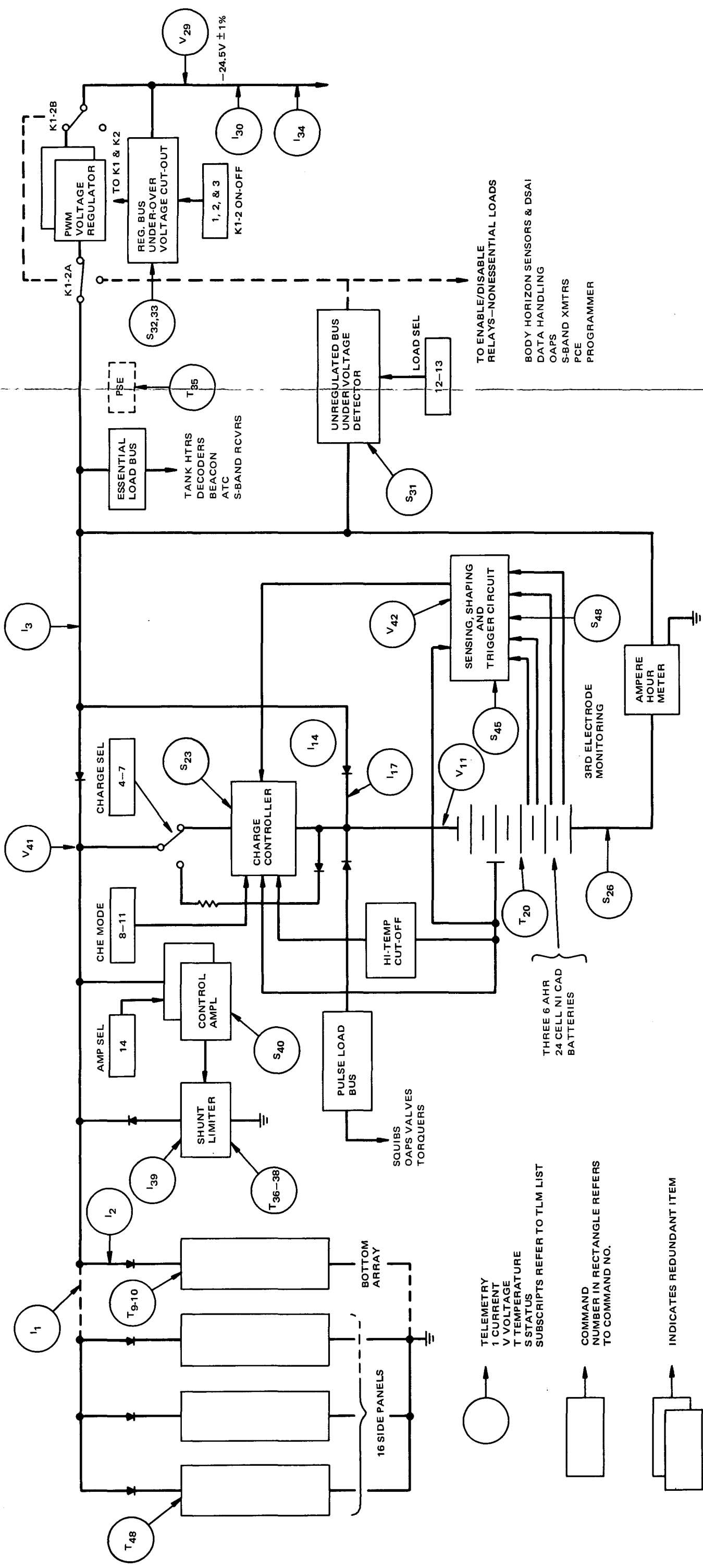
Figure IV-12. AE Power Subsystem, Block Diagram

IV-39/40

TABLE IV-IX. UNIT LOAD ESTIMATES

Subsystem/ Component	Type Load	Bus	Nominal Load (Watts)					Notes
			Fixed	Record	PB	RT	R&RR	
ATTITUDE CONTROL								
MASC								1.0 watt on 10 orbits every 4 months
QOMAC								1.4 watts, on 30 orbits per month
DSA1	NE	UNG	0.735					Based on 4 units
PCE	E	UNG	6.33					Includes horizon splitting load
Mom Wheel Assy	NE	UNG	120mA					120mA @ 34.5V Day; 28.0V Night
Solar Gate Elect	NE	UNG						Small
Body Horiz. Sen.	NE	UNG						Small
Magnetometer	NE	REG		3.1		3.1		
COMMUNICATIONS								
S-Band XMTR	NE	UNG			37.5	37.5	37.5	
Dual Beacon/Tele	E	UNG	2.0					
Dual PMP	NE	UNG			1.0	1.0	1.0	May be on during R&RR plus RT and/or PB
COMMAND & DATA HAND.								
Recorder	NE	REG		4.5	9.2	4.5		
Dual Decoder	E	UNG	8.2					Includes S-Band Rcvr's (5W Total, 2.5 W each)
Dual Programmer	E	UNG	2.3					Includes power for LIU unit
PCM Assy	NE	UNG		3.2		3.2		Includes S/C clock
Command Mem. Unit								Small
OAPS								
Electronics	NE	UNG	0.25					
Thruster Valves								2.4 amps when firing
Tank Valves								12 watts when energized
Squib	NE	Battery						5 amp pulse
ENGINEERING MEAS.								
PSA	NE	REG		1.5		1.5		
PSB	NE	REG		2.0		2.0		
EXPERIMENTS								
Reg. Bus*	NE	REG		91.45				
Unreg Bus (GFE)	NE	UNG		19.5		19.5		
SOLAR POINTING SUBSYS	NE	REG		6.0		6.0		
THERMAL CONTROL								
Tank Heaters	E	UNG						5 watts as required
Base Plate Heaters	E	UNG						25 watts as required
PSE								
Shunt Losses Day		UNG	305.5mA					
Night		UNG	223.3mA					
Temperature Controllers			2.93					
TOTALS								
Unregulated:								
Essential			18.83					
Nonessential			120 Ma					
Current								
Power			0.985	22.7	38.5	61.2	38.5	
Total								
Current			120mA					
Power			19.82					
PSE Shunt Losses								
Day			305.5mA					
Night			223.3mA					
REGULATED				108.55	9.2+.6	108.55		Minimum load on Reg Bus is 9.8W
Efficiency				0.90	0.64	0.90		
Total				120.61	15.28	120.61		

*Excluding Magnetometer, which is shown under Attitude Control for the purposes of this report.

become an unrestricted load on the solar array bus and be subject to damage from hydrogen gas evolution. Normal charge current will be diverted from the remaining batteries in the event of an electrical short to the solar array bus during orbit daytime operation and the battery will try to power the control amplifiers during orbit nighttime operation in addition to contributing to the nighttime load. If a failure occurs such that the battery cannot be charged, the battery will eventually discharge sufficiently and no longer contribute to the spacecraft electrical load.

In order to protect against either type of charge controller failure without re-moving the battery from the power subsystem, a commandable by-pass resistor has been connected in parallel with each charge controller. When the resistor is commanded, the battery will be charged at a C/10 maximum charge rate. A diode in series with the by-pass resistor isolates the unregulated bus from the battery during discharge periods. The three battery disconnect commands have been removed.

5.   Ampere Hour Meter

An ampere hour meter which performs the integration of battery current has been incorporated in the system to provide an accurate indication of the "state of charge" of the battery. Battery recharge ampere-hours effectively cancel discharge ampere-hours. Correction of battery efficiency as a function of battery temperature is also provided. The system capacity relative to 100% depth of discharge is 18 ampere hours, however the inherent surplus capacity of the up-down counters used provides registration to over 600% before over-flow occurs. The system operates over a current range of 100 mA to 10 amperes with the charge/discharge ratio adjustable from 1.04 to 1.50. Two telemetry signals are developed by the system. One channel indicates the state of charge in percent with 100% equivalent to 18 ampere hours. The second channel indi-cates peak depth of discharge in percent with 100% equivalent to 18 ampere hours.

A more detailed discussion of the ampere hour meter is contained in Appendix IV.E.

F. COMMUNICATIONS

The major changes in the spacecraft communications and ranging subsystem from that defined at the outset of the study and described in attachment A, have evolved as a result of the integration by NASA of the MSFN and STADAN networks.

These changes place emphasis on the S-band facilities of the combined network and include:

- Expansion of the spacecraft S-band communications capability to provide simultaneous command, ranging, real time telemetry and playback telemetry functions.

- Deletion of VHF command capability.

In the following paragraphs these modifications, together with related changes in overall subsystem performance, are described. At the time of preparation of this report a potential change to a single whip VHF antenna is still under consideration. Also a transponder subcontractor has not yet been selected; thus, certain design and performance parameters for the components remain to be finalized.

1. Subsystem Configuration

a. VHF COMMUNICATIONS SUBSYSTEM

Figure IV-13 shows the VHF communications subsystem as previously configured prior to network integration. Deletion of the VHF command capability results in the considerably simplified revised system configuration shown in Figure IV-14.

The revised system consists of two dual mode VHF beacon/telemetry transmitters, an rf switch assembly, a VHF antenna coupling network and a crossed dipole antenna system. Beacon capability has been retained for S-band antenna acquisition and back up; VHF capability for real time telemetry into VHF facilities.

The dual mode beacon/telemetry transmitters are similar in configuration to those previously described, except for the following interface differences:

- A dc/dc converter-regulator has been included as part of each transmitter. This modification is required in order to provide continuous beacon transmission independent of the power status of the spacecraft regulated (-24.5V) bus.

- Dual, resistively isolated, modulation inputs have been incorporated to facilitate cross strapping of the signals from the dual PCM assemblies.
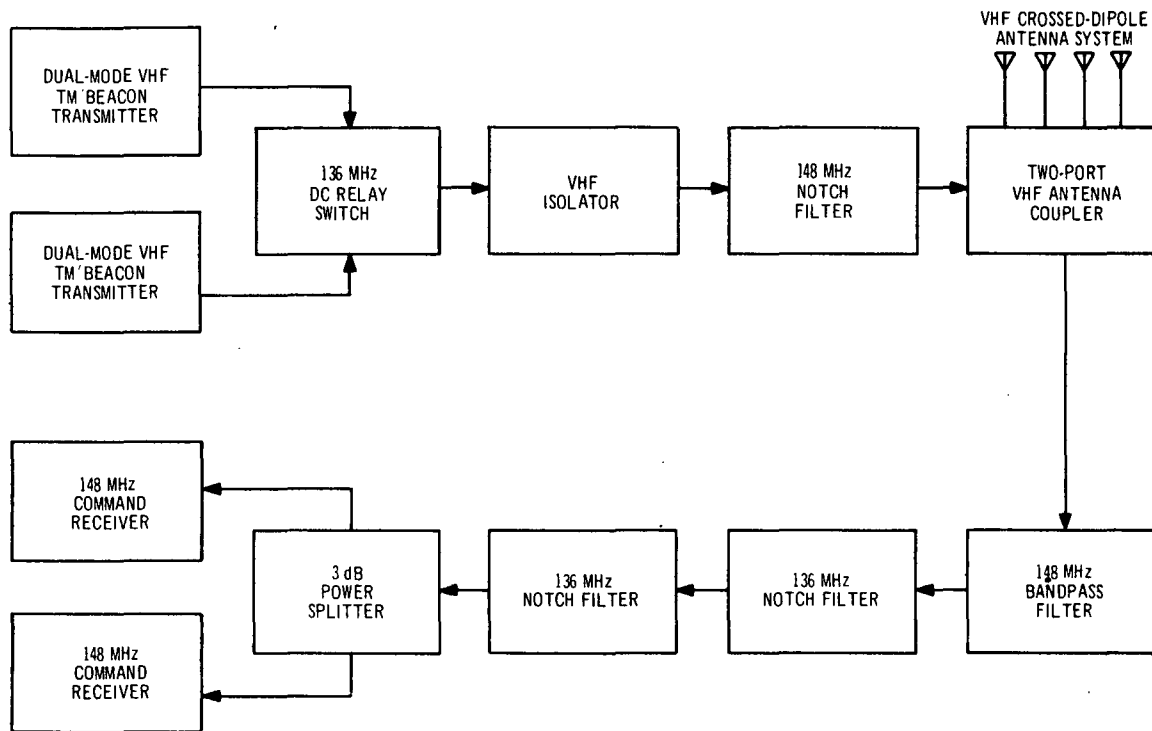
Figure IV-13. Original VHF Communications Subsystem
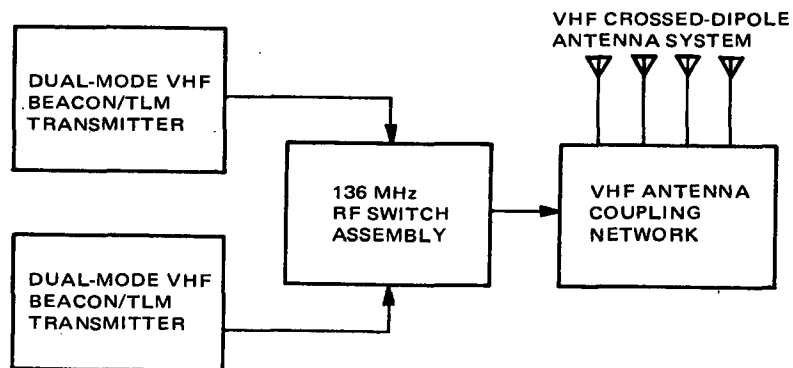
Figure IV-14. Revised VHF Communications Subsystem

- A latching relay memory has been added to the mode control circuitry for standardization with the major mode command interfaces called for in the General Interface Specification.

The VHF antenna coupling network is simplified by the elimination of the receiver output port. The only function of the antenna coupling network in the revised system is to split the rf signal to the four antenna elements in the phase relationship required to achieve the desired antenna radiation pattern.

The rf switch assembly and VHF crossed dipole antenna system are unchanged from the previously described system configuration.

The separate VHF isolator, 148-MHz notch filter, 148-MHz bandpass filter, 136-MHz notch filters, 3 dB power splitter and command receivers are all deleted in the revised system configuration.

b.   S-BAND COMMUNICATIONS AND RANGING SUBSYSTEM

Figure IV-15 shows the S-band ranging subsystem as originally configured for operation with the GRARR system. The revised system configuration is shown in Figure IV-16.

The revised system consists of two S-band transponders, an S-band coupling assembly, a dual pre-modulation processor and an S-band belt antenna system.

The S-band transponders are new in concept compared to those previously described. The major differences are as follows:

- The receivers in the redundant transponders will both be continuously powered throughout the mission. This is required to provide continuous, redundant command capability throughout the spacecraft lifetime. A separate dc/dc converter in each transponder receiver has been added to provide the required power directly from the spacecraft unregulated power bus.

- Provision of cross-strapping facilities is being examined to permit use of the transmitter section of either transponder with either receiver section, providing full redundancy. A decision on whether to implement this feature will await detail reliability data from the potential transponder subcontractor.

- Separate dc/dc converters in each transponder transmitter have been added to alleviate the peak power requirements on the spacecraft regulated bus, to increase overall efficiency, and to make it possible to perform ranging and telemetry transmission independent of the power status of the spacecraft regulated (-24.5V) bus.
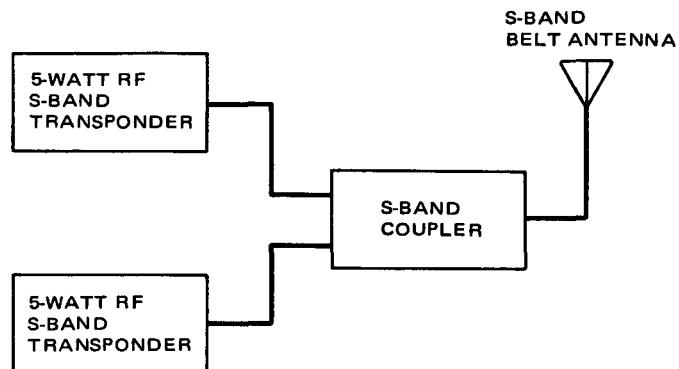
Figure IV-15. Original S-Band Ranging Subsystem
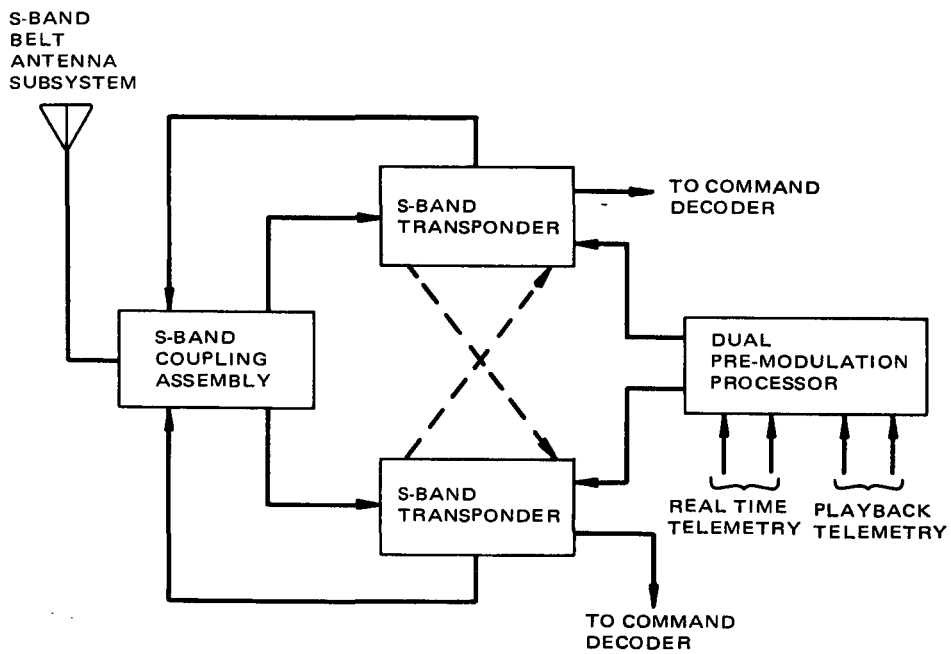
Figure IV-16. Revised S-Band Communications and Ranging Subsystem

- The receive and transmit frequencies and ranging modulation transfer function have been changed to be compatible with the combined Stadan*/MSFN** (Apollo) ground network.

- Uplink and Downlink modulation spectra have been changed to perform the simultaneous functions of command, ranging, real time telemetry and playback telemetry.

A detailed description and specification summary of the revised S-band transponder is included in Section IV-F-3 of this report.

The S-band coupling assembly is a modification of the coupling system previously described. The major differences are as follows:

- Only one diplexer is used and the commom port is directly connected to the antenna, with no switches intervening.

- The receiver part of the diplexer is connected to both receivers through a passive 3 dB hybrid coupler, thus providing a continuous signal input to both receivers at all times.

- The transmitter part of the diplexer is connected to either transmitter by means of a switchable circulator, similar to the one in the previously described coupling system

A detailed description and specification summary of the revised S-band coupling assembly is included in Section IV-F-3 of this report.

The dual pre-modulation processor is a new device not previously included in the system. Its function is to generate two subcarriers, one phase modulated with real time telemetry and the other phase modulated with playback telemetry. These subcarriers are supplied to the modulation input of the active S-band transponder, where they are added to the turnaround ranging signals for transmission to Earth as modulation on the S-band downlink carrier.

A detailed description and specification summary of the dual pre-modulation processor is also included in Section IV-F-3 of this report.

The S-band belt antenna system is unchanged in concept from that previously described in the Phase B/C Study Report.

---

*Tone Ranging
**Pseudo random noise ranging.

2. System Performance

a. VHF BEACON/TELEMETRY DOWNLINK

At any given time, the spacecraft will transmit either (1) an unmodulated 0.25 watt beacon, or (2) a modulated 1.0 watt telemetry signal, of which the carrier component can be tracked as a beacon.

Performance characteristics of the beacon-telemetry downlink are essentially unchanged from those defined at the outset of the study except that spacecraft circuit losses have been reduced from 3.0 dB to 1.6 dB by elimination of the external VHF isolator and 148 MHz notch filter from the rf transmission path. These components are no longer required due to the deletion of the VHF command capability. The elimination of these components results in a 1.4 dB improvement in link margin.

Other changes in the link analysis entries (see Table IV-X) reflect the inclusion of worst case spacecraft parameter tolerances in the individual entries rather than leaving these items lumped together as part of the link margin. In this manner the effects of individual equipment tolerances become more evident and can be reviewed for their effect on the system.

One item presently undergoing further study is the possible change of the VHF antenna configuration from a set of 4 quadrature fed dipoles to a single quarter-wave or shorter monopole antenna. This change is desired to reduce the cross section of the VHF antenna to achieve better accuracy in the Cylindrical Electrostatic Probe (CEP) experiment.

(1) BEACON TRACKING DURING BEACON MODE OF OPERATION

During the beacon mode of operation, the spacecraft may be tracked by the STADAN Minitrack System. Table IV-X summarizes the link calculations pertaining to the 0.25 watt unmodulated beacon mode.

Note that in these calculations a polarization loss of -3 dB is indicated. In reality the Minitrack antenna fields are linearly polarized so that, in theory, much greater polarization losses are possible. The measured spacecraft antenna patterns, however, indicate that over the majority of look angles, there is substantial radiated power in both orthogonal linear polarizations as transmitted, so a value of -3 dB, corresponding to 45° angle of axis between linearly polarized antennas is a reasonable value to use. Systems utilizing quadrature fed antennas such as the one considered here have been successfully flown (TIROS, ESSA spacecraft). Systems utilizing a linear monopole antenna, such as new undergoing further study, have been successfully flown (ITOS, NOAA spacecraft). The substantial margins in these links assure compatible performance with the Minitrack System of either type of antenna system.

TABLE IV-X. VHF BEACON/TELEMETRY LINK: BEACON MODE

Parameter	Value	Remarks
Transmitter Power	23.98 dBm	0.25 watt spec. value (SK-PS-2270711)
Transmitting Circuit Loss	- 1.60 dB	RF switch, cable and reflection losses
Transmitting Antenna Gain	- 6.80 dB	Spec. value (PS-SK-2260204)
Transmitting Pointing Loss	0.00 dB	Included in gain figure
Path Loss	-152.85 dB	Altitude = 4000 km
		Range = 7646 km
		Frequency = 137.00 MHz
		Elevation = 5 degrees
Polarization Loss	- 3.00 dB	See text
Rx Noise Spectral Density	-166.32 dBm/Hz	System Temp = 1690 deg. K
		Receiver F = 3 dB (NASA X-530-66-33)
		T_{sky} = 1400°K (NRL Report 5668)
"FINE" SYSTEM		
Receiving Circuit Loss	0.00 dB	NASA X-530-66-33
Receiving Antenna Gain	16.30 dB	NASA X-525-64-222
Receiving Pointing Loss	0.00 dB	Included in gain figure
Net Circuit Loss	-147.95 dB	
Total Receiver Power	-123.97 dBm	
Carrier Modulation Loss	0.00 dB	Unmodulated
Received Carrier Power	-123.97 dBm	
Carrier APC Noise Bandwidth	10.00 dB-Hz	2 BLD = 10 Hz (NASA X-530-66-33)
Noise Power in APC Loop	-156.32 dBm	
APC Loop CNR	32.35 dB	
Threshold CNR	6.00 dB	Gardner, "Phaselock Techniques"
Performance Margin	26.35 dB	
"AMBIGUITY" SYSTEM		
Receiving Circuit Loss	0.00 dB	NASA X-530-66-33
Receiving Antenna Gain	6.40 dB	NASA X-525-64-222
Receiving Pointing Loss	0.00 dB	Included in gain figure
Net Circuit Loss	-154.85 dB	
Total Received Power	-130.87 dBm	
Carrier Modulation Loss	0.00 dB	Unmodulated
Received Carrier Power	-133.87 dBm	
Carrier APC Noise Bandwidth	3.01 dB-Hz	BLD = 2 Hz (NASA X-530-66-33)
Noise Power in APC Loop	-163.31 dBm	
APC Loop CNR	29.44 dB	
Threshold CNR	6.00 dB	Gardner, "Phaselock Techniques"
Performance Margin	23.44 dB	

(2) BEACON TRACKING DIVING TELEMETRY MODE OF OPERATION

During the Telemetry mode of operation, the carrier component of the transmitted signal may be tracked by the Minitrack System. The tracking system is not affected by the PCM split phase modulation since the latter does not have frequency components near the carrier frequency. Table IV-XI summarizes the link calculations pertaining to Minitrack operation with the spacecraft transmitter in the telemetry mode.

Note that worst case spacecraft tolerances have been included in calculation of the modulation losses.

The same comments regarding polarization losses previously discussed in the unmodulated beacon case also apply to this case. The link margins, although reduced from the unmodulated case, are still ample.

(3) VHF TELEMETRY

During the telemetry mode of operation, VHF telemetry is transmitted at a 1 watt level from the beacon/telemetry transmitter, which is phase modulated ±1.25 radians nominal with the 16,384 bit/second bi-phase real time telemetry data stream. Table IV-XII summarizes the link calculations pertaining to STADAN ground stations equipped with the Satellite Automatic Tracking Antenna (SATAN). Operationally, the SATAN ground antennas and associated receivers make up a polarization diversity system.

Note that worst case spacecraft equipment tolerances have been included in calculation of the modulation losses.

Aside from the possible change of VHF antenna configuration previously noted at the beginning of this section, one item presently undergoing further study is in the area of the pre-modulation filtering requirements. With only one bit rate (16,384 b/s) to consider it may be possible to ease the pre-modulation filtering requirements and thereby reduce the filter energy loss and inter-symbol interference loss quantities.

b. S-BAND UPLINK

All commands from Earth to the spacecraft are transmitted via a phase modulated S-band rf carrier. This carrier is also capable of being modulated by ranging signals which are coherently translated in frequency and retransmitted by the spacecraft. The functions of command and turn-around ranging (as well as downlink telemetry), may be accomplished simultaneously at either a Manned Space Flight Network (MSFN) unified S-band ground station or a

TABLE IV-XI. VHF BEACON/TELEMETRY LINK: BEACON TRACKING DURING TELEMETRY MODE

Parameter	Value	Remarks
Total Transmitter Power	30.00 dBm	1 watt spec. value (SK-PS-2270711)
Transmitting Circuit Loss	- 1.60 dB	RF switch, cable and reflection losses
Transmitting Antenna Gain	- 6.80 dB	Spec. value (PS-SK-2260204)
Transmitting Pointing Loss	0.00 dB	Included in gain figure
Path Loss	-152.85 dB	Altitude = 4000 km
		Range = 7646 km
		Frequency = 137.00 MHz
		Elevation = 5 degrees
Polarization Loss	- 3.00 dB	See text
Rx Noise Spectral Density	-166.32 dBm/Hz	System Temp = 1690 deg. K
		Receiver NF = 3 dB (NASA X-530-66-33)
		T_{sky} = 1400°K (NRL Report 5668)
"FINE" SYSTEM		
Receiving Circuit Loss	0.00 dB	NASA X-530-66-33
Receiving Antenna Gain	16.30 dB	NASA X-525-64-222
Receiving Pointing Loss	0.00 dB	Included in gain figure
Net Circuit Loss	-147.95 dB	
Total Received Power	-117.95 dBm	
Carrier Modulation Loss	- 14.20 dB	Square wave modulation ±1.375 rad
Received Carrier Power	-132.15 dBm	
Carrier APC Noise Bandwidth	10.00 dB-Hz	2 BLD = 10 Hz (NASA X-530-66-33)
Noise Power in APC Loop	-156.32 dBm	
APC Loop CNR	24.17 dB	
Threshold CNR	6.00 dB	Gardner, "Phaselock Techniques"
Performance Margin	18.17 dB	
"AMBIGUITY" SYSTEM		
Receiving Circuit Loss	0.00 dB	NASA X-530-66-33
Receiving Antenna Gain	6.40 dB	NASA X-525-64-222
Receiving Pointing Loss	0.00 dB	Included in gain figure
Net Circuit Loss	-157.85 dB	
Total Received Power	-127.85 dBm	
Carrier Modulation Loss	- 14.20 dB	Square wave modulation ±1.375 rad
Received Carrier Power	-142.05 dBm	
Carrier APC Noise Bandwidth	3.01 dB-Hz	2 BLD = 2 Hz (NASA X-530-66-33)
Noise Power in APC Loop	-163.31 dBm	
APC Loop CNR	21.26 dB	
Threshold CNR	6.00 dB	Gardner, "Phaselock Techniques"
Performance Margin	15.26 dB	

TABLE IV-XII. VHF BEACON/TELEMETRY LINK: TELEMETRY MODE

Parameter	Value	Remarks
Total Transmitter Power	30.00 dBm	1 watt spec. value (SK-PS-2270711)
Transmitting Circuit Loss	− 1.60 dB	RF switch, cable and reflection losses
Transmitting Antenna Gain	− 6.80 dB	Spec. value (PS-SK-2260204)
Transmitting Pointing Loss	0.00 dB	Included in gain figure
Path Loss	−152.85 dB	Altitude = 4000 km
		Range = 7646 km
		Frequency = 137.00 MHz
		Elevation = 5 degrees
Polarization Loss	− 1.00 dB	Polarization diversity
Receiving Circuit Loss	0.00 dB	NASA X-530-66-33
Receiving Antenna Gain	22.24 dB	Satan antenna (NASA X-525-64-222)
Receiving Pointing Loss	0.00 dB	Included in gain figure
Net Circuit Loss	−140.01 dB	
Total Received Power	−110.01 dBm	
Rx Noise Spectral Density	−165.95 dBm/Hz	System temp = 1840 deg. K
		Receiver NF = 4 dB (NASA X-530-66-33)
		T_{sky} = 1400 (NRL Report 5668)
CARRIER CHANNEL		
Carrier Modulation Loss	− 14.20 dB	Square wave modulation ±1.375 rad
Received Carrier Power	−122.21 dBm	
Carrier APC Noise Bandwidth	24.77 dB-Hz	2 BLD = 300 Hz (NASA X-530-66-33)
Noise Power in APC Loop	−141.18 dBm	
APC Loop CNR	16.97 dB	
Threshold CNR	6.00 dB	Gardner, "Phase Lock Techniques"
Performance Margin	10.97 dB	
DATA CHANNEL		
Data Modulation Loss	− .90 dB	Square wave modulation ±1.125 rad
Received Data Power	−108.91 dBm	
Intersymbol Interference Loss	− 1.00 dB	RCA AED P-5270-A (See text)
Premodulation Filter Energy Loss	− 2.00 dB	RCA AED P-5270-A (See text)
Worst Case Data Power	−111.91 dBm	
Bit Rate Reference Bandwidth	42.14 dB-Hz	BW = 16,384 Hz
Noise Power in Data BW.	−123.81 dBm	
Worst Case S/N in Data BW.	9.90 dB	
Required S/N in Data BW.	10.30 dB	PSK; BER = 1×10^{-5}
Worst Case Data Margin	0.40 dB	

Satellite Tracking and Data Acquisition Network (STADAN) ground station with modified rf frequencies and subcarrier modulators.

Depending on the type of ground station used, the uplink baseband modulation spectrum will appear as in Figure IV-17 (a) or (b). Table IV-XIII indicates the 5 major uplink modulation modes, together with the primary signal characteristics and possible deviation range limits.

(1) MSFN UNIFIED S-BAND OPERATION

Table IV-XIV summarizes the link calculations pertaining to the S-band uplink when operating from a MSFN Unified S-band ground station (Modes 1, 2 or 4 of Table IV-XIII). The value of spacecraft antenna gain shown in the table does not include additional pattern degradation due to spacecraft holes or protrusions from experiment sensors.

The carrier and command subcarrier modulation losses shown are those existing under the worst case combination of modulation indices. With nominal modulation indices the carrier margin would increase an additional 9.9 dB and the command margin would increase an additional 7.5 dB.

The modulation loss shown for the ranging channel is that resulting with simultaneous command and ranging with nominal modulation indices. The performance margin as shown is insufficient. With the worst case combination of modulation indices, the margin would degrade an additional 7.9 dB. If, on the other hand a modulation index equal to the upper limit is used, the margin would improve 4.6 dB during simultaneous ranging and command operation and 5.0 dB during ranging – only operation (Mode 2 of Table IV-XIII).

Thus, if it is desired to obtain the required PRN uplink performance at maximum start range with the 30 ft USR stations, then either (a) perform PRN ranging only with a modulation index of 0.8 radians or higher or (b) increase the ground station transmitter power above 2 KW.

According to the MSFN Network User's Guide (MSFN No. 101.1), the USB ground station transmitters are capable of 20 KW output for single carrier operation, such as in AE. This would provide 10 dB additional margin above those shown in Table IV-XIV.

(2) STADAN (GRARR) S-BAND OPERATION

Table IV-XV summarizes the link calculations pertaining to the S-band uplink when operating from a SATAN (GRARR) station (Modes 1, 3 or 5 of Table IV-XV). The spacecraft parameters utilized are the same as for MSFN Unified S-Band Operation. The ground station parameters used represent

COMMAND FM SUBCARRIER
(θ = 0.4—1.4 rad, 0.8 rad nominal)

PRN RANGING CODE, 992 KB/S
(θ = 0.5—0.8 rad, 0.5 rad nominal)

70   1008   1513

f (kHz)
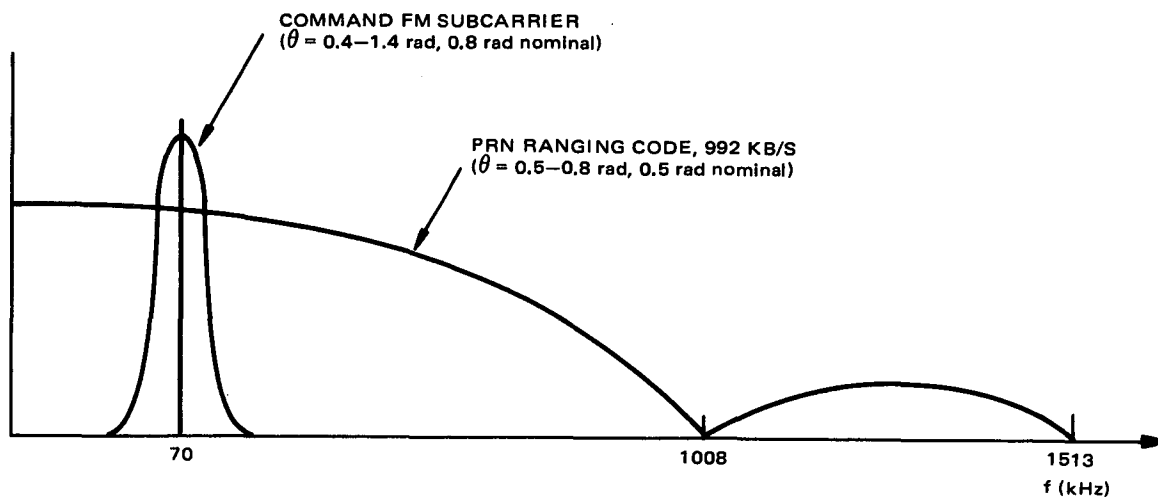
(a) MSFN (APOLLO) UNIFIED S-BAND STATION

GRARR RANGING (MINOR TONE)
(θ = 0.2—0.7 rad)

COMMAND FOR SUBCARRIER
(θ = 0.4—1.4 rad, 0.8 rad nominal)

GRARR RANGING (MAJOR TONE)
(θ = 0.5—1.06 rad, 0.5 rad nominal)

4.0—4.8 OR 20   70   100   f (kHz)
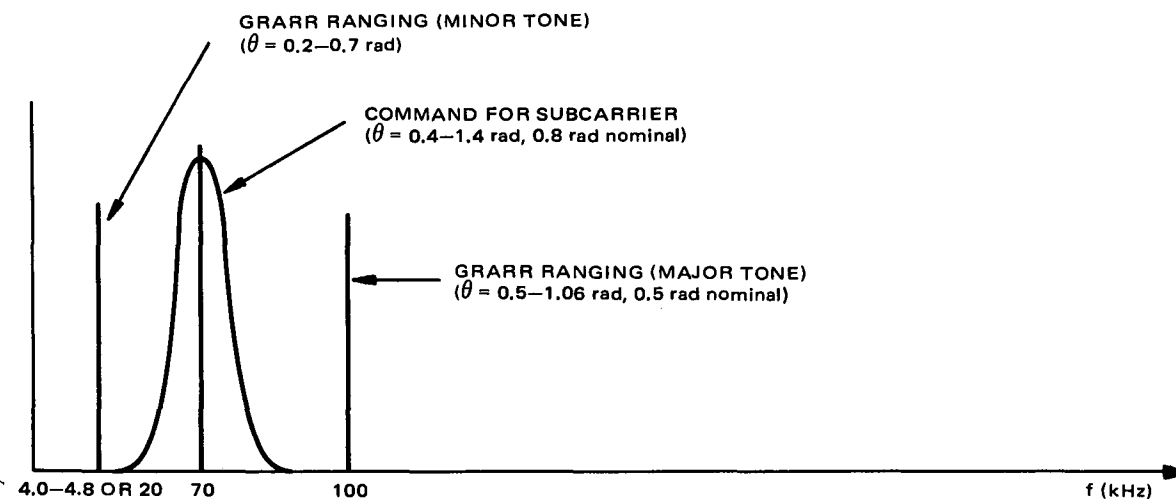
(b) STADAN (GRARR) S-BAND STATION

NOTE: θ = PEAK CARRIER MODULATION INDEX.

Figure IV-17. S-Band Uplink Modulation Spectra

TABLE IV-XIII. EARTH TO SPACECRAFT (UPLINK) MODULATION MODES

Uplink Mode	Information Channel	Modulation Technique	Peak Carrier Deviation (radians)	Subcarrier Frequency	Subcarrier Deviation (peak)
1	Command	FM/PM	0.4 to 1.8	70 kHz	5.0 kHz ±10%
2	PRN Ranging	PM on Carrier	0.5 to 0.8	—	—
3	GRARR Ranging	CW/PM	0.5 to 1.06	100 kHz	—
	GRARR Minor Tone (1)	CW/PM	0.2 to 0.7	4.0–4.8 kHz or 20 kHz	—
4	Command	FM/PM	0.4 to 1.6 (2)	70 kHz	5.0 kHz ±10%
	PRN Ranging	PM on Carrier	0.5 to 0.8	—	—
5	Command	FM/PM	0.4 to 1.55 (2)	70 kHz	5.0 kHz ±10%
	GRARR Ranging	CW/PM	0.5 to 1.06	100 kHz	—
	GRARR Minor Tone (1)	CW/PM	0.2 to 0.7	4.0–4.8 kHz or 20 kHz	—

NOTES: (1) Present only during ranging acquisition.

(2) Upper limit shown for the command signal carrier deviation is the maximum allowed value to retain 10% power in the carrier when the ranging signals are at the maximum deviation indices. To retain 10% power in the carrier, the assignment of carrier deviation among the various information channels will be constrained by expressions:

$$J_o^2 (\theta_1) \, \cos^2 (\theta_2) \geq 0.1 \text{ for mode \#4}$$

and

$$J_o^2 (\theta_1) \, J_o^2 (\theta_3) \, J_o^2 (\theta_4) \geq 0.1 \text{ for mode \#5}$$

where
θ_1 = peak carrier deviation of command S/C
θ_2 = peak carrier deviation of PRN Ranging S/C
θ_3 = peak carrier deviation of GRARR Ranging S/C
θ_4 = peak carrier deviation of GRARR Minor Tone

$J_o(\theta)$ = Zero Order Bessel Function of the First Kind.

TABLE IV-XIV. S-BAND UPLINK: MSFN (USB) GROUND STATION

Parameter	Value	Remarks
Total Transmitter Power	63.01 dBm	2 KW (see text)
Transmitting Circuit Loss	0.00 dB	Included in gain figure
Transmitting Antenna Gain	43.00 dB	30 ft USB antenna (MSFN 101.1)
Transmitting Pointing Loss	0.00 dB	Included in gain figure
Path Loss	-176.60 dB	Altitude = 4000 km
		Range = 7646 km
		Frequency = 2108.25 MHz
		Elevation = 5 degrees
Polarization Loss	- 3.00 dB	Circular to linear
Receiving Circuit Loss	- 5.00 dB	SCA, cable and reflection losses
Receiving Antenna Gain	- 11.00 dB	Spec. value (PS-SK-2260206) (see text)
Receiving Pointing Loss	0.00 dB	Included in gain figure
Net Circuit Loss	-152.60 dB	
Total Received Power	- 89.59 dBm	
Rx Noise Spectral Density	-167.38 dBm/Hz	System temp = 1326 deg. K
RCVD Power/Noise Spec. Den.	77.79 dB-Hz	
CARRIER TRACKING		
Carrier Modulation Loss	- 12.50 dB	Worst case (see text)
Received Carrier Power	-102.09 dBm	
Carrier APC Noise Bandwidth	29.03 dB-Hz	2 BLD = 800 Hz (PS-2265304)
Noise Power in APC Loop	-138.34 dBm	
APC Loop CNR	36.26 dB	
Threshold CNR	29.00 dB	Required for 90% probability of acquisition with 35 kHz/sec sweep rate.
Performance Margin	7.26 dB	Worst case (see text)
COMMAND CHANNEL		
Modulation Loss	- 14.30 dB	Worst case (see text)
Received Subcarrier Power	-103.89 dBm	
Subcarrier Noise Bandwidth	43.01 dB-Hz	BW = 20 kHz (PS-2260581)
Subcarrier Noise Power	-124.37 dBm	
Subcarrier SNR	20.48 dB	Not including interference from PRN
S/C Threshold SNR	12.00 dB	
Subcarrier Margin	8.48 dB	
Baseband SNR	27.88 dB	S/C Freq = 70 kHz, S/C Dev = 4.5 kHz Baseband BW = 4.8 kHz
Required Baseband SNR	14.00 dB	(PS-2260581)
Performance Margin	13.88 dB	Worst case (see text)
RANGING CHANNEL (PRN)		
Modulation Loss	- 7.90 dB	Nominal (see text)
Power in Data Channel	- 97.49 dBm	
Noise Bandwidth of Data Channel	61.76 dB/Hz	BW = 1.5 MHz (PS-2265304)
Noise Power in Data Channel	-105.61 dBm	
Data Channel SNR	8.13 dB	
Required SNR	13.24 dB	75 dB-Hz S/QN, BW = 1.5 MHz (71-AE-0038)
Performance Margin	- 5.11 dB	See text

TABLE IV-XV. S-BAND UPLINK: STADAN (GRARR) GROUND STATION

Parameter	Value	Remarks
Total Transmitter Power	63.01 dBm	2 kW (See text)
Transmitting Circuit Loss	0.00 dB	Included in gain figure
Transmitting Antenna Gain	43.00 dB	30 ft antenna
Transmitting Pointing Loss	0.00 dB	Included in gain figure
Path Loss	-176.60 dB	Altitude = 4000 kM
		Range = 7646 kM
		Frequency = 2108.25 MHz
		Elevation = 5 degrees
Polarization Loss	- 3.00 dB	Circular to linear
Receiving Circuit Loss	- 5.00 dB	SCA, cable and reflection losses
Receiving Antenna Gain	- 11.00 dB	Spec value (PS-SK-2260206) See text
Receiving Pointing Loss	0.00 dB	Included in gain figure
Net Circuit Loss	-152.60 dB	
Total Received Power	- 89.59 dBm	
RX Noise Spectral Density	-167.38 dBm/Hz	System Temp = 1326 Deg. K
RCVD Power/Noise Spec. Den.	77.79 dB-Hz	
CARRIER TRACKING		
Carrier Modulation Loss	- 13.30 dB	Worst case (See text)
Received Carrier Power	-102.89 dBm	
Carrier APC Noise Bandwidth	29.03 dB-Hz	2 BLD = 800 Hz (PS-2265304)
Noise Power in APC Loop	-138.34 dBm	
APC Loop CNR	35.46 dB	
Threshold CNR	29.00 dB	Required for 90% probability
		of acquisition at 35 kHz/sec sweep rate.
Performance Margin	6.46 dB	Worst case
COMMAND CHANNEL		
Modulation Loss	- 15.10 dB	Worst case (See text)
Received Subcarrier Power	-104.69 dBm	
Subcarrier Noise Bandwidth	43.01 dB-Hz	BW = 20 kHz (PS-2260581)
Subcarrier Noise Power	-124.37 dBm	
Subcarrier SNR	19.68 dB	
S/C Threshold SNR	12.00 dB	
Subcarrier Margin	7.68 dB	
Baseband SNR	27.08 dB	S/C Frequency = 70 kHz
		S/C Dev = 4.5 kHz
		Baseband BW = 4.8 kHz
Required Baseband SNR	14.00 dB	(PS-2260581)
Performance Margin	13.08 dB	Worst Case
GRARR RANGING (MAJOR TONE)		
Modulation Loss	- 19.90 dB	Worst case (See text)
Received Ranging Power	-109.49 dBm	
Received Power/Noise Spec. Den.	57.89 dB-Hz	
Required Uplink Power/Spec.	40.00 dB-Hz	Equal Uplink and Downlink
		Degradations, No IF limiter
		(See text)
Performance Margin	17.89 dB	
GRARR RANGING (MINOR TONE)		
Modulation Loss	- 29.20 dB	Worst case (See text)
Received Ranging Power	-118.79 dBm	
Received Power/Noise Spec. Den.	48.59 dB-Hz	
Required Uplink Power/Spec. Den.	40.00 dB-Hz	Equal Uplink and Downlink
		Degradations, No IF limiter
		(See text)
Performance Margin	8.59 dB	

a 2 kW transmitter and a 30-foot antenna. If a 14-foot antenna and 10 kW power are used all uplink margins should be increased by 1.0 dB.

The modulation losses shown correspond to the worst case combination of modulation indices (separately calculated for each signal) for the command subcarrier, GRARR Major tone and GRARR minor tone, all occuring simultaneously. If the only signals present are the command tone and the GRARR major tone, both at their nominal indices, the carrier tracking margin would increase by 11.3 dB, the command margin by 8.9 dB and the GRARR major tone margin by 9.1 dB.

The requirements for received signal power of the ranging signals have assumed equal weight for both uplink and downlink degradations (for an overall goal of -37 dB-Hz in accordance with document 71-AE-0038). Also assumed are that the transponder will be of the coherent AGC type, without an IF limiter, as per PS-2265304. If an IF limiter is used in the transponder the effective signal-to-noise ratio after the limiter will be reduced by 1.0 dB and, in addition, the downlink modulation index will change in accordance with the presence or absence of the ranging minor tone and/or command subcarrier. *

c.   S-BAND DOWNLINK

The S-Band downlink is capable of simultaneous transmission of real time telemetry, playback telemetry and turnaround ranging to either Manned Space Flight Network (MSFN) ground stations or modified Satellite Tracking and Data Acquisition (STADAN) stations.

The composite downlink will appear either as Figure IV-18 (a) or (b) depending on the type of ranging signal modulated on the uplink carrier. There is provision on the spacecraft to disable the turn-around ranging function, on command, to reduce spurious noise on the downlink carrier when ranging is not desired.

Table IV-XVI indicates the five major downlink modulation modes, together with the primary signal characteristics.

Real time telemetry from the spacecraft dual PCM assembly consisting of a 16,384 bit/second bi-phase data stream, PSK modulates a 1024 kHz sinusoidal subcarrier. This subcarrier, in turn, phase modulates the carrier with a modulation index of ±0.70 radians peak. The frequency of 1024 kHz for the subcarrier has been selected because of the availability of ground station demodulators and because the frequency is near the energy minimum of the PRN ranging spectrum. This frequency was previously used in the Apollo program.

---

*Assuming a 3 MHz IF noise bandwidth the S/N for the GRARR major tone at the input to the limiter will be -6.9 dB, under the above worst case conditions.
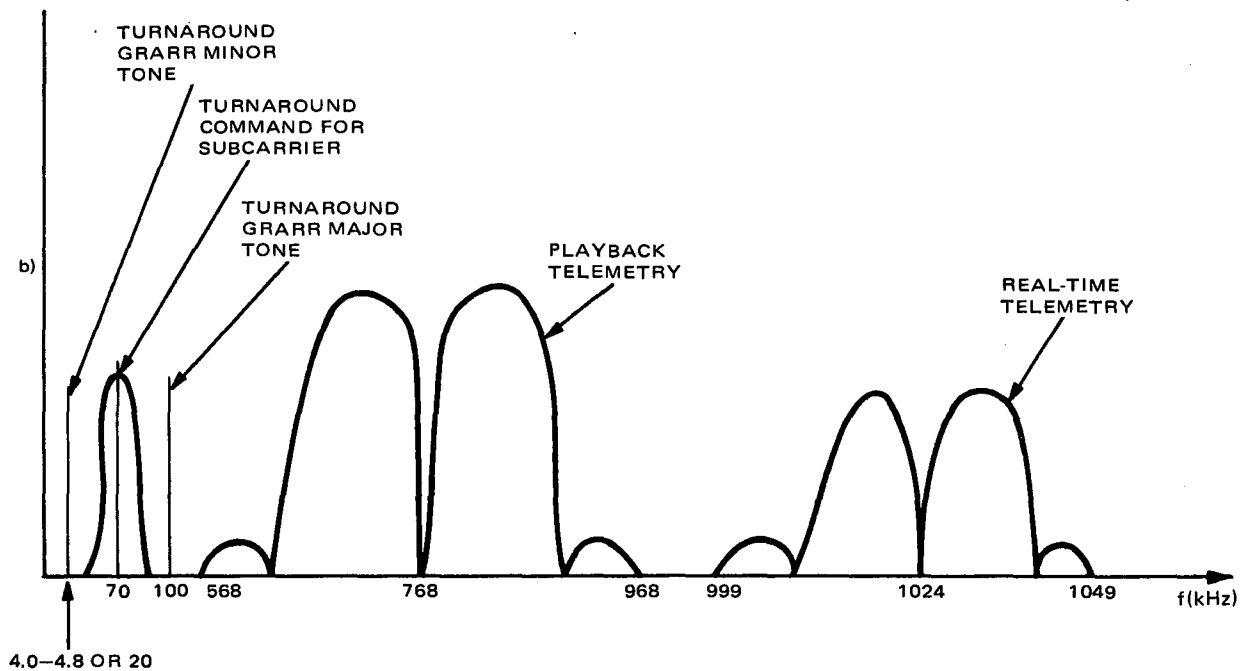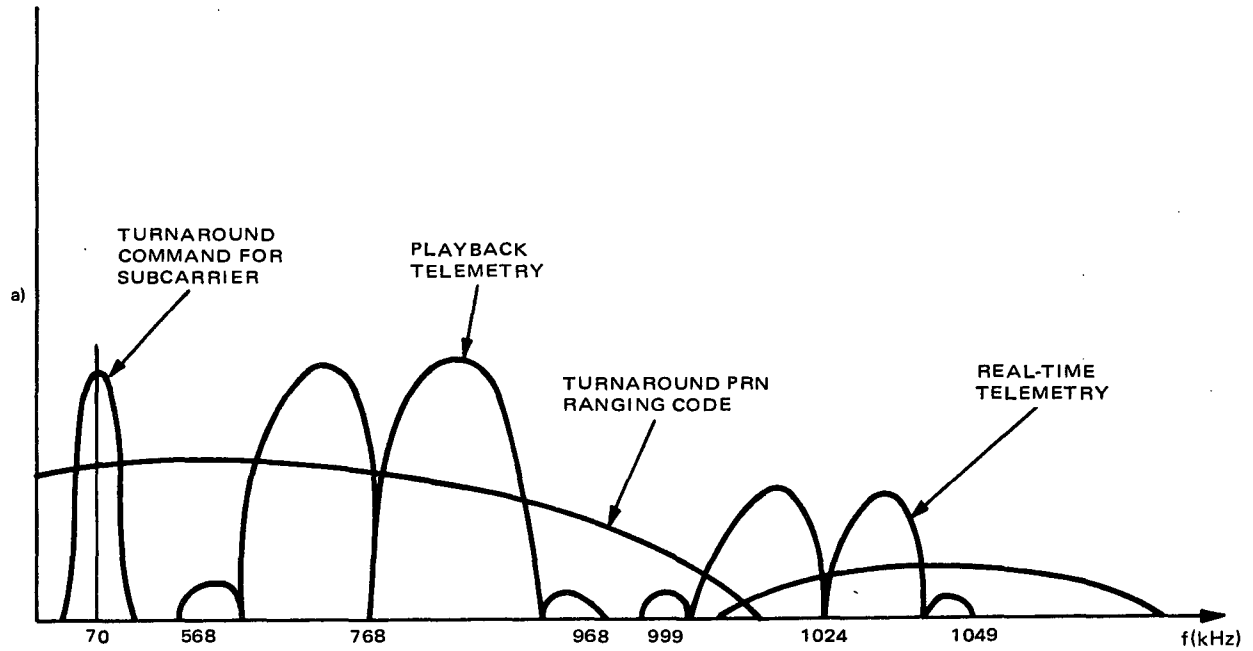
Figure IV-18. S-Band Downlink Modulation Spectra

TABLE IV-XVI. SPACECRAFT TO EARTH (DOWNLINK) MODULATION MODES

Downlink Mode	Information Channel	Modulation Technique	Peak Carrier Deviation	Subcarrier Frequency (KHz)	Subcarrier Deviation (Peak)
1	Real Time TLM	PSK/PM	0.70 ± 0.07	1024	±90°
	Playback TLM	PSK/PM	1.10 ± 0.11	768	±90°
2	PRN Ranging*	PM on Carrier	Note 1	-	-
3	GRARR Ranging*	CW/PM	Note 1	100 kHz	-
	GRARR Minor Tone**	CW/PM	Note 1	4.0 - 4.8 kHz or 20 kHz	-
4	Real Time TLM	PSK/PM	0.70 ± 0.07	1024	±90°
	Playback TLM	PSK/PM	1.10 ± 0.11	768	±90°
	PRN Ranging*	PM on Carrier	Note 1	-	-
5	Real Time TLM	PSK/PM	0.70 ± 0.07	1024	±90°
	Playback TLM	PSK/PM	1.10 ± 0.11	768	±90°
	GRARR Ranging*	CW/PM	Note 1	100 kHz	-
	GRARR Minor Tone**	CW/PM	Note 1	4.0 - 4.8 kHz or 20 kHz	-

*Signal includes command subcarrier as spurious.
**Present only during ranging acquisition.

NOTE 1: Downlink ranging carrier modulation index, within the linear range of the signal transfer characteristic of Paragraph 3.1.1.1.3.3, is given approximately by the expressions:

$$\theta_{PRN} \cong \frac{1}{\sqrt{2}} \left[\frac{S/N}{4/\pi + S/N} \right]^{1/2} \sin(\theta_2) \, J_o(\theta_1) \quad \text{for PRN Ranging}$$

$$\theta_{GRARR} \cong \left[\frac{S/N}{4/\pi + S/N} \right]^{1/2} J_1(\theta_3) \, J_o(\theta_1) \, J_o(\theta_1) \, J_o(\theta_4) \quad \text{for GRARR Ranging}$$

where θ_1, θ_2, θ_3, θ_4, and $J_o(\theta)$ are as defined in Table IV-XIII, and S/N is the Signal-to-Noise ratio at the input to the receiver IF limiter, if used. (If no limiter is used, the quantity in the brackets may be assumed to be unity).

Playback telemetry, from either of the spacecraft tape recorders, consisting of a 131,072 bit/second bi-phase data stream, PSK modulates a 768 kHz sinusoidal subcarrier. This subcarrier, in turn, phase modulates the carrier with a modulation index of ±1.10 radians peak. The frequency of 768 kHz has been selected because of the availability of ground station demodulators. The frequency has been selected for use on the ERTS spacecraft.

In addition to telemetry data, the downlink may simultaneously carry the turned around uplink modulation consisting of both the desired ranging signal and the undesired command signal. The turnaround gain for a single sinusoidal tone modulation the uplink has been selected at 0.5, based on previous experience with similar unified S-Band Systems in the Apollo program. For the actual ranging signals, the downlink modulation indices are given by the expressions shown in Table IV-XVI.

(1) MSFN UNIFIED S-BAND OPERATION

Table IV-XVII summarizes the link calculations pertaining to the S-band downlink when operating to a MSFN Unified S-Band ground station (Modes 1, 2 or 4 of Table IV-XVI). As in the uplink calculations, the value of the spacecraft antenna gain shown in the table does not include additional pattern degradation due to spacecraft holes or protrusions from experiment sensors.

The subcarrier modulation losses shown are those applicable during simultaneous ranging, telemetry and command and are calculated using nominal modulation indices.

The signal margins have been computed relative to the data thresholds supplied to RCA in document 71-AE-0038.

(2) STADAN (GRARR) S-BAND OPERATION

Table IV-XVIII summarizes the link calculations pertaining to the S-band downlink when operating in conjunction with a STADAN GODDARD range and range rate (GRARR) station (Modes 1, 3 or 5 of Table IV-XVI). The spacecraft parameters are the same as for the MSFN Unified S-Band operation. The ground station parameters are applicable to a 30 foot diameter antenna. For the 14 foot antenna systems, the margins shown will degrade by 8.4 dB.

The subcarrier modulation losses shown are those applicable during simultaneous telemetry, ranging and command and are calculated using nominal modulation indices.

TABLE IV-XVII. S-BAND DOWNLINK: MSFN (USB) GROUND STATION

Parameter	Value	Remarks
Total Transmitter Power	36.99 dBm	5W Spec (PS-2265304)
Transmitting Circuit Loss	- 2.00 dB	SCA, cable and reflection losses
Transmitting Antenna Gain	- 7.00 dB	Spec value (PS-SK-2260206) See text
Transmitting Pointing Loss	0.00 dB	Included in gain figure
Path Loss	-177.31 dB	Altitude = 4000 kM
		Range = 7646 kM
		Frequency = 2289.50 MHz
		Elevation = 5 degrees
Polarization Loss	- 3.00 dB	Linear to circular
Receiving Circuit Loss	0.00 dB	Included in gain figure
Receiving Antenna Gain	44.00 dB	30 ft antenna (MSFN 101.1)
Receiving Pointing Loss	0.00 dB	Included in gain figure
Net Circuit Loss	-145.31 dB	
Total Received Power	-108.32 dBm	
RX Noise Spectral Density	-176.15 dBm/Hz	System Temp = 176 Deg. K
RCVD Power/Noise Spec. Den.	67.82 dB-Hz	
CARRIER CHANNEL		
Carrier Modulation Loss	- 4.40 dB	Nominal (See text)
Received Carrier Power	-112.72 dBm	
Carrier APC Noise Bandwidth	28.45 dB-Hz	2 BLD = 700 Hz
Noise Power in APC Loop	-147.70 dBm	
APC Loop CNR	34.97 dB	
Threshold CNR	20.00 dB	Corresponds to $S/\emptyset R$ = 48.5 dB-Hz
Performance Margin	14.97 dB	
RANGING CHANNEL (PRN)		
Modulation Loss	- 18.20 dB	Nominal (See text)
Received Ranging Power	-126.52 dBm	
Ranging $S/\emptyset R$	49.63	
Required $S/\emptyset R$	42.50 dB-Hz	(71-AE-0038)
Ranging Margin	7.13 dB	
REAL TIME TELEMETRY CHANNEL		
Modulation Loss	- 9.90 dB	Nominal (See text)
Received Telemetry Power	-118.22 dBm	
Reference Bandwidth	42.14 dB-Hz	Bandwidth = Bit Rate = 16,384 Hz
Noise Power in Ref. BW	-134.00 dBm	
Received SNR	15.78 dB	(Not including PRN interference)
Required SNR in Ref. BW	13.00 dB	
Performance Margin	2.78 dB	
PLAYBACK TELEMETRY CHANNEL		
Modulation Loss	- 5.00 dB	Nominal (See text)
Received Telemetry Power	-113.32 dBm	
Reference Bandwidth	51.18 dB-Hz	Bandwidth = Bit Rate = 131,072 Hz
Noise Power in Ref. BW	-124.97 dBm	
Received SNR	11.65 dB	(Not including PRN interference)
Required SNR in Ref. BW	13.00 dB	
Performance Margin	- 1.35 dB	

TABLE IV-XVIII. S-BAND DOWNLINK: STADAN (GRARR) GROUND STATION

Parameter	Value	Remarks
Total Transmitter Power	36.99 dBm	Spec value (PS-2265304)
Transmitting Circuit Loss	- 2.00 dB	SCA, cable and reflection losses
Transmitting Antenna Gain	- 7.00 dB	Spec value (PS-SK-2260206) See text
Transmitting Pointing Loss	0.00 dB	Included in gain figure
Path Loss	-177.31 dB	Altitude = 4000 kM
		Range = 7646 kM
		Frequency = 2289.50 MHz
		Elevation = 5 Degrees
Polarization Loss	- 1.00 dB	Diversity Loss
Receiving Circuit Loss	0.00 dB	Included in gain figure
Receiving Antenna Gain	42.00 dB	30 ft GRARR 2 antenna (NASA X-530-69-109)
Receiving Pointing Loss	0.00 dB	Included in gain figure
Net Circuit Loss	-145.31 dB	
Total Received Power	-108.32 dBm	
RX Noise Spectral Density	-174.91 dBm/Hz	System Temp = 234 Deg. K
RCVD Power/Noise Spec. Den.	66.58 dB-Hz	
CARRIER CHANNEL		
Carrier Modulation Loss	- 4.10 dB	Simultaneous TLM, command and ranging
Received Carrier Power	-112.42 dBm	
Carrier APC Noise Bandwidth	22.04 dB-Hz	2 BLD = 160 Hz (NASA X-530-69-109)
Noise Power in APC Loop	-152.87 dBm	
APC Loop CNR	40.44 dB	
Threshold CNR	20.00 dB	Assumed
Performance Margin	20.44 dB	
GRARR RANGING (MAJOR TONE)		
Modulation Loss	- 21.00 dB	Uplink Mod index = 0.5 rad
Received Ranging Power	-129.32 dBm	
Received Power/Noise Spec. Den.	45.59 dB-Hz	
Required Power/Noise Spec Den.	37.00 dB-Hz	71-AE-0038
Performance Margin	8.59 dB	
GRARR RANGING (MINOR TONE)		
Modulation Loss	- 29.00 dB	Uplink mod index = 0.25 rad
Received Ranging Power	-137.32 dBm	
Received Power/Noise Spec. Den.	37.59 dB-Hz	
Received Power/Noise Spec. Den.	37.00 dB-Hz	71-AE-0038
Performance Margin	0.59 dB	
REAL TIME TELEMETRY CHANNEL		
Modulation Loss	- 9.70 dB	Simultaneous TLM, Command and Ranging
Received Telemetry Power	-118.02 dBm	
Reference Bandwidth	42.14 dB-Hz	Bandwidth = Bit Rate = 16,384 Hz
Noise Power in Ref. BW	-132.76 dBm	
Received SNR in Ref. BW	14.74 dB	
Required SNR in Ref. BW	13.00 dB	
Performance Margin	1.74 dB	
PLAYBACK TELEMETRY CHANNEL		
Modulation Loss	- 4.70 dB	Simultaneous TLM, Command and Ranging
Received Telemetry Power	-113.02 dBm	
Reference Bandwidth	51.18 dB-Hz	Bandwidth = Bit rate = 131,072 Hz
Noise Power in Ref. BW	-123.73 dBm	
Received SNR in Ref. BW	10.71 dB	
Required SNR in Ref. BW	13.00 dB	
Performance Margin	- 2.29 dB	

The margins have been computed relative to the required data thresholds supplied to RCA in document 71-AE-0038.

(3)   STADAN 40 AND 85 FT S-BAND OPERATION

Table IV-XIX summarizes the link calculations pertaining to telemetry reception using a STADAN 40 foot Data Acquisition Antenna System. The margins are applicable to telemetry reception during simultaneous ranging by a GRARR station. If no ranging is taking place the real time telemetry margin would increase by 0.2 dB and the playback telemetry margin by 0.5 dB.

If an 85 foot antenna is used, all margins will increase by an additional 6.5 dB.

All margins have been computed relative to the required data thresholds supplied to RCA in document 71-AE-0038.

TABLE IV-XIX. S-BAND DOWNLINK: STADAN 40 FT ANTENNA

Parameter	Value	Remarks
Total Transmitter Power	36.99 dBm	
Transmitting Circuit Loss	- 2.00 dB	
Transmitting Antenna Gain	- 7.00 dB	
Transmitting Pointing Loss	0.00 dB	
Path Loss	-177.31 dB	Altitude = 4000 kM
		Range = 7646 kM
		Frequency = 2289.50 MHz
		Elevation = 5 Degrees
Polarization Loss	- 1.00 dB	
Receiving Circuit Loss	0.00 dB	
Receiving Antenna Gain	46.00 dB	
Receiving Pointing Loss	0.00 dB	
Net Circuit Loss	-141.31 dB	
Total Received Power	-104.32 dBm	
RX Noise Spectral Density	-174.91 dBm/Hz	System Temp = 234 Deg. K
RCVD Power/Noise Spec. Den.	70.58 dB-Hz	
REAL TIME TELEMETRY CHANNEL		
Modulation Loss	- 9.70 dB	See text
Received Telemetry Power	-114.02 dBm	
Reference Bandwidth	42.14 dB-Hz	Bandwidth = bit rate = 16,384 Hz
Noise Power in Ref. BW	-132.76 dBm	
Received SNR in Ref. BW	18.74 dB	
Required SNR in Ref. BW	13.00 dB	
Performance Margin	5.74 dB	
PLAYBACK TELEMETRY CHANNEL		
Modulation Loss	- 4.70 dB	See text
Received Telemetry Power	-109.02 dBm	
Reference Bandwidth	51.18 dB-Hz	Bandwidth = bit rate = 131,072 Hz
Noise Power in Ref. BW	-123.73 dBm	
Received SNR in Ref. BW	14.71 dB	
Required SNR in Ref. BW	13.00 dB	
Performance Margin	1.71 dB	

3. S-Band Hardware Summary

a. S-BAND TRANSPONDER

The revised S-Band Transponder performs the simultaneous functions of command reception, coherent turnaround ranging, and transmission of real time and playback telemetry. The transponder is an integrated package containing, as major components, a receiver and a transmitter, each with its associated dc/dc power converter.

The receiver is a high sensitivity superheterodyne employing a phase lock carrier tracking loop, a separate wideband (modulation) phase detector, IF limiting, and a coherent AGC detector.

The transmitter is a high efficiency solid state unit incorporating a linear phase modulator and having the capability of generating an output rf carrier coherently related to the received frequency or, on command, derived from a local frequency reference.

The transmitter has provisions for automatic turn-on upon the receipt of an up-link rf carrier to facilitate ranging operations. This automatic mode can be inhibited by ground command.

Figure IV-19 is a block diagram of the transponder interfaces. The principal transponder specifications are summarized in Table IV-XX, and appear in complete form in RCA Specification PS-2265304.

b. S-BAND COUPLING ASSEMBLY

The S-band coupling assembly couples the two S-band Transponders to the S-band antenna system. It is composed of a frequency diplexer, a 3 dB hybrid coupler, and a switchable circulator. A block diagram of the coupling assembly is shown in Figure IV-20. The functions of the various components are as follows:

The frequency diplexer separates the received and transmitted signals present at the common antenna port and provides isolation between the transmitter output and the receiver inputs.

The 3 dB coupler splits the received signal power equally to both receivers and provides isolation between them.
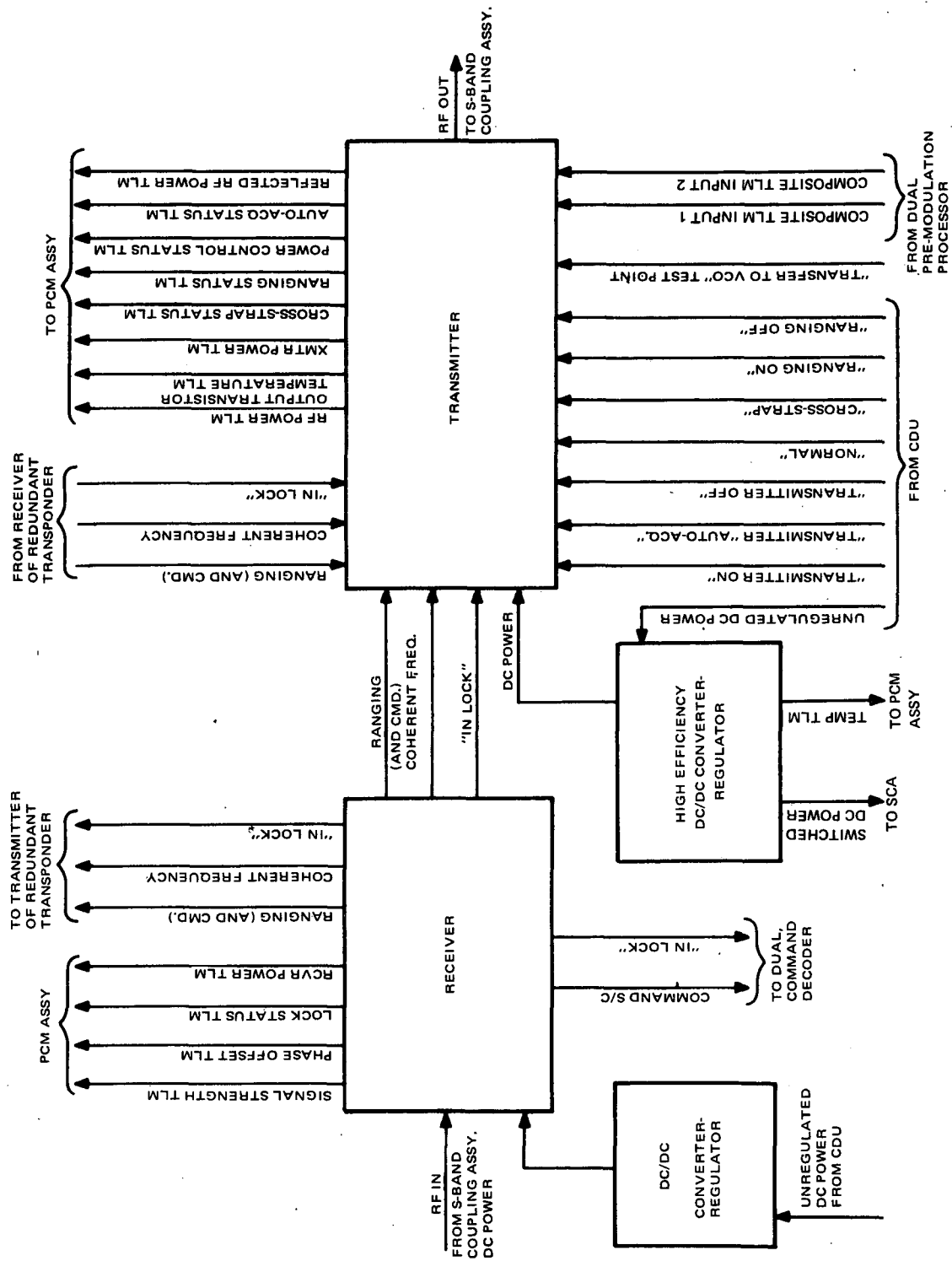
Figure IV-19.   Transponder Functional Interconnections

TABLE IV-XX. S-BAND TRANSPONDER SPECIFICATION SUMMARY

Parameter	Specification
Receive Frequency	2108.25 MHz
Transmit Frequency	2289.50 MHz
Coherent turnaround ratio	240/221
Input RF Level	-110 to -40 dBm
Receiver Noise Figure	7 dB
Uplink Modulation	Simultaneous command and ranging
Noise Bandwidths:	
carrier tracking	800 Hz
command	20 kHz
ranging	1.5 MHz
RF Power Output	5 watts
Downlink modulation	Simultaneous ranging and real time telemetry and playback telemetry.
Modulation Bandwidth	4 kHz to 1.4 MHz
DC Voltage Input	
receiver	-21 to -38.5 volts
transmitter	-26 to -38.5 volts
DC Power Input	
receiver	2.5 watts
transmitter	37.5 watts
Duty cycle	
receiver	continuous
transmitter	8% typical, capable of continuous operation
Weight	10 pounds
Size	400 cubic inches

The switchable circulator switches the output of the active transmitter to the transmitter port of the diplexer and provides isolation between the active and inactive transmitters.

The principal specifications of the S-band coupling assembly are summarized in Table IV-XXI, and appear in complete form in RCA Specification SK-PS-1972215.

c.   DUAL PRE-MODULATION PROCESSOR (PMP)

The Dual Pre-Modulation Processor (PMP) consists of two identical redundant units, within a common assembly, only one of which will be powered at any given time. The function of the PMP is to:

a)   Generate a 1024 kHz subcarrier, phase modulated by a 16,384 bit/ second bi-phase data stream from either of two spacecraft PCM Assemblies.

b)   Generate a 768 kHz subcarrier, phase modulated by a 131,072 bit/second bi-phase data stream from either of two spacecraft tape recorders.

c)   Perform amplitude conditioning and bandpass filtering of the two modulated subcarriers, combine them into a composite frequency division multiplex spectrum, and provide the composite signal as an output to both redundant spacecraft S-Band Transponders.

A functional block diagram of one redundant section of the PMP is shown in Figure IV-21. Either redundant section of the PMP can be selected, on command, to provide the modulation input to either of the redundant transponders.

The principal PMP specifications are summarized in Table IV-XXII, and appear in complete form in RCA specification SK-PS-2270710.
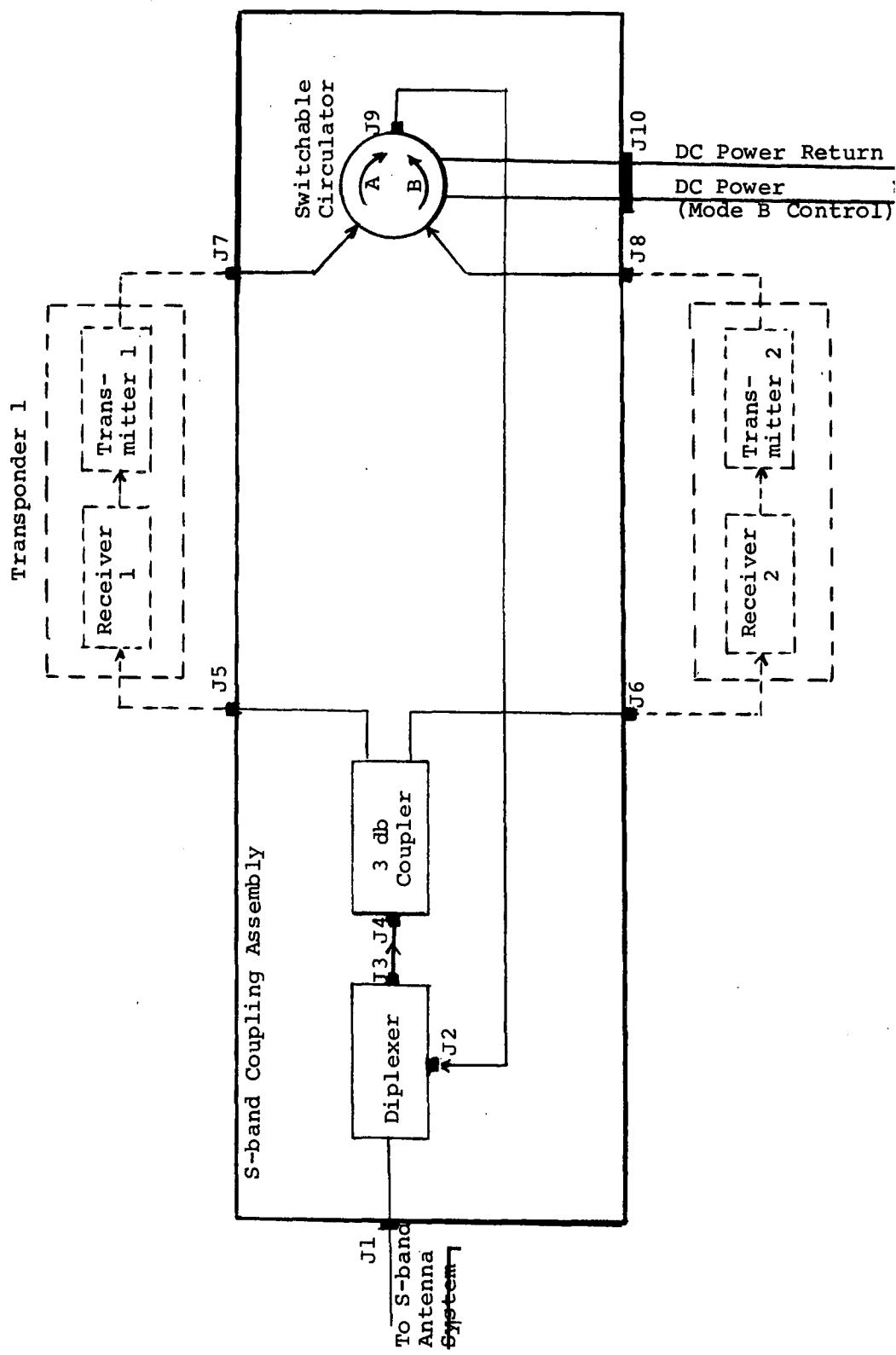
Figure IV-20. Functional Block Diagram of S-Band Coupling Assembly

TABLE IV-XXI. S-BAND COUPLING ASSEMBLY SPECIFICATION SUMMARY

Parameter	Specification
Receive Frequency (Fr)	2108.25 MHz
Transmit Frequency (Ft)	2289.50 MHz
Insertion Losses	
Antenna to either receiver	4.0 dB max @ Fr
Active transmitter to antenna	0.7 dB max @ Ft
Isolation	
Active transmitter to receiver	54 dB min @ Ft 54 dB min @ Fr
Receiver to Receiver	25 dB min
Active transmitter to inactive transmitter	25 dB min
Impedance	50 ohms, all ports
DC Voltage Input	
(to switchable circulator)	-26 to -38.5 volts
DC Current	
Transponder 1 active (Mode A)	0 mA
Transponder 2 active (Mode B)	40 mA max
Weight	4 pounds
Size	180 cubic inches

FUNCTIONAL BLOCK DIAGRAM OF PRE-MODULATION PROCESSOR

Figure IV-21. Functional Block Diagram of Pre-Modulation Processor
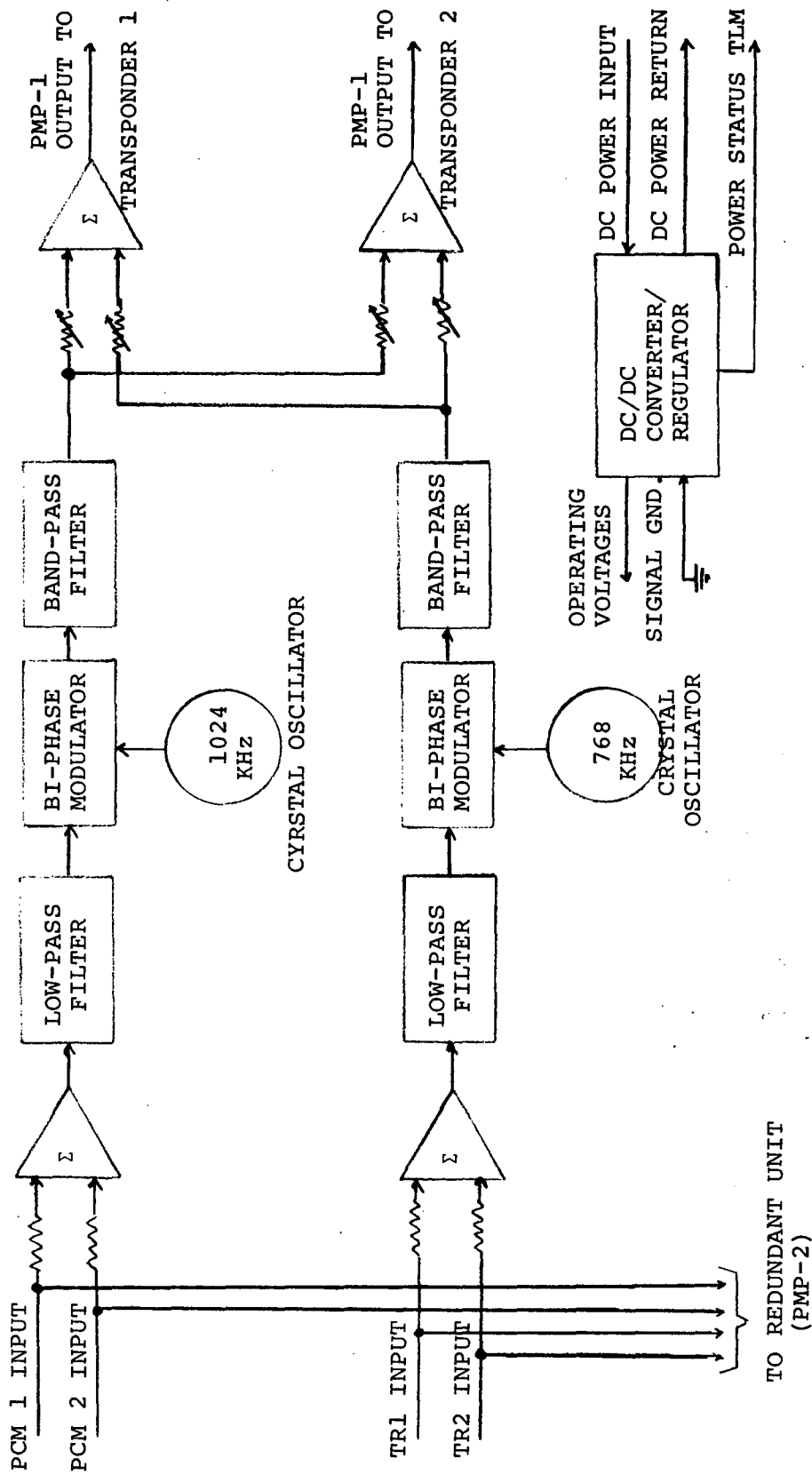
NOTES: 1. ONLY ONE REDUNDANT UNIT (PMP-1) SHOWN.

TABLE IV-XXII. DUAL PRE-MODULATION PROCESSOR SPECIFICATION SUMMARY

Parameter	Specification
Inputs	
Real-Time Signal	16,384 bit/sec. bi-phase digital data from either of two PCM assemblies.
Playback Signal	131,072 bit/sec bi-phase digital data from either of two PCM assemblies
Subcarrier Frequencies	
Real-time	1024 kHz ±0.005%
Playback	768 kHz ±0.005%
Subcarrier Modulation	PSK
Subcarrier Amplitudes	
Real-Time	1.40 ±0.07 volts p-p
Playback	2.20 ±0.11 volts p-p
DC voltage input	-26 to -38.5 volts
DC Power Input	1.0 watt
Weight	4 pounds
Size (estimated)	☐

G. COMMAND AND DATA HANDLING SUBSYSTEM

1. Summary

The Command and Data Handling subsystem (CD & H) which has evolved as a result of experiment requirements identified during the study and operating constraints imposed by the new combined STADAN/MSFN network is shown in block diagram form in Figure IV-22. The system provides all command information, both in real-time and remote modes of operation, all sync and timing signals, and the means of gathering and formatting the telemetry data into a single serial digital bit stream for direct transmission to the ground station or for storage in the spacecraft tape recorders.

The basic functional capabilities are as follows:

- The subsystem will turn the experiments on and off by the generation of power commands*. In real time the power commands will be generated as received; in remote operation, power command generation will be achieved with a granularity of four seconds.

- The subsystem will generate all command information, in the form of major and minor mode commands*, with the attendant command clock, as required by the experiments. As for power, in real time, the information will be distributed as received; in remote operation it will be distributed with a granularity of four seconds.

- The subsystem will operate from either a pre-defined fixed format for the main frame and subcom telemetry or from a programmable main frame format which can be commanded from the ground.

- The subsystem will generate the appropriate signals to acquire telemetry from the experiments, in either digital or analog form and generate a serial digital bit stream of the output telemetry in accordance with the format in use (fixed or programmed).

- The subsystem will generate and supply all sync signals as required by the experiments.

- The subsystem is configured to be fully redundant.
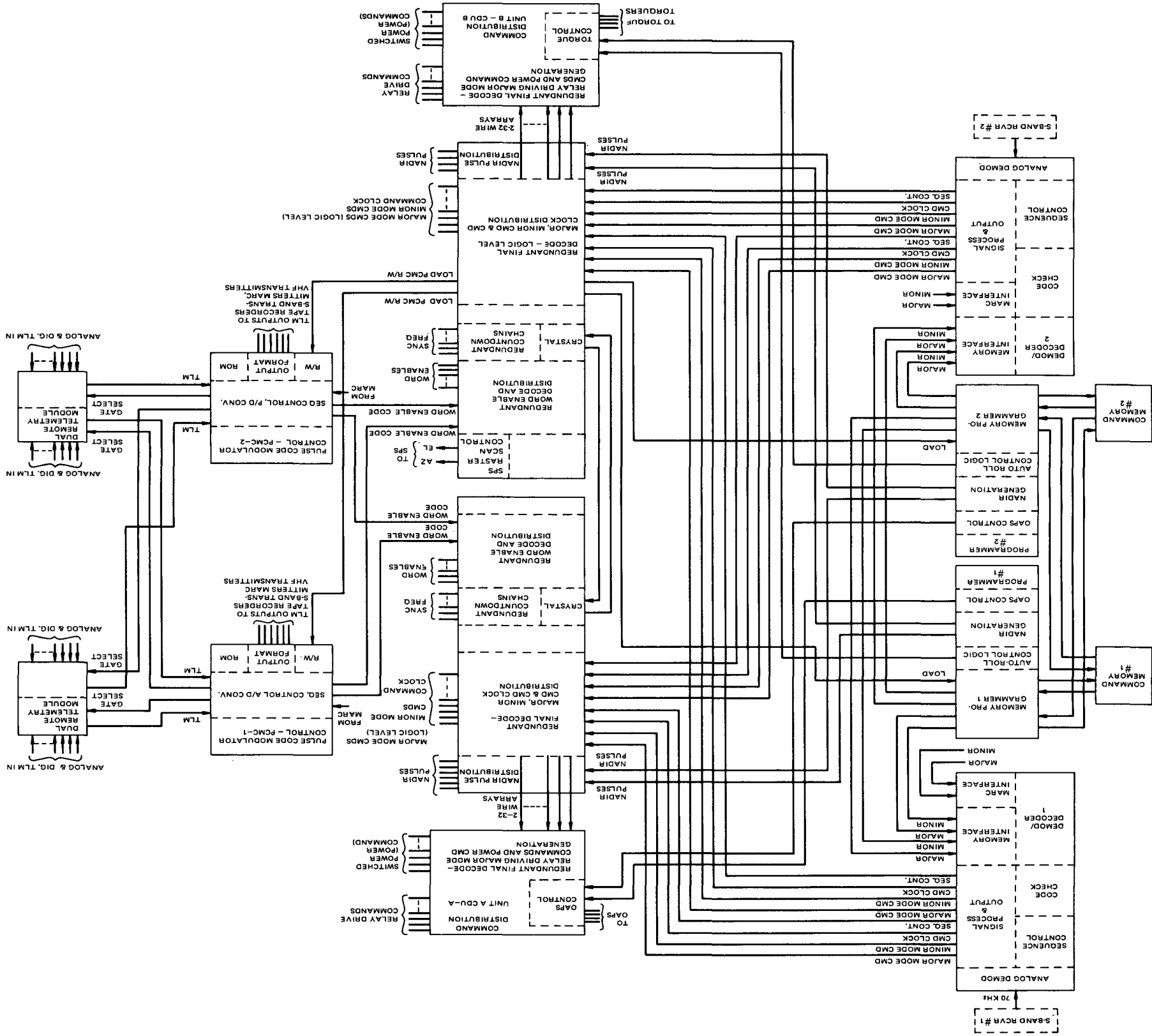
---

*Defined in Table IV-XXIII.

Figure IV-22. AE Spacecraft Command and Data Handling System, Block Diagram

2. Signals

The specific signals generated by the subsystem to implement the above capabilities, in the general categories of command, sync and telemetry are given in Table IV-XXIII. Brief descriptions of the function of each signal are included.

TABLE IV-XXIII. CD & H SUBSYSTEM SIGNALS

Command

1. Power Commands - Switched power levels to initiate and terminate operation of equipment. These may be generated either in real time or in remote operation.

2. Major Mode Commands - Pulse commands of two types; those with a power capability to operate relays and those designed to interface with all families of IC logic circuitry which operate between a positive supply and ground. These may be generated in real time or in remote operation.

3. Minor Mode Commands - 32 bit serial data stream designed to interface with all families of IC logic circuitry which operate between a positive supply and ground. These may be generated in real time or remote operation.

4. Command Clock - A burst of 34 clock pulses phase related to the Minor Mode Commands which appear when any command is executed in the spacecraft. The command clock is designed to interface with all families of IC logic operating between a positive supply and ground.

Sync

All sync signals are generated as required within the spacecraft. The following sync signals are designed to interface with all families of IC logic which operate between a positive supply and ground.

1. Experiment Clock - 16,384 bps continuous clock rate

2. Assorted additional clock rates which are binarily related to the experiment clockrate

3. Main Frame Sync - A pulse train related to the telemetry main frame rate of 16 frames per second with one pulse appearing at the start of each main frame.

4. Subcom sync - A pulse train related to the main frame rate but with one pulse appearing at the start of the main frame which contains the first word of the subcom frame.

TABLE IV-XXIII. CD&H SUBSYSTEM SIGNALS (Continued)

Sync cont'd

5. Digital Word Enables - A series of pulses with duration equal to the length of the digital telemetry word being read out of a unit occurring when that digital word is interrogated.

6. Nadir Pulses - A series of pulse trains related to the spin rate of the body of the spacecraft and generated at the time the particular user experiment is aligned with the nadir.

7. Spin/Despin - A two level signal which will indicate whether the spacecraft is in the spinning or oriented mode of operation.

Telemetry

1. Digital words - Digital telemetry words of 8, 16, or 24 bit length which are assembled into the serial telemetry output of the spacecraft.

2. Analog Words - Analog telemetry which is converted into 8-bit digital words and assimilated into the serial telemetry output.

3. Flag Bits - Discreet two level telemetry signals which are formatted into 8-bit words in the spacecraft and assimilated into the serial telemetry output of the spacecraft.

3. CD&H Equipment

The following equipment comprises the Command and Data Handling Subsystem:

Dual* Demod/Decoder

Dual* Programmer

Two Command Memories

Dual* PCM Controller

Dual* Remote Telemetry Modules A and B**

Logic Interface Units A and B**

Command Distribution Units A and B**

The basic functions of each of the units in the Command and Data Handling Subsystem are given in Table IV-XXIV through IV-XXV. Details of the operation of these units are discussed in subsequent paragraphs in this section. Specific interfaces with the experiments are addressed in Section II.

---

*Two fully redundant units packaged in one assembly
**A and B units not redundant to each other but internally piecewise redundant

TABLE IV-XXIV. DEMOD/DECODER

1. Demodulate the 70 kHz command subcarrier and present command information and the transmitted command clock signal to the decoder for real-time commands.

2. Decode received real-time command information and check for proper address and overall code validity.

3. If information is correct, sequence final decode in LIU's and output minor mode command information.

4. Sequence final decode in LIU's and output minor mode command information from the on board memory.

5. Generate command clock for commands extracted from memory.

6. Provide telemetry of decoder operation and of real-time command code validity.

TABLE IV-XXV. PROGRAMMER

1. Operate either command memory for execution of stored commands.

2. Provide nadir-referenced pulses to those units requesting same.

3. Perform "Delta V" comparison during OAPS operation.

4. Perform attitude control auto-roll calculations and modulate magnetic torquing programs as required.

TABLE IV-XXVI. COMMAND MEMORIES

1. Store major and minor commands for remote execution via either of the redundant programmers.

2. Maintain memory of command after execution.

TABLE IV-XXVII. PCM CONTROLLER

1. Provide control for both fixed and dynamic telemetry main frame formats.

TABLE IV-XXVII. PCM CONTROLLER (Continued)

2. Provide for four subcoms (fixed) of either 64 or 128 word length and one 4 word subcom.

3. Generate coded information to identify unique word enables and supply to LIU's for decode and distribution.

4. Generate coded information to operate data gates in remote telemetry modules (RTM's) to commutate digital or analog data into PCM controller.

5. A to D convert all analog telemetry in either a 0 to +5.12 Vdc or a 0 to -5.12 Vdc telemetry range.

6. Format a biphase output and deliver same to
    Two Tape Recorders
    Two Beacon/Telemetry Transmitters
    Two S-band Telemetry (Transponder) Transmitters

7. Format one NRZ (non-biphase) output for an off-line flight central processor.

TABLE IV-XXVIII. REMOTE TELEMETRY MODULES

1. Commutate telemetry into the serial data stream under control of PCM Controller.

TABLE IV-XXIX. COMMAND DISTRIBUTION UNITS

1. Provide the final decode and distribution of major mode commands at the relay driving level.

2. Provide relays to respond to relay driving major mode commands to generate commands and house the redundancy selection of S/C equipment.

3. Provide fusing of -24.5 Vdc regulated bus for generation of separate fused sources for individual units.

TABLE IV-XXX. LOGIC INTERFACE UNITS

1. Provide final decode of major mode commands and translate same into a 2 of 32 matrix for output driving and redundant coupling of all required major mode logic level commands for the experiments and spacecraft.

2. Provide 2 of 32 matrices to associated CDU (Command Distribution Unit) for output driving and redundant coupling of all required major mode relay drive commands and for operation of CDU located relays (generation of power commands.)

3. Distribute minor mode commands and command clocks.

4. Provide decode of PCM Controller generated codes and translate same into a 2 of 32 matrix final decoding, output driving, and redundant coupling of all telemetry word enables.

5. Provide redundant countdown chains for generation of all required time base frequencies; generate spacecraft time code.

6. Provide raster scan program generation for Solar Pointing Subsystem.

7. Provide logic interface to PCM Controller, real-time S-band link, and Demod/Decoder for an off-line flight central processor.

8. Provide for redundancy cross-strapping at the logic signal level and for other logic functions such as 1) assembly of flag bits into 8-bit telemetry words, 2) distribution of nadir pulses, 3) distribution of spin/despin signals.

4. Subsystem Configuration

Evaluation of the volume of interface traffic and considerations of the spacecraft configuration has resulted in the following design approach for information distribution and collection.

The two-baseplate configuration of the spacecraft and the restrictions on baseplate to baseplate harnessing through the center section of the spacecraft pose possibly severe noise coupling problems if signal distribution and "fan out" were performed on one baseplate for logic-receiving circuits located on the other baseplate. Analysis of the potential noise coupling line to line, based on the number of signals which must make phase coherent fast transitions over extended harness runs, indicates a potentially severe noise environment. To minimize the effects of such potential noise sources and to provide a flexible and efficient layout capability for the spacecraft, the following technique was adopted.

a. LOGIC INTERFACES

Logic level interfaces from the spacecraft support equipment to the experiments (and, in general, from spacecraft units to spacecraft units) will be performed via a logic interface unit (LIU) which is located on the same baseplate as the unit receiving the signal. Thus, there is one LIU on each baseplate. The redundancy coupling between the redundant sources which generate the signal will be performed in the LIU and the active circuitry required to generate the signal in the LIU will be powered by the source dc/dc converter of the (i.e. decoder, programmer, PCMC) which is generating the signal. Information from the source unit to the LIU will be delivered to the LIU in a serial bit stream, final decoding and fan out will be accomplished in the LIU.

Present considerations of the characteristics of the serial information which will be distributed from source units to the LIU's indicates that active line drivers and receivers for this information may be required. Such drivers are expected to be required when the source unit is on one baseplate and the load unit is on the other baseplate-the interface being accomplished in the LIU on the baseplate mounting the load unit.

By the nature of the functions that the LIU's perform, they do not have a dedicated function within themselves other than to serve as extensions (fan-out terminals) for the various source units on the spacecraft. Accordingly, the two LIU's are not redundant to each other but the internal circuitry associated with specific functions from redundant source units are piecewise redundant.

b. RELAY INTERFACES

Also located on each baseplate is a Command Distribution Unit (CDU). These units perform a function quite similar to the LIU's with the restriction that they deal with command interfaces only and are restricted to commands (either major mode or power commands) which operate at the non-logic level. The CDU's house the final decoding of all relay driving major mode commands and also house the relays used to switch power on and off to various loads (both spacecraft and experiment) which are located on their baseplate. The separation of the power switching functions into CDU's on each baseplate has been made to minimize the harnessing problems and improve the noise environment associated with the power distribution between the two baseplates.

Generation of power commands for experiments or spacecraft equipment is accomplished via the use of latching relays which are operated by major mode commands. The physical separation of the power switching functions from the location of the logic circuitry has been made to prevent the high current, high noise level power lines and switching transients from interfering with the logic. Consistent with this is the physical configuration of the spacecraft harness which will have the logic interfaces bundled separately from the power harnesses on each of the two baseplates.

c.   TELEMETRY

The third area where a "distributed" function approach was taken is telemetry commutation. The actual commutation of the telemetry information into the serial data stream is performed in commutation stations located on each baseplate. The stations are fully redundant on each baseplate. A PCM subsystem consists of a selected PCM controller (PCMC) and two Remote Telemetry Modules (RTM's), one on each baseplate, which are uniquely associated with that PCMC. The PCMC in use distributes serial information to two locations on one baseplate when requesting telemetry: one serial burst of data is transmitted to the LIU on the baseplate where the telemetry data is originating and another serial burst of data is transmitted to the RTM on that baseplate. The serial data in the LIU is code converted and decoded to be fanned out from the LIU via the specific word enable (to the experiment or spacecraft equipment) associated with the telemetry word to be sampled. The code transmitted to the RTM is decoded in the RTM to activate the particular commutator gate for the telemetry point in question. As generated, the telemetry is commutated back from the RTM's to the PCMC in use for formatting and for A/D conversion, if required. By so doing, the possibility for contamination of the telemetry information, especially the analog information is minimized as the interface from source to commutator will be kept short, while the interface from RTM to PCMC will be accomplished by an actively driven noise immune line.

5.   Subsystem Operation

With the above configuration and approach to interface control, the operation of the subsystem is as displayed in Figure IV-22.

a.   COMMAND FLOW (REAL TIME OR REMOTE)

   (1)   REAL TIME COMMANDS

The word structure of the transmitted command is shown in Figure IV-23. The command word is 64 bits long. The first 7 bits are assigned by the combined STADAN/MSFN network as the spacecraft address. The next two bits are used by the spacecraft to identify which of the redundant demod/decoders are to be used to process the commands. Following are two bits used for data bus control, an internal function which indicates whether the command being transmitted includes minor mode data. Following these eleven bits is a spare interval of 5 bits and nine bits used for encoding of the major mode command. The next 32 bits contain the minor mode command, if used, or a spacer of 32 zeros. The last 7 bits of the 64 bit command frame contain a 7 bit cyclic check code.
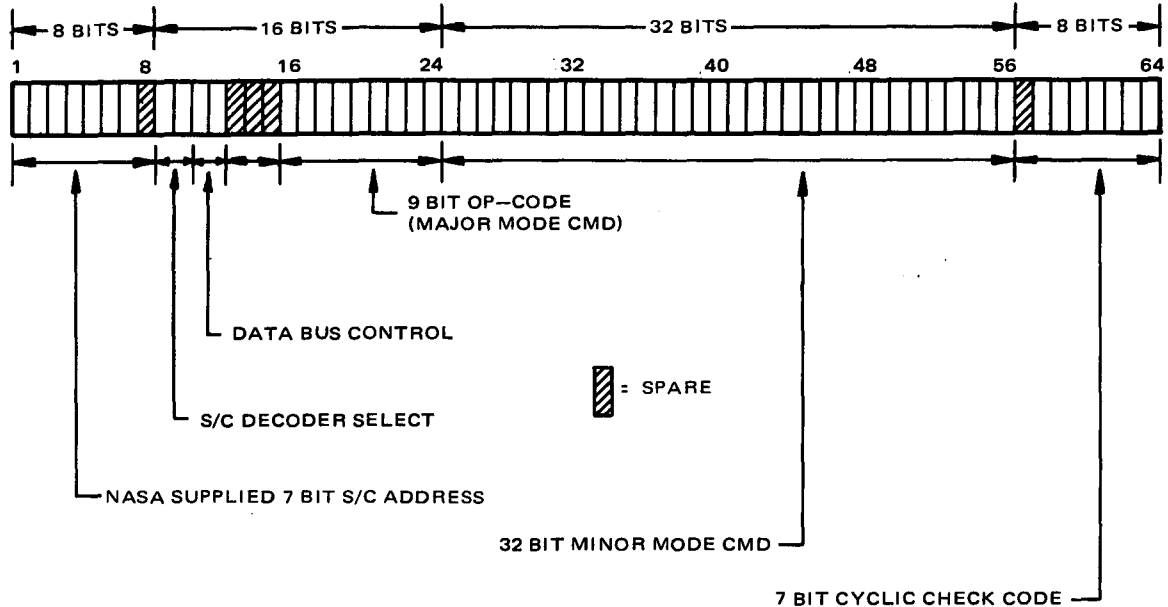
Figure IV-23. Command Word Structure - Real Time Command

In operation, once a sync pattern is recognized (presently n zeros followed by a one where n is greater or equal to 13) both decoders search the next 9 bits for proper spacecraft address and decoder address. If not found, the decoders return to a sync search operation. Once found, the decoder which has properly been addressed assembles and holds the 9 bit op-code and, if the Data Bus Control bits indicate that a minor mode command is included in the command frame assembles the 32 bit minor mode command in a 32 bit shift register. During reception of the minor mode command or the spacer, the nine bit op-code is shifted to both LIU's as a serial nine bit word where it is code converted to a 2 of 32 code. The circuitry associated with the LIU code conversion is dedicated to and powered by the decoder which has been properly addressed and is processing the command. During reception of the 64 bit word, the serial information passed into the decoder is being circulated through a feedback shift register with selected exclusive OR'ing to the register input. The register is configured to indicate all zeros if the code check is valid. When this condition occurs, the decoder sequencer (internal to the decoder) permits the code converted major mode command to be executed and delivered to the load circuit. Once the major mode command execute is initiated, the minor mode command (if required) is shifted out of the register in the decoder. The exact timing relationships of the major and minor command and the relationship of the command clock, which is also distributed during execution of each major mode command are shown in General Interface Specification RCA PA-2260216.

(2)   REMOTE COMMANDS

Commands which are executed from the active Command Memory
are executed via the same path as those received in real time. When the command
memory outputs a major mode command, it is in the form of the nine bit op-code,
serially read into the output gate of the decoder. The minor mode data from
the command memory is read into the register in the decoder used for real time
minor mode data. The major mode information is code converted in the LIU's
under the sequence control of the decoder and the minor mode data and command
clock are read out of the decoder in the identical fashion to those received in
real time. The timing relationships of commands read out of the command
memory are such that any such command execution can be completed even if the
decoder starts to receive real time commands during execution of the memory
command.

An interlock is provided between the two (redundant) decoders and the two
(redundant) memory programmers (contained within the Dual Programmer)
which is used to select the decoder for execution of the memory commands.
Functionally, whichever command memory programmer is in use (exclusive
selection of redundant S/C programmers) uses for remote command execution
the decoder which was last used for real time commanding.

(3)   MEMORY PROGRAMMER OPERATION

The memory and memory programmer operate to execute commands
based on a time tag comparison to a clock which is phase related to the space-
craft time code. The entire contents of the memory are searched during each 4
second clock interval and all commands tagged for execution when their time
tags match the programmer clock are assembled and executed. As the memory
programmer executes commands on a "match only" condition for the time tags,
a facility is provided to accommodate an excessive number of commands tagged
for one time period, and to inhibit execution when the real time command link
is active. The technique can be thought of as establishing a "bookmark" in
time within the memory programmer such that if interrupted, the memory
programmer can, when the interruption is terminated, go back to where it was
and execute commands until it has removed the "backlog". The length of the
bookmark period is under evaluation at present; the final value will be selected
based on the expected times required for real time commanding.

Information is loaded into the command memories by using Minor Mode Com-
mands. To load, a preamble message is first transmitted to establish where,
in the memory, the loading will be initiated and how many words are to be loaded.
The actual load data is then transmitted in either of two minor mode commands.
One load contains the time tag information and the op-code while the other load
command is used only for loading minor mode 32 bit words into the memory.

When the memory programmer finds a time tag match, it transmits the op-code (9 bits) to the output stage of the decoder (see discussion of remote command flow above) and checks information stored with the op-code to determine whether an adjacent block in the memory contains minor mode data which is to be also read out with that command.

(4) REAL-TIME/REMOTE COMMAND INTERLOCKS

Referring back to the real time command reception behavior of the decoders, if the spacecraft and decoder address are not immediately recognized after the sync pattern, the decoder returns to the sync search pattern. If the address and decoder select are proper but the cyclic code check (last seven bits) fails, execution of the command information in that command frame is inhibited. In this condition, the decoder then starts to search for the address and decoder select again in the next received 9 bits. If this check fails, the decoder returns to sync search. The logic flow of this sequence permits the command link to be maintained without "locking up" the decoder to preclude execution of commands from memory during a real time contact while real time commands are not being executed. The interlock is established such that real time commands take precedence over memory stored commands. The command link, therefore, can be maintained by transmitting commands with the proper spacecraft address but with the improper decoder address for either decoder. Alternately, if it is desired to maintain the command link, and inhibit commands out of memory, an "idle" pattern can be established by properly addressing the spacecraft and one of the decoders, and then intentionally transmitting a bad check code in the last seven bits of the 64 bit frame.

(5) FINAL COMMAND DECODING

The final decode technique which is performed in the LIU is shown in Figure IV-24. The configuration shown is for the function on one baseplate with the redundant source information from both decoders. The nine bit op-code is serially received from the decoder in use and is code converted during the time the decoder is operating on the last 40 bits of the command frame. The resulting 2 of 32 matrix is established in a 32 bit register. When the code check has been satisfactorily completed, the decoder in use generates an execute signal which is 34 counts of the command bit rate in length. This execute signal locks the code converter and is AND gated with the outputs of the 32 bit register. This results in two active signals in the 32 bit array. For logic level major mode commands, these two active lines are hard wire connected to a dedicated AND gate which results in the output of the AND gate going to ground.* This output is OR gated with the identical command as generated by the other decoder.

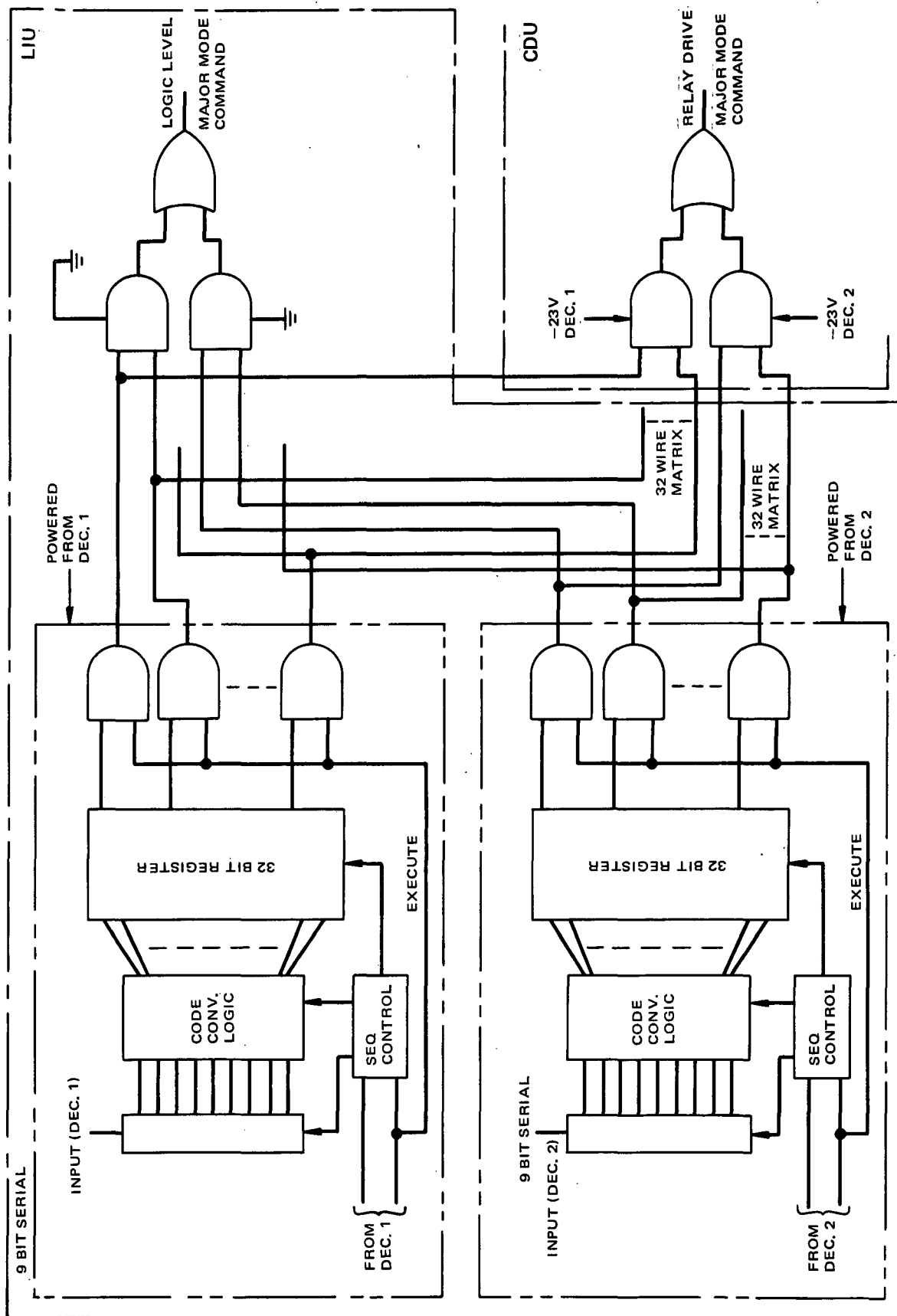*The circuit configuration is shown in the General Interface Specification.

Figure IV-24. Major Mode Command Decode and Distribution

To generate the major mode commands for relay driving the identical circuitry is used with the following modifications. The outputs of the 32 execute gated and gates which form the matrix are transmitted from the LIU to the associated CDU. In the CDU the decoding technique is identical except that instead of the hard-wired AND gate going to ground in the active state, -23 Vdc is switched on for the 34 count duration.* It should be noted that the same circuit is used for both logic level interfaces and relay driving interfaces with the exception being that for the logic application the OR function is resistive while for the relay driving application, the OR gate is made up of diodes.

Utilizing this approach, all of the commands in the command glossary may be decoded either as relay driving pulses or as logic level pulses in either CDU or LIU on either baseplate. The hard-wire decoding connections to the final AND gates determine which commands are actually decoded in each unit and at what levels.

The distribution of the minor mode commands and the command clock is performed in the LIU's in the same fashion as the distribution of the major mode commands at the logic level. The same AND gate/OR gate configuration is used to achieve the redundancy source and coupling. In these applications, however, one input to the final AND gate is either the command clock or the minor mode data. In the case of the command clock, the second input to the AND gate is the execute command. In the case of the minor mode command, the second input to the AND gate is an enable which is generated by the decoder in use only when Minor Mode Commands are being distributed. This enable is 32 counts of the command bit rate long and is coherent with the last 32 counts of the 34 count Major Mode/Load Command associated with the minor mode command.

b.   PCM OPERATION FLOW

    (1)   GENERAL OPERATION

        The subsystem includes a fully redundant PCM facility, comprising a dual PCM Controller (PCMC), dual RTM A and dual RTM B. When one of the redundant PCM Controllers is selected for operation, it utilizes two dedicated Remote Telemetry Modules, are on each baseplate. Thus, if one PCMC is selected, it always operates with the same RTM in the redundant RTM A and the same RTM in RTM B.

As stated previously, the PCMC sequences through the telemetry format and causes digital word enables to be generated for each digital word in the telemetry format. These word enables are distributed to the units providing the telemetry to indicate that the digital words are to be read out serially phased to a continuous clock signal supplied by the spacecraft. At the same time, the PCMC opens a data gate in the appropriate RTM to accept the digital data. For analog

---

*The circuit configuration is shown in the General Interface Specification.

data, the same basic operation is performed except that (in general) the word enable signals are not required by the telemetry generating unit.

Once the data, either digital or analog, has been commutated into the RTM, it is transmitted back to the PCMC. The digital data is buffered and then directly inserted into the serial digital telemetry output stream. Analog data is AtoD converted in the PCMC in use and then inserted into the serial output stream. The output data, which is bi-phase coded, is distributed to the spacecraft tape recorders, the beacon/telemetry transmitters, and the pre-modulation processor for application to the S-band transmitters. Routinely, the information is distributed to all of the above noted redundant receiving units; the receiving unit of the redundant pair which is in operation will accept the data while the other, which is not in operation, will, of course, not process it.

The system has been configured such that all digital eight bit word telemetry from a source which is to be inserted in the main frame of the telemetry format is multiplexed onto redundant outputs (one output dedicated to each of the redundant RTM's located on the same baseplate). All digital eight bit word telemetry from a unit which is to be inserted in the subcoms of the telemetry format is multiplexed onto another set of redundant outputs (again one output is dedicated to each redundant RTM on the same baseplate). Analog data is not commutated onto common outputs in the source units; separate redundant outputs of each analog point are provided.

(2) TELEMETRY FORMATTING

The telemetry sequence for the operational mission of each of the AE spacecraft is defined in a ROM (read-only-memory) peculiar to that spacecraft.* The PCM also has the capability of modifying the telemetry format by the use of a read/write memory which can be substituted for the ROM, logically, in the PCMC. In this mode of operation, the main frame format can be modified as desired, including the facility to "bring up" words in the fixed sub-coms into the main frame.

(3) DIGITAL WORD ENABLE DISTRIBUTION

During the study, a tradeoff was performed on the technique of distributing the digital word enables to the experiments. If the subsystem contained only a fixed format for the telemetry data, the digital word enables to a particular unit could be either multiplexed onto a single wire or distributed on a one signal per wire basis. The reduction in hardware and interface circuitry to multiplex the data onto the single line in the spacecraft was balanced by the increased logic in the users to identify which word enable corresponded to which

---

*Word assignments for the main telemetry frame are presented in Section III. Spacecraft support equipment telemetry tests are included in Attachment B.

data word. However, with the requirement to provide a flexible main frame, thereby providing for selective data word examination in the experiments, it is more desirable to distribute the word enables on a one signal per wire basis. Thus, many different word enable input interfaces to a unit will result in digital output data appearing at the multiplexed output of the unit.

To generate the information required for the word enable generation and to control the RTM gating the following approach has been taken. The PCMC sends a serial nine bit word to the LIU on the baseplate where the particular digital data word is generated. This nine bit word is code converted to a 2 of 32 matrix in the same fashion as the op-codes of the command system are converted. Decoding of the word enable is performed in the same fashion (the speed is faster as the word rate is faster than the command rate) and the signal is distributed in the same fashion as a major logic level command. The information in Figure IV-24 for the logic level major mode command is exactly the same with the input signals coming from the PCMC in use instead of the decoder.

A separate nine bit word is sent to the RTM to be used for the data gate. This is required as many different nine bit words (decoded into digital word enables) are associated with a telemetry source unit which send data back via the same RTM gate. The information contained in the PCMC, either in ROM or Read/Write memory, has the capability of maintaining a word enable continuously for multiple adjacent eight bit words. This facility is used when the output digital data word is 16 or 24 bits long. Under these conditions, the RTM gate is similarly maintained in an ON condition.

When operating in the Read/Write mode, the PCMC automatically enters a "self dump" mode of operation of a periodic basis. This capability has been put into the system to ensure that data gatered while not in the ROM (fixed) main frame format can be identified if examined in other than real time.

(4)   COMMAND DUMP

As was noted in the discussion of command flow, the command memories are equipped with a dump facility. This dump is not automatic but is performed in response to a command. When a command memory is dumped, selected words in the PCM main frame are pre-empted. The words selected for this function will exclude sync, time code, command verification, and a word in the main frame identifying whether the PCM data is ROM or Read/Write controlled and whether a memory dump is in process. The number of words selected for preemption is 32 which, when de-commed at the receiving site in real time resulted in an effective 4k bps data rate which is compatible with the minimum station to OCC long line bandwidth.

Routinely, only one PCMC will be in operation at a time. The redundant PCMC will either be in a power OFF state or will be in a quiescent mode. This quiescent

mode is provided to preclude destroying the contents of the R/W memory should it be desired for subsequent use.

5.   OFF LINE CENTRAL PROCESSOR

Included in the design of the C&DH subsystem are interface terminals to permit a central processor to be added to the spacecraft complement. The objective of this function is to evaluate the capabilities of the processor as regards growth potential in capability for the system. The configuration of the system is such that the off line processor, if it is flown, can behave like a command memory, and/or replace the PCMC programming and control function. In addition, the processor will have interface capability to examine both the PCM output data stream and, by using the PCMC which is not in use, independently access the telemetry points of the experiments to perform diagnostics and adaptive control operations. The configuration of the system is such that this may be done in parallel with or in place of the routine PCM function.

To provide this evaluation capability, the LIU's include logic to permit the processor to access the command memory function and the PCMC function as well as providing a means of establishing the I/O trunk on either of the two spacecraft baseplates. This latter facility is provided to permit installation of the processor into the spacecraft on either baseplate well into the spacecraft integration program.

H.   SOLAR POINTING SUBSYSTEM

The Solar Pointing Subsystem (SPS) is designed to support and provide solar orientation for the EUVS experiment to enable this instrument to perform solar measurements in the extreme ultra-violet region. The SPS is comprised of 2 units, as 2-axis az-el gimballed platform mounted within the spacecraft adapter section and an ancilliary electronics package located on the spacecraft lower baseplate. The functions of the SPS are to:

- Acquire the sun from initial error of up to 360° in azimuth and 85° in elevation within 30 seconds.

- Track the center of the sun to within 1 minute of arc, rms in both axes.

- Provide an offset pointing capability in any one of 256 positions (16 x 16 matrix) enveloping the solar disk.

- Provide a raster scan of these positions at a step frequency of 1 per 2 seconds.

- Provide a one-dimensional scan over 16 positions in either elevation or in a direction normal to the elevation plane.

- Furnish electrical and mechanical interfaces between the experiment and the electronics package.

The platform consists of two gimbals, one providing azimuth rotation, the second, which supports the experiment, providing elevation rotation. Each are driven by brushless dc motor servos under the control of sun sensors mounted on both the platform and the experiments. The outer gimbal contains the azimuth bearings, brushless torque motor, brushless resolver, position potentiometer and slip rings. The minor gimbal contains the elevation bearings, a brushless limited angle torque motor, a polytwist flexible cable unit and a linear position potentiometer.

Sun sensors mounted on the platform provide coarse error information for azimuth acquisition. Coarse elevation is obtained by command from the spacecraft command memory. When the platform optical axis falls within 4-1/2 degrees of the center of the sun, a "target eye" transfers control to two sets of "fine eyes", or limited field of view, mounted on the instruments. In this fine mode the error is reduced to 1 are minute. To achieve offset pointing or raster scan, the eyes will be biased electrically to pre-calibrated levels under the control, in the latter case, of a read-only memory module located in the spacecraft logic interface unit.

Commands furnished by the spacecraft include one power command, possibly one major mode pulse command and a minor mode word indicating desired offset pointing position (8 bits) and initial elevation (4 bits). Telemetry includes azimuth and elevation shaft positions, fine eye error signals, motor currents and selected status signals. The azimuth drive assembly contains 40 slip rings dedicated to experiment/spacecraft interface functions.

MAGNETIC FIELD MAPPING PROGRAM

A computer program was written to generate the magnetic field maps presented in Section III.D. The program calculates the magnetic flux at a point due to a number of permanent magnets or electromagnets.

The model is based on the following assumptions:

a. The magnetic field is static

b. The magnets creating the field can each be represented by a pair of magnetic charges

c. The permeability of the space is that of free space. (No ferromagnetic materials are present other than the magnets.)

The magnetic potential (V) due to a single magnetic charge can be described by:

$$V = \frac{m}{r}$$

where: m is the magnetic strength in poles

r is the distance from the pole to the test point in centimeters.
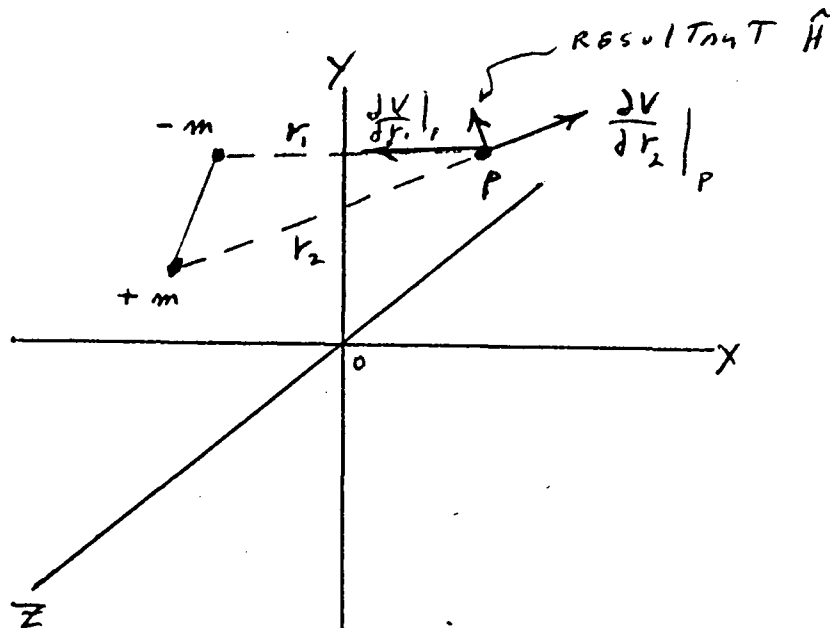
The magnetic field (H) is calculated from V by:

$$\overline{H} = - \text{grad } \overline{V}$$

In cartesian coordinates:

$$\hat{H} = \begin{bmatrix} - \dfrac{\partial V}{\partial x} \\[2mm] - \dfrac{\partial V}{\partial y} \\[2mm] - \dfrac{\partial V}{\partial z} \end{bmatrix}$$

$$V = \frac{m}{\sqrt{x^2 + y^2 + z^2}}$$

$$H = \begin{bmatrix} m\,x \\ m\,y \\ m\,z \end{bmatrix} \cdot \frac{1}{(x^2 + y^2 + z^2)^{3/2}}$$

Super position holds here since the equations are linear, therefore the H vectors due to each magnetic charge can be added together to get the total magnetic field.

The magnetic flux (B) is:

$$\overline{B} = \mu_0 \hat{H}$$

where μ_0 is the permeability of free space. In the CGS system μ_0 is unity.

The H or B vector is calculated and printed out in the cartesian S/C coordinates along with the absolute magnitude. Also, the vector is printed out in coordinates tangential and normal to the S/C sides, i.e., rotating the axes $\emptyset$ degrees about the Z axis where:

$$\emptyset = \tan^{-1} \frac{y}{x}$$

Thus
$$H_{rad} = H_x \cos \emptyset + H_y \sin \emptyset$$
$$H_{taw} = H_y \cos \emptyset - H_x \sin \emptyset$$
$$H_z = H_z$$

Program Usage

The program is presently stored on the AL/COM time sharing system. This program is interactive but uses system default files for the storage of input data.

The present file system set is as follows:

> File 1. Torquer configurations
>
> File 2. #2 Experiment magnetic data
>
> File 3. #3 Experiment magnetic data
>
> File 4. Test point locations

The program first accepts input data on the torquer file and experiment magnets files.

$$\text{Type A, } B_1, B_2, B_3$$

A is an integer referring to the torquer configuration in file 1 to be used.

B_1, B_2, B_3 are integers referring to those experiments magnets that are to be added to the torquer file.

Output Options

> Type 0 – asks for a test point location and prints the field at that point.
>
> 1 – asks for plot information for a radial search routine.
>
> > R_{max} – maximum radius of sweep from Z axis (in/cm)
> >
> > THI – angular increment of sweep in degrees
> >
> > Z – Z coordinate of search plane (plane always parallel to XY plane)
> >
> > H – magnetic field magnitude being searched for in the specified region.

2 - Prints out current input data.

3 - Prints field at those experiment locations listed in file 4. Type in 2 integers to specify the first and last experiment in file to be printed.

Numerical Data

Field intensity values given in Section III.D. of this report are based on the specific torquer locations shown in Table I. Also shown in the table are the strengths of the torquer dipoles in the "on" state. Table II and III list the actual combinations of dipole directions which have been analyzed.

TABLE I. TORQUER CONFIGURATIONS

1. Near-Polar Orbit (High Inclination)

   Torquer locations in cm. (end points of magnets)

	End 1			End 2		
	X	Y	Z	X	Y	Z
Momentum Torquer 1:	22.9,	-58.4,	51	22.9,	58.4,	51
Momentum Torquer 2:	-22.9,	-58.4,	51	-22.9,	58.4,	51
Attitude Torquer 1:	-28.9,	-25.4,	38	-28.9,	-25.4,	-38
Attitude Torquer 2:	-31.5,	-27.9,	38	-31.5,	-27.9,	-38

Magnitude of Torquer Dipoles ('on')

   Momentum:- 13 ATM^2
   Attitude:- 98 ATM^2

2. Near-Equatorial Orbit (Low Inclination)

   Torquer Locations in cm (End points of magnets)

	End 1			End 2		
	X	Y	Z	X	Y	Z
Momentum Torquer 1:	22.9,	-58.4,	51	22.9,	58.4	51
Momentum Torquer 2:	-22.9,	-58.4,	51	-22.9,	58.4,	51
Attitude Torquer 1:	22.9,	-58.4,	51	22.9,	58.4	51
Attitude Torquer 2:	-22.9,	-58.4,	51	-22.9,	58.4,	51

Magnitude of Torquer Dipoles ('on')

   Momentum:- 47 ATM^2
   Attitude:- 161 ATM^2

TABLE II. SOURCE CONDITIONS – POLAR ORBIT

Case A - Experiments off

    - Torquers on

    - Momentum Torquers   End 1 North

                                  End 2 South

    - Attitude Torquers   End 1 North

                                  End 2 South

Case B - Experiments off

    - Torquers on

    - Momentum Torquers   End 2 North

                                  End 1 South

    - Attitude Torquers   End 1 North

                                  End 2 South

Case C and D - Same as above but torquers off (with 2% of 'on' value in magnitude to represent the expected residual magnetism).

Case E - Experiments on

    - Residual Torquer Field (2%)

    - Momentum Torquers   End 1 North

                                  End 2 South

    - Attitude Torquers   End 1 North

                                  End 2 South

Case F - As in E except:

    Momentum Torquers   End 2 North

                                  End 1 South

Case G - As in E except:

    Attitude Torquers   End 2 North

                                  End 1 South

Case H - As in F except:

    Attitude Torquers   End 2 North

                                  End 1 South

TABLE III. SOURCE CONDITIONS - EQUATIOAL ORBIT

Case A1 - Experiments off

        - Torquers on

        - For all Torquers   End 1 North

                                           End 2 South

Case B1 - Experiments off

        - Residual Torquer field

        - For all Torquers   End 1 North

                                           End 2 South

Case C1 - Experiments on

        - Residual Torquer field as in B1

Case C1 - Experiments on

        - Residual Torquer field as in B1

Case D1 - As in C1 except Torquers reversed.

APPENDIX IV. A

POTENTIAL MODIFICATION TO WHEEL HORIZON SENSOR
PROCESSING ELECTRONICS

A. INTRODUCTION AND SUMMARY

A study has recently been conducted to examine the effects on performance at the high scanning rate (up to 400 rpm) employed on the AE spacecraft of certain modifications to the wheel mounted horizon sensor electronics. These modifications include peaking as previously employed on both the TIROS and NIMBUS programs, and dc restoration as employed on NIMBUS. The inclusion of these modifications in the sensor electronics can provide a better than two to one improvement in sensing accuracy (i.e., better than ±0.4 degree, 3σ in pitch), but at the cost of a decreased threshold to noise ratio and of added circuit complexity. The threshold to noise ratio, while less than that of the originally proposed sensor, is adequate for sensing in the CO_2, spectral region; the hardware impact - cost and complexity - remains to be evaluated.

B. DISCUSSION AND ANALYSIS

To provide pitch and roll/yaw information for attitude determination, two dc coupled CO_2 band horizon sensors, scanned by the flywheel mirror, will be employed. The sensors and electronics, as originally proposed, have an overall transfer function given by

$$G(S) = \frac{K}{(S + 333)(S + 1571)} \tag{1}$$

The frequency response of the sensor is shown in Figure 1.

Because of the narrow bandwidth of the sensor, the response is not as fast as is desirous, giving rise to significant errors due to earth radiance changes. Computer simulations were conducted of the sensor and electronics with different radiance extremes input on the sky/earth and earth/sky scan transitions. The resulting responses at the input to the threshold detector given in Figure 2 show the shift in the response from the hot/cold to the cold/hot transition. This shift results in a pitch attitude error of ±0.97 degree-commensurate with S/C specification pointing requirements of ±2.0 degrees in pitch.

Where greater sensing accuracy may be desirable, it therefore becomes desirable to shorten the response time of the sensor and reduce the susceptibility to radiance variations. It was found that this could be accomplished by including peaking and clipping in the sensor electronics. A block diagram of the resulting scheme is
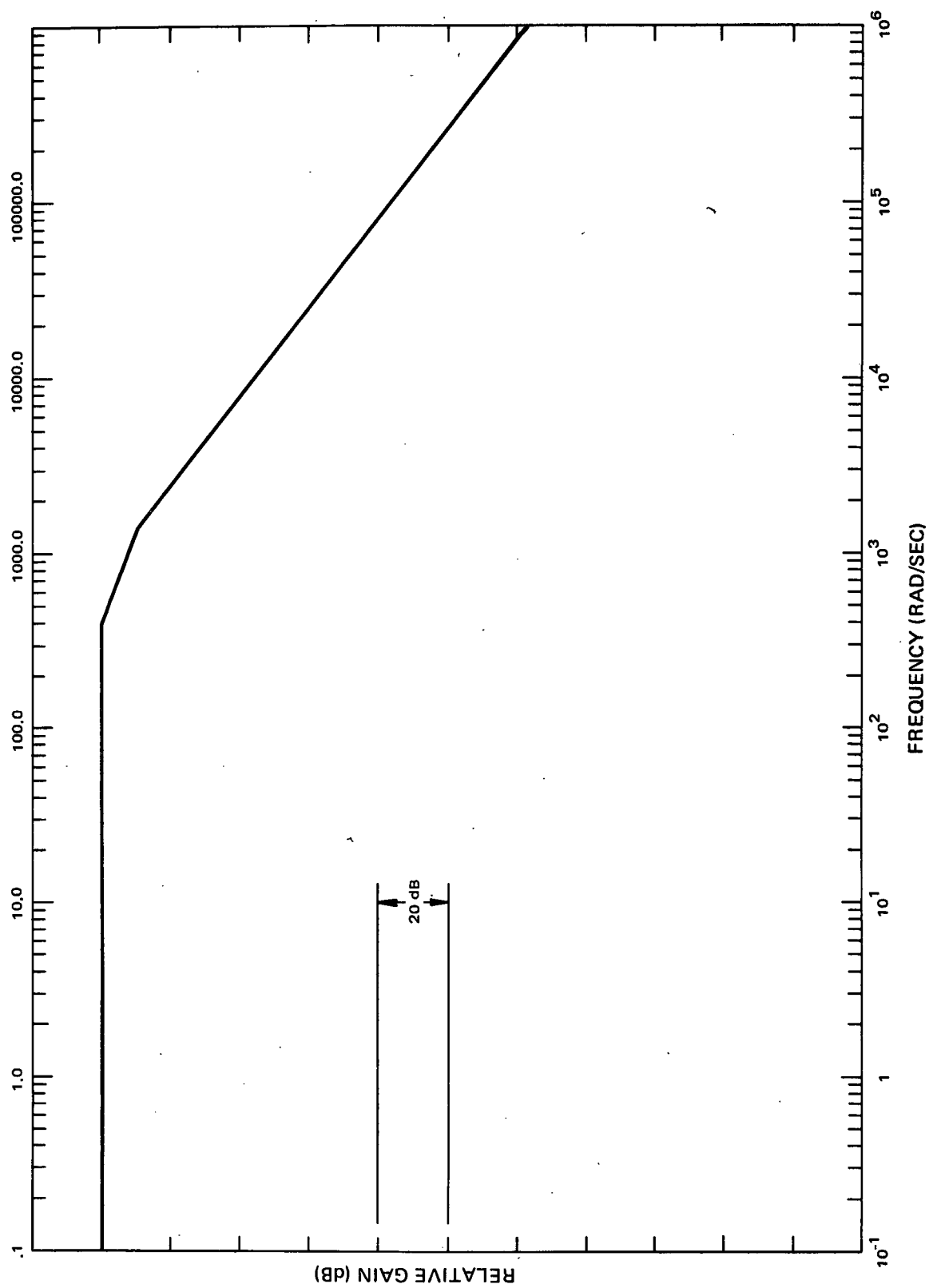
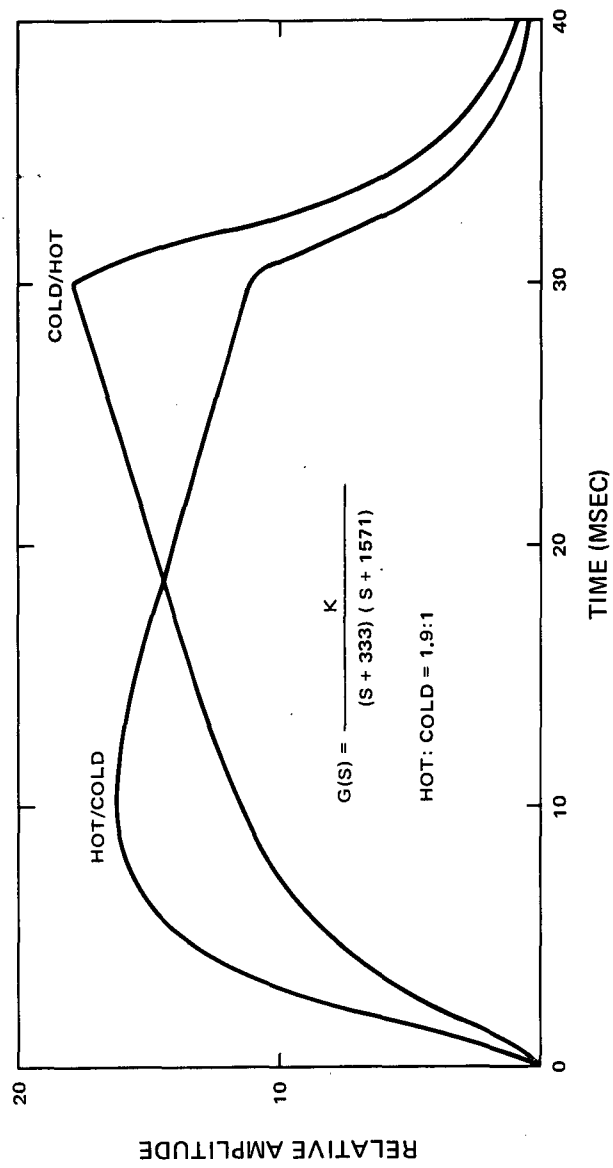Figure 1. Frequency Response – Originally Proposed Sensor

Figure 2. Response of Originally Proposed Sensor

shown in Figure 3. The dc restorer shown in the figure acts as a soft clamp to reference the signal to zero during the sky portion of the scan. Using this technique eliminates any possibility of clamping to the earth during capture, which might result from the use of a hard clamp triggered geometrically, while also minimizing the effects of 1/f noise at low frequencies. The transfer function for the modified sensor is

$$G(S) = \cfrac{KS^4 (S + 312) (S + 5 \times 10^5)}{\cfrac{(S +0.0142) (S^2 +0.485S +0.21) (S +0.5) (S + 400) (S +5.46 \times 10^3)^2}{(6 + 10^4) (S + 2 \times 10^4) (S + 2.4 \times 10^4) (S + 4.5 \times 10^4)}} \qquad (2)$$

which produces a frequency response as shown in Figure 4. By comparing Figures 1 and 4 it can be seen that the net result of the modified design is to extend the high frequency response to provide the desired faster response.

A digital simulation of the modified sensor was made to evaluate the response in terms of the radiance effect. Runs for a hot/cold and cold/hot transition were made which showed a reduction in the radiance error from ±0.97 degree to ±0.25 degree. The sky/earth edge responses of these simulations are given in Figure 5. The net effect is to reduce the overall pitch sensing error from ±1.0 degree to approximately ±0.4 degree, as will be shown below.

Naturally, by introducting peaking into the detection circuitry, noise becomes a major concern. Thus, an evaluation was made of the predictable threshold to noise ratio of the modified sensor electronics. For the evaluation, equation (2) was approximated by the transfer function

$$G(S) = \frac{3.74 \times 10^3 (1 + 3.2 \times 10^{-3}S)}{(1 + 10^{-4}S) (1 + 1.83 \times 10^{-4}S)^2} \qquad (3)$$

Utilizing Johnson noise and 1/f noise for the noise model, the threshold to noise ratio was determined to be approximately 7.5. By reducing the frequency of the double pole break at 870 Hz to 477 Hz, it was further determined that a threshold to noise ratio of 8.8 can be achieved with little degradation in the response. Additional work can be performed in this area if it is found desirous to further optimize the threshold to noise ratio. While these signal to noise ratios are an order of magnitude lower than that of the originally proposed sensor, they are adequate and will not produce excessive error (see Table 1).

With the modified sensor as configured in Figure 3, one potential problem area exists, namely that a low signal to noise ratio (approximately 1) at the input to the dc restorer may cause the restorer to clamp on noise rather than on zero. It is felt that this problem can be alleviated by removing the peaking amplifier from the location shown in Figure 3 and reinserting it after the dc amplifier.
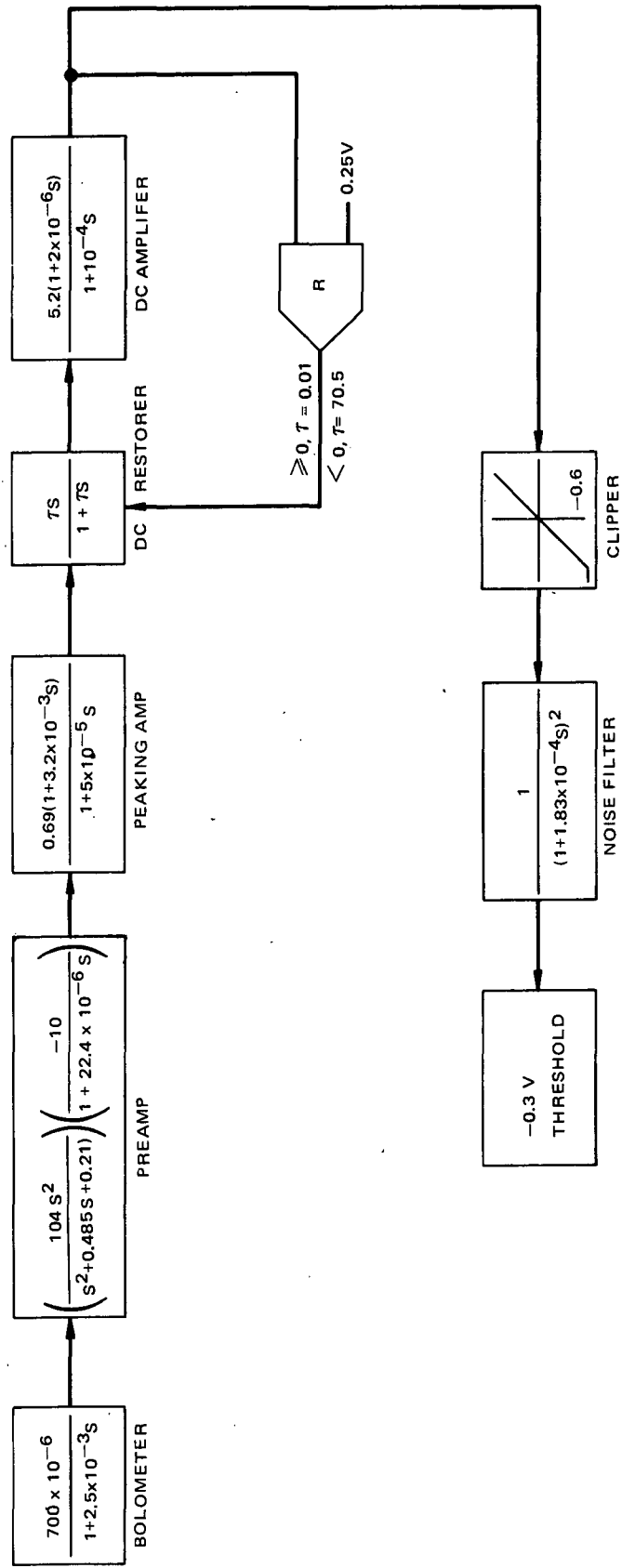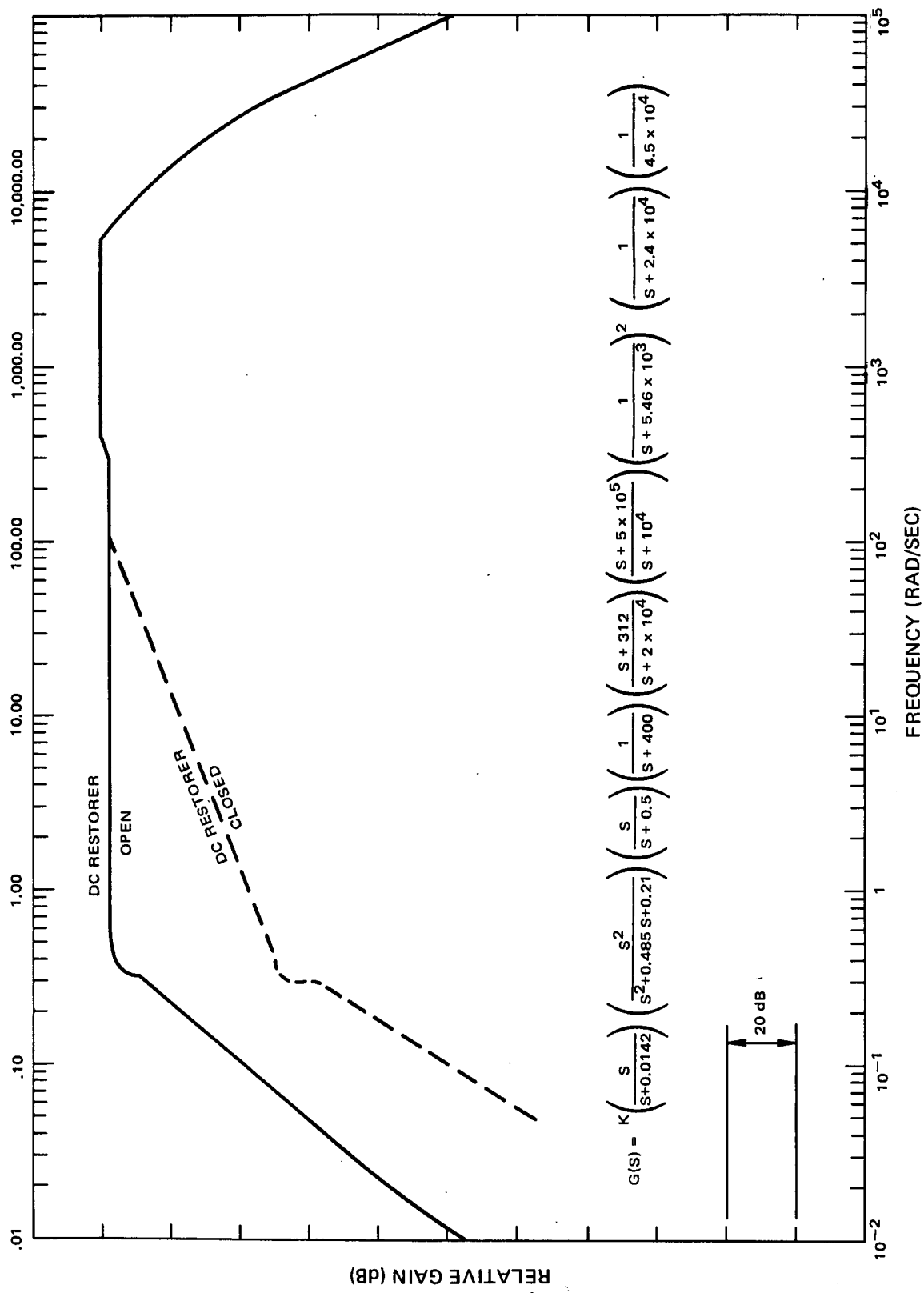
Figure 3. Revised Sensor Block Diagram

$$G(S) = K\left(\frac{S}{S+0.0142}\right)\left(\frac{S^2}{S^2+0.485\,S+0.21}\right)\left(\frac{S}{S+0.5}\right)\left(\frac{1}{S+400}\right)\left(\frac{S+312}{S+2\times10^4}\right)\left(\frac{S+5\times10^5}{S+10^4}\right)\left(\frac{1}{S+5.46\times10^3}\right)^2\left(\frac{1}{S+2.4\times10^4}\right)\left(\frac{1}{4.5\times10^4}\right)$$

Figure 4. Frequency Response – Modified Sensor
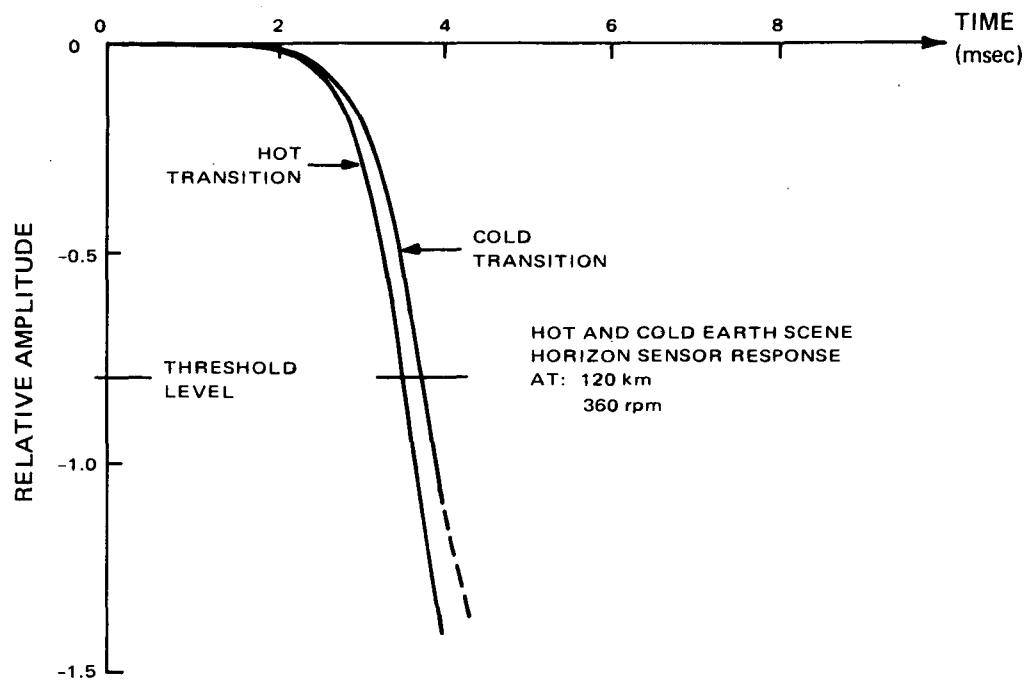
Figure 5. Modified Sensor-Sky/Earth Responses

TABLE 1

AE PITCH AND ROLL/YAW ATTITUDE DETERMINATION ACCURACY AT PERIGEE

	Error Source	Pitch	2 Sensors Roll	62° Sensor plus Altitude Roll
1	Alignment Uncertainty	0.050	0.032	0.011
2	Sensor Dynamics/Radiance	0.247	0.096	0.442
3	Wheel Speed Variation	0.021	0.002	0.006
4	Threshold Drift	0.013	0.073	0.024
5	Threshold Jitter*	0.024	0.133	0.043
6	CO_2 Horizon Variation	0.150	0.012	0.311
7	Hard Earth Calibration	0.1	—	—
8	Oblateness	0.174	0.1	0.370
9	Altitude Uncertainty	—	—	0.095
	RSS Summation	0.357	0.208	0.664

*Assumes Data Averaging

This is shown in Figure 6. The net effect is to increase the signal to noise ratio into the dc restorer without impairing the signal at the threshold detector. With this change, residual overshoot at the threshold detector does not appear to be a problem.

Utilizing the sensor configuration of Figure 6, an analysis was made of the attitude sensing errors at perigee. These errors are tabulated in Table 1. As is evident, the worst contributor to pitch attitude determination is still the effect of radiance variations. The largest roll contributors are due to noise and drift in the threshold circuitry.
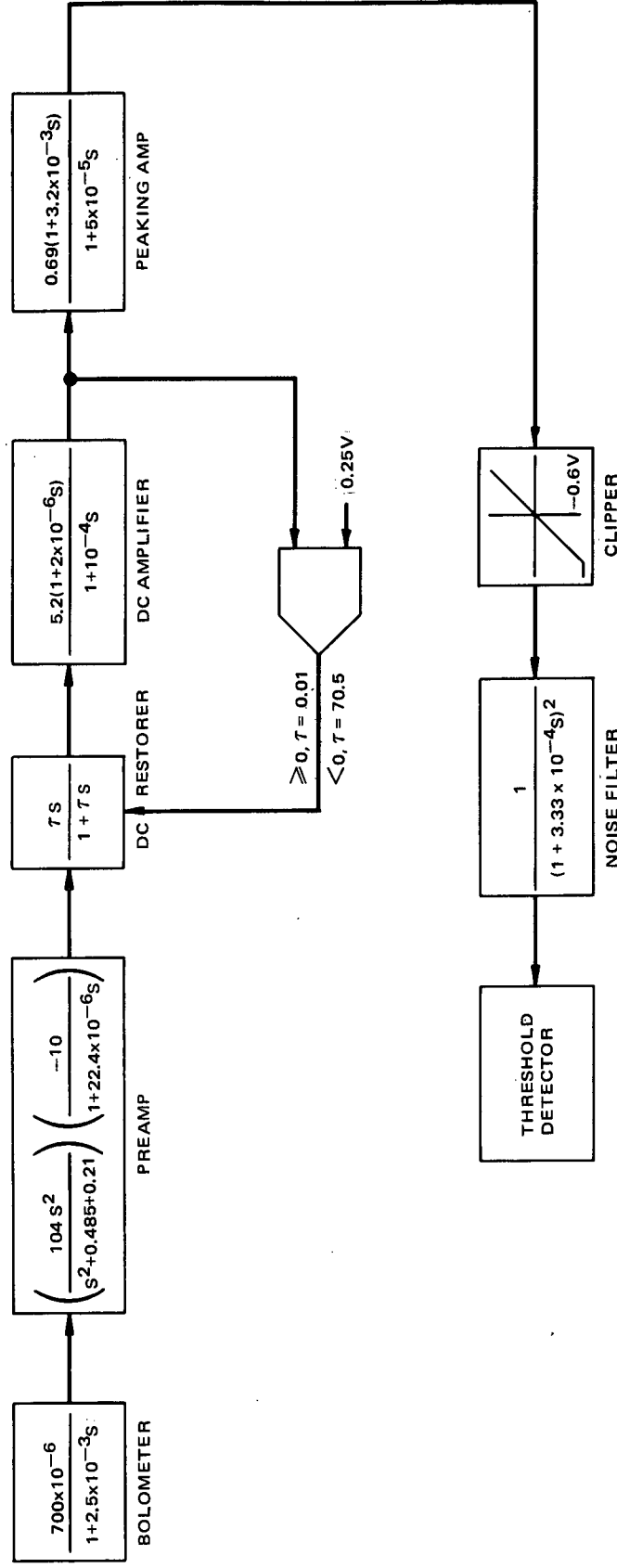
$$\frac{700\times10^{-6}}{1+2.5\times10^{-3}S}$$

BOLOMETER

$$\left(\frac{104\,S^2}{S^2+0.485+0.21}\right)\left(\frac{-10}{1+22.4\times10^{-6}S}\right)$$

PREAMP

$$\frac{\tau S}{1+\tau S}$$

DC RESTORER

$$\frac{5.2(1+2\times10^{-6}S)}{1+10^{-4}S}$$

DC AMPLIFIER

$$\frac{0.69(1+3.2\times10^{-3}S)}{1+5\times10^{-5}S}$$

PEAKING AMP

$\geqslant 0,\ \tau = 0.01$

$< 0,\ \tau = 70.5$

0.25V

$$\frac{1}{(1+3.33\times10^{-4}S)^2}$$

NOISE FILTER

−0.6V

CLIPPER

THRESHOLD DETECTOR

Figure 6. Alternate Electronics Configuration

PARAMETRIC STUDY OF BASEPLATE TEMPERATURE
PERFORMANCE AND DUTY CYCLE CAPABILITY OF THE
AE SPACECRAFT WITH BOTH PASSIVE AND ACTIVE CONTROL

1.0 INTRODUCTION AND SUMMARY

Information developed in the Interface Definition Study
indicates that the spacecraft design and mission constraints
(baseplate power distribution and minimum sun angle) on which
the tailored passive thermal design presented in the Phase D
Proposal is based, may no longer apply because of experiment
placement requirements and new ranges of mission orbit inclina-
tion angles (midrange, in addition to originally proposed near
polar and near equatorial). A universal (0 to 90° sun angle
range) thermal design is now indicated. In addition the
experiment accommodation requirements may lead to a baseplate
power distribution which is less favorable thermally than the
70 - 30% upper-lower baseplate distribution in the original
baseline design.

In order to evaluate the impact of these changes on the required
thermal design, an orbit average temperature study was performed
using the following items as parameters:

- coupling from upper baseplate-equipment complex to top
  (-Z surface)
- baseplate power distribution
- experiment duty cycle.

Results of this study indicate that passive control cannot pro-
vide adequate temperature margins for the equivalent max 30% -
100 w duty cycle and available end-of-life 19% - 100 w duty cycle
range* for the practical range of baseplate power distribution.
A reduction of the worst-case hot equivalent duty cycle to 6%
or less would be required to provide the necessary margin with
this type of control. On the other hand active control using
rotary shutter type devices driven by a heated bimetal spring
as described in Reference 1 will provide adequate temperature
performance at these limiting duty cycles with some margin

for changes in experiment aperture requirements. If the fraction of power dissipation on the upper baseplate is greater than 60%, additional duty cycle capability under worst case hot conditions can be obtained.

2.0 DISCUSSION

2.1 The Analytical Model

A relatively detailed 24 node analytical model was used for this analysis. The nodes are identified in Table 1. Internal radiative couplings were selected to give as nearly as possible, balanced temperature conditions at 0° and 90° sun angles. The magnitude of coupling between the upper baseplate and the top is one of the study parameters since this coupling controls the spacecraft temperature level and is the means of temperature control with the ATC. The couplings from the top to the side insulation and the momentum wheel support will also vary directly with this parameter. An average effective emittance of .02 is taken for all insulation between the spacecraft internals and the solar arrays except that between the lower BP-equip complex and the side array. This insulation has a larger effective emittance to provide the necessary coupling for control of the temperature difference between the two baseplates. The couplings used in this model are relatively close to optimum values.

2.2 Spacecraft Power Profile

The profile used as a baseline in the Phase B/C study was based on a total experiment power during the record cycle of 100 watts. The updated profile used in this analysis is based on later information available from the Interface Definition Study. The principal differences between this updated power profile and the baseline, is an increase in total experiment power during the record cycle to 123 watts*,

---

*Subsequent to the analysis estimates have been reduced to approximately 115 watts, see Section IV.5.

TABLE 1.   IDENTIFICATION OF NODES IN ANALYTICAL MODEL

NODE NO.	DESCRIPTION
1	Upper baseplate - equipment complex
2	Lower baseplate - equipment complex
3	Propellant tanks
4	Momentum wheel drive
5	Support - momentum wheel drive
6	Center column
7	Lower column & adapter
8	Solar EUV experiment
9	Solar EUV exp - gimbal platform
10	Accelerometer pkg.
11	Exposed interior surface of side array insulation above upper BP equip complex
12	Lower surface of insulation over lower BP equipment complex
13	Momentum wheel
14	ATC hub
15	ATC bi-metal drive
16	Side array above upper BP equip complex
17	Side array upper BP equip complex to belt antenna
18	Side array belt antenna to lower BP equip complex
19	Side array below lower BP equip complex
20	Bottom Array
21	Top
22	Momentum wheel mirror
23	Belt antenna + side non-cell area
24	Shield - Solar EUV experiment

2.3 Orbit Average Parametric Analysis

2.3.1 Power distribution parameter

The temperature performance as predicted in the Phase D proposal was based on a distribution of total baseplate power dissipation of 70% on the upper BP and 30% on the lower. Latest IDS information indicates that balance and experiment placement requirements will probably not permit a distribution this favorable. A more likely distribution now appears to be one with 50% to 60% of the total baseplate dissipation on the upper baseplate. In order to evaluate the effect of this parameter, values from 70% to 40% on the upper BP were used in the analysis.

2.3.2 Duty cycle parameter

The nominal specified (S-620-P-1) beginning of life duty cycle is 30% based on a total experiment power of 100 watts. At the end of the mission this magnitude of duty cycle will not be attainable at certain sun angles due to array power availability. Worst case cold temperature conditions will occur for some combination of sun angle and array power availability. In the original baseline design, the estimated minimum available experiment duty cycle with the given internal power profile was 19% which occurred at a 90° sun angle. This was the worst case cold condition for a 'tailored' thermal design since the minimum sun angle for the two missions considered (near polar and near equatorial) was 15°. A mid-range (63°) inclination mission is now planned in which the entire sun angle range of 0 to 90° can occur. This will require a universal thermal design, with worst case cold conditions now occuring at a 0° sun angle. The end of mission power availability at this sun angle is estimated to be approximately the same as that for the 90° sun angle. The worst case hot sun angle is 45° where sufficient power will always be available to maintain the equivalent of the 30% - 100 watt duty cycle.

In order to determine the effect of varying the duty cycle, a wide range of duty cycles from 0 to 50% was used in the analysis.

2.3.3 Coupling parameter

Active temperature control would be accomplished by varying the coupling between the upper BP equipment complex and the top using 4 rotating shutter devices as described in Ref. 1. The range of coupling variation which could be accomplished by these devices is as follows:

Effective emittance of area not covered by shutter	Coupling in^2		Ratio Max/Min
	Min	Max	
.05	55	275	5
.9	368	590	1.6

In the parametric analysis a range of values for this coupling from 100 to 500 in^2 was used. This range embraces that required for temperature control with ample margins at both open and closed conditions.

2.4 Results of Parametric Analysis

2.4.1 Temperature vs coupling

Figures 1 and 2 present temperature vs coupling curves, for various values of the power distribution and duty cycle parameters, at worst case hot (45°) and cold (0°) sun angle conditions. Information can be obtained from these curves for determination of temperature performance, and thus temperature margin, with various values of power distribution for both passive and active control.

Temperature margin is the difference between the orbit average temperature and the required maximum or minimum operating temperature. For the two baseplates these operating temperature limits are:

Condition	Temperature Limits $^\circ C$	
	Upper BP	Lower BP
Hot	30	40
Cold	-5	-5

Figure 3 presents curves of worst-case hot vs worst case cold BP temperature margins for duty cycles of 26% (eq., 30% - 100w) and 10% (eq., 19% - 100w) for various values of BP power distribution for both passive and active control. For the type of analysis used (lumped orbit average for baseplates) a temperature margin of 10° at both hot and cold conditions is desirable to allow for:

- Baseplate location temperature variation
- Orbital temperature variation
- Analytical errors (coupling, difference between spacecraft and analytical model)
- Variation in surface and material properties and power dissipation from assumed values
- Probability of increase in size of experiment ports which will change effectiveness of insulation system.

It can be observed that this magnitude of margin cannot be maintained for the limiting duty cycles using passive control but is attainable within the range of expected baseplate power distribution with active control.

Figure 4 presents curves of temperature margin vs BP power distribution for equal margin at worst case hot and cold conditions with the previously discussed duty cycle limits for both passive and active control.

2.4.2 Duty cycle vs temperature margin

Figure 5 presents curves of worst case hot duty cycle vs temperature margin for various values of BP power distribution for both passive and active control. With active control and

an upper baseplate power distribution greater than 60% this margin is greater than 10° for the specified 26% (eq., 30% - 100w) duty cycle which indicates increased duty cycle capability over specification requirements. For a 70% upper BP distribution the duty cycle capability is increased to 30.5% (eq., 37.5% - 100w). Duty cycles vs BP power distribution curves are presented in Figure 6 which are based on a 10° margin at worst case hot and cold conditions.

2.5 Active Controller Operation

All performance data for active temperature control presented in Section 2.4 is based on the shutters being 100% open at worst case hot conditions and fully closed at worst case cold. This is readily achieved with the type of electronic controller actuating circuit proposed in Reference 1 since the operating bandwidth from closed to open is about 1^OC. In case of failure of the control circuit the bimetallic spring would be actuated by radiation from the upper BP but a change of baseplate temperature of 24° would be required to move the shutter from the closed to open position. If the controller were set to begin opening at an upper BP temperature of 5^OC it would be fully open at an upper BP temperature of 29^OC. A curve of coupling to top vs upper BP temperature for this condition is included in Figure 1 for the 60 - 40 power distribution at worst case hot conditions. The temperature margin for the specified 26% duty cycle would be:

- upper baseplate - 11^OC
- lower baseplate - 6^OC

In order to reestablish the 10° margin the duty cycle would have to be cut back to 20% (eq., 24% - 100w).

REFERENCE

DN-505-4.5(AE), "Atmosphere Explorer Active Temperature Control System", R. Scott, 7 July 1971

FIGURE I
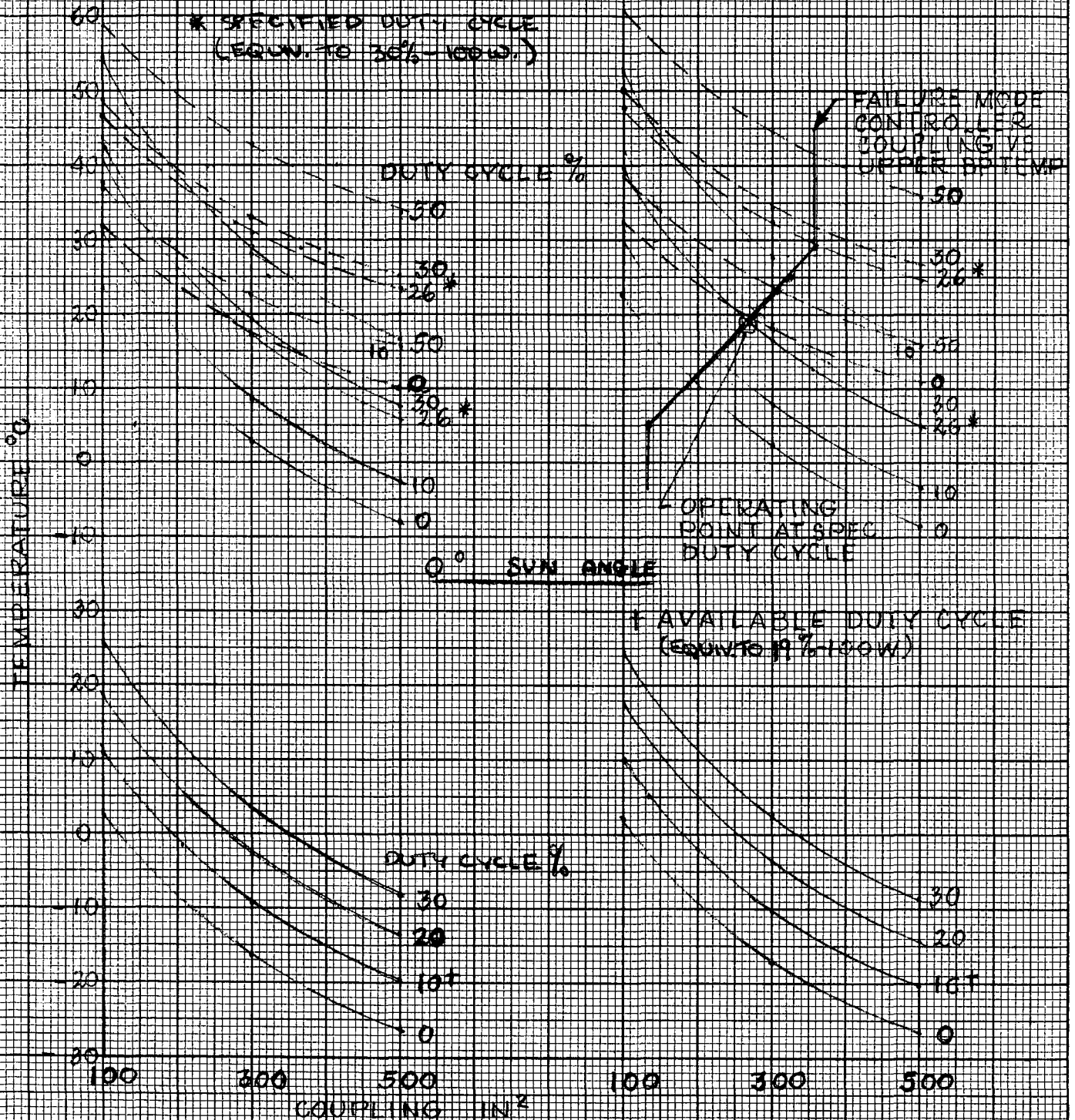BASE PLATE TEMPERATURE VS COUPLING FROM UPPER BP TO TOP FOR WORST CASE HOT & COLD SUN ANGLES
— UPPER BP
— — LOWER BP

FIGURE 2
BASEPLATE TEMPERATURE VS COUPLING FROM UPPER BP
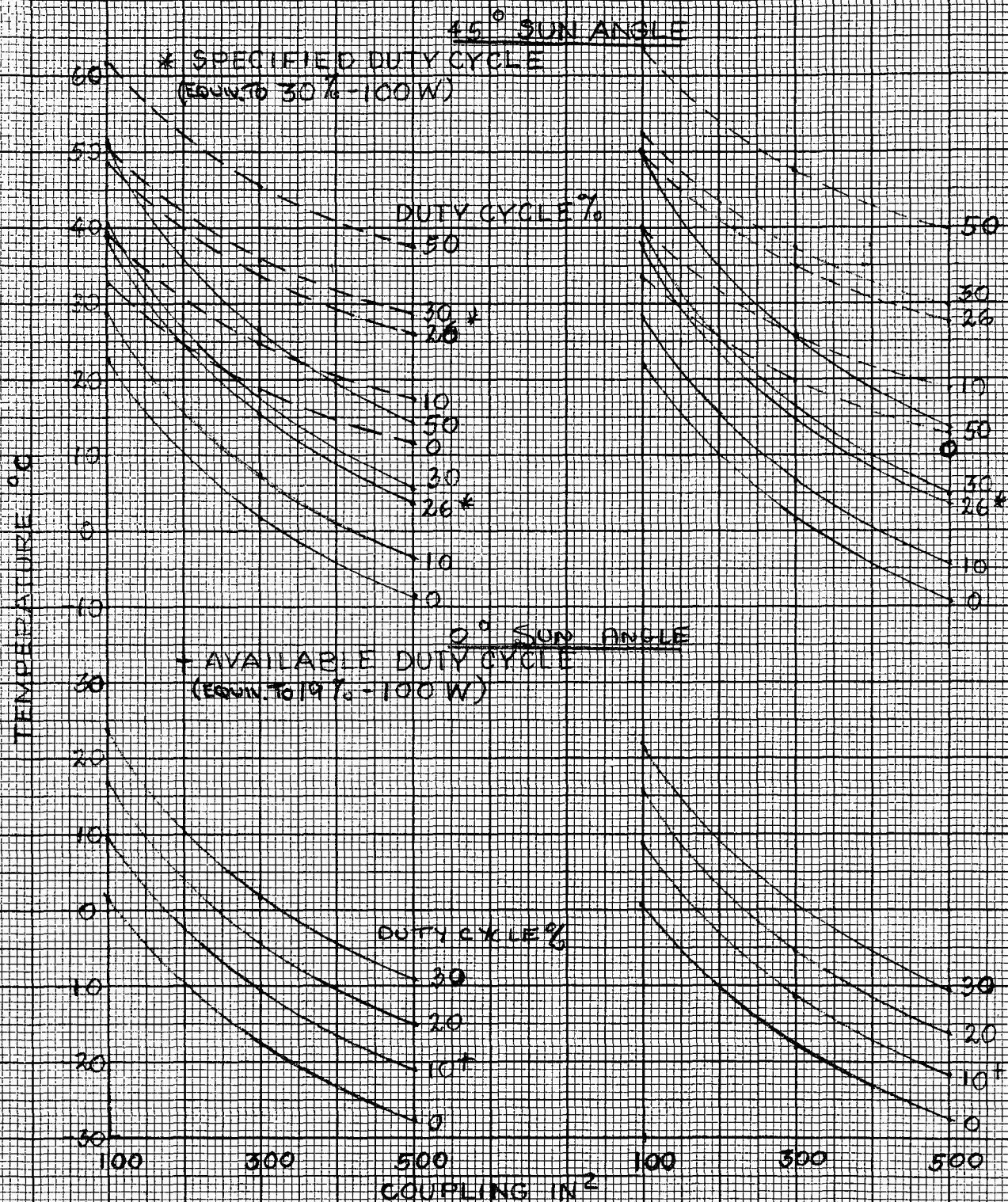TO TOP FOR WORST CASE HOT & COLD SUN ANGLES
—— UPPER BP
— — LOWER BP

FIGURE 3

WORST CASE HOT ORBIT-AVERAGE BASE PLATE TEMP MARGIN AT SPECIFIED DUTY CYCLE (EQ 30%-100W) VS. W/C COLD MARGIN AT AVAILABLE DUTY CYCLE (EQ 19%-100W) WITH PASSIVE AND ACTIVE CONTROL

NOTE: COUPLING CAN BE ADJUSTED TO IMPROVE MARGIN AT ONE END OF RANGE AT THE EXPENSE OF THE OTHER.
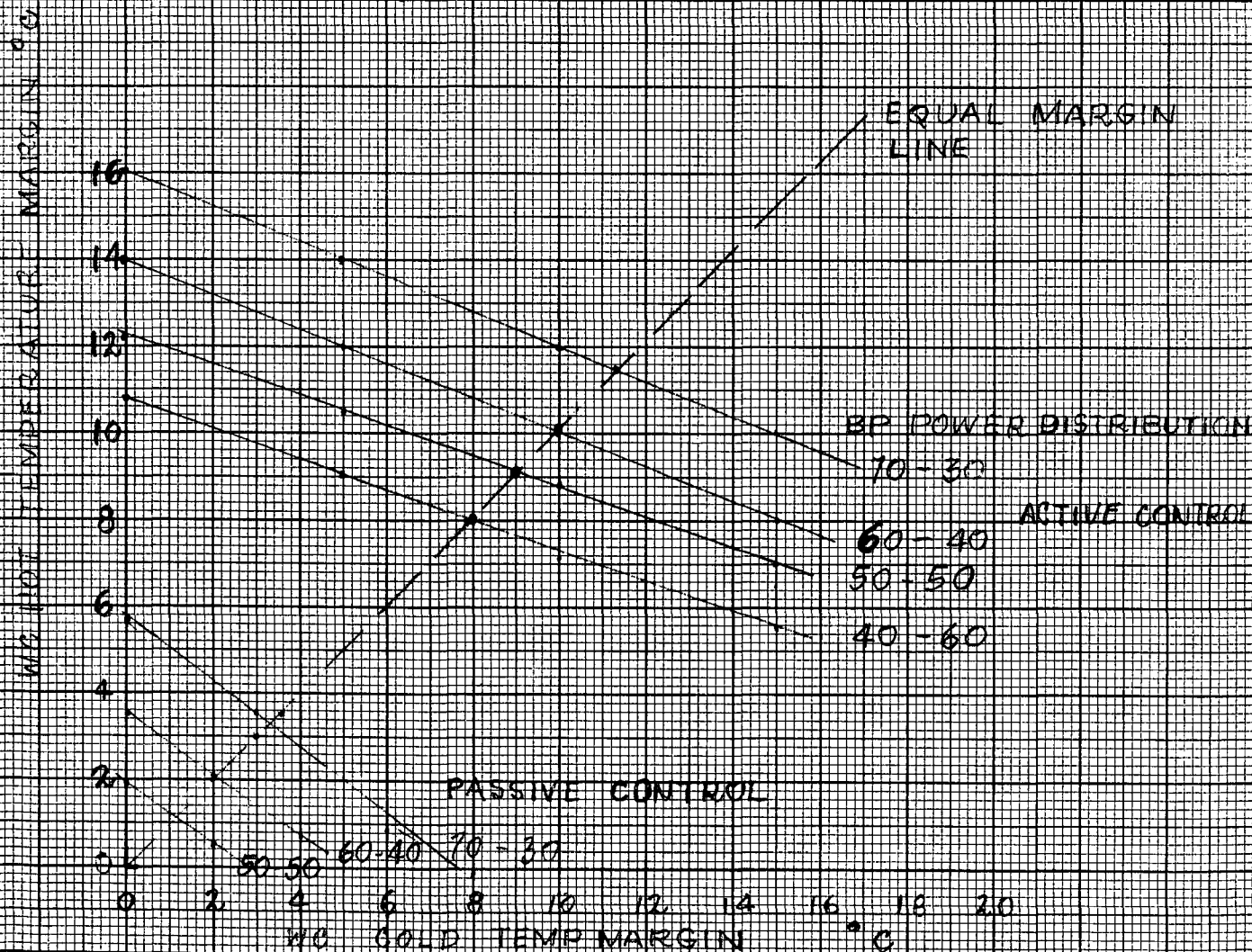
FIGURE 4

ORBIT AVERAGE BASEPLATE WC HOT & COLD TEMPERATURE
MARGIN VS % POWER DISTRIBUTION ON UPPER BP
FOR EQUAL MARGIN AT WORST CASE HOT AND COLD
CONDITIONS
— — PASSIVE CONTROL
— ACTIVE CONTROL

TEMPERATURE MARGIN °C

% BP PWR DISSIPATION ON UPPER BP
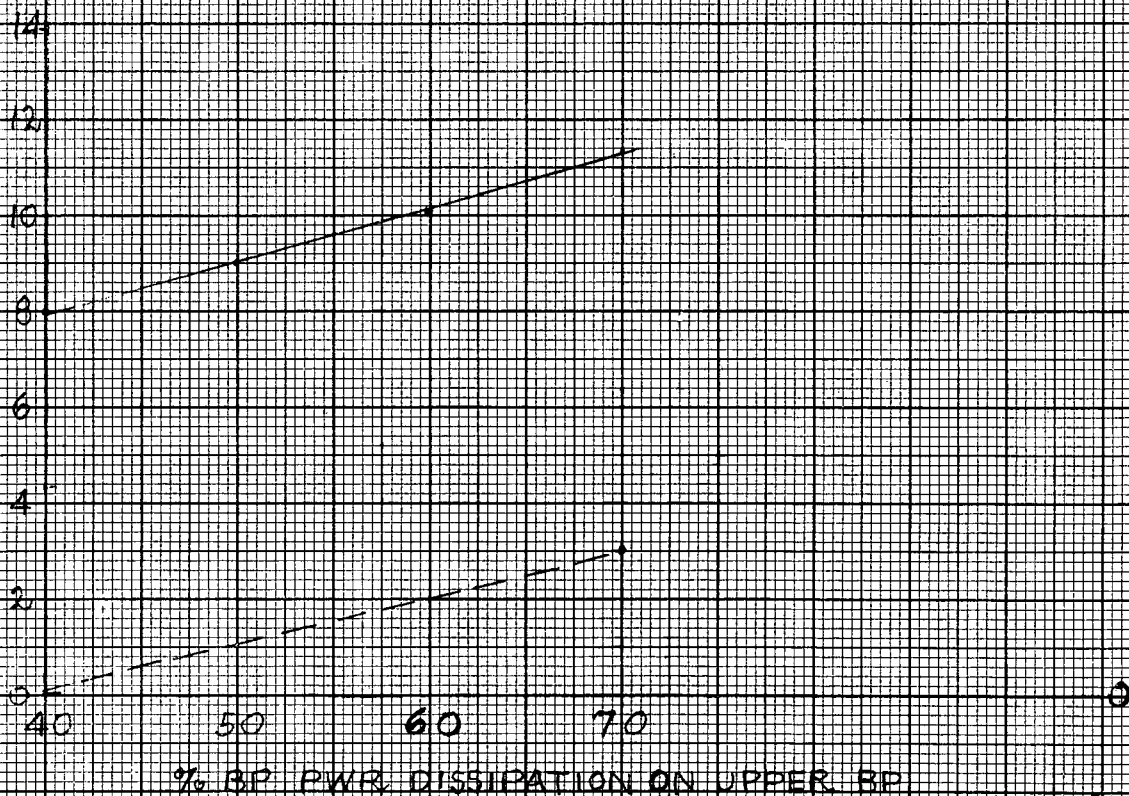
FIGURE 5
WC HOT DUTY CYCLE VS TEMPERATURE MARGIN, FOR EQUAL
HOT & COLD CONDITION MARGINS, FOR PASSIVE AND ACTIVE
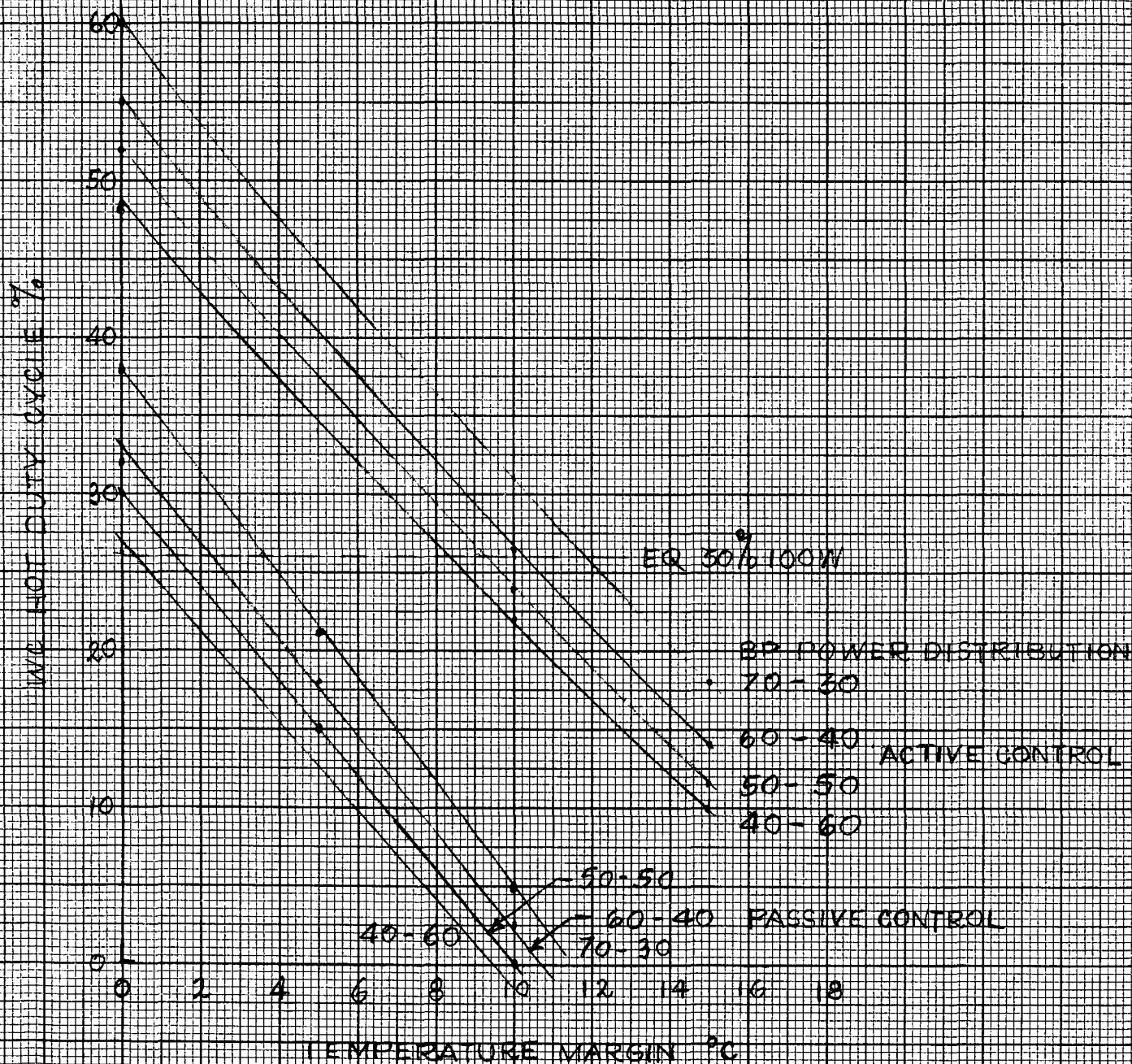CONTROL

WORST CASE COLD DUTY CYCLE 10% (EQUIV TO 19% 100W)

EQ 50% 100W

BP POWER DISTRIBUTION
70 - 30
60 - 40   ACTIVE CONTROL
50 - 50
40 - 60

50 - 50
60 - 40   PASSIVE CONTROL
40 - 60   70 - 30

WC HOT DUTY CYCLE %

TEMPERATURE MARGIN °C

FIGURE 6
WORST CASE HOT DUTY CYCLE VS % TOTAL BP POWER
DISSIPATION ON UPPER BP WITH A 10°C TEMPERATURE
MARGIN AT WORST CASE HOT AND COLD CONDITIONS
WORST CASE COLD DUTY CYCLE 10% (EQUIV. 19% - 100W)
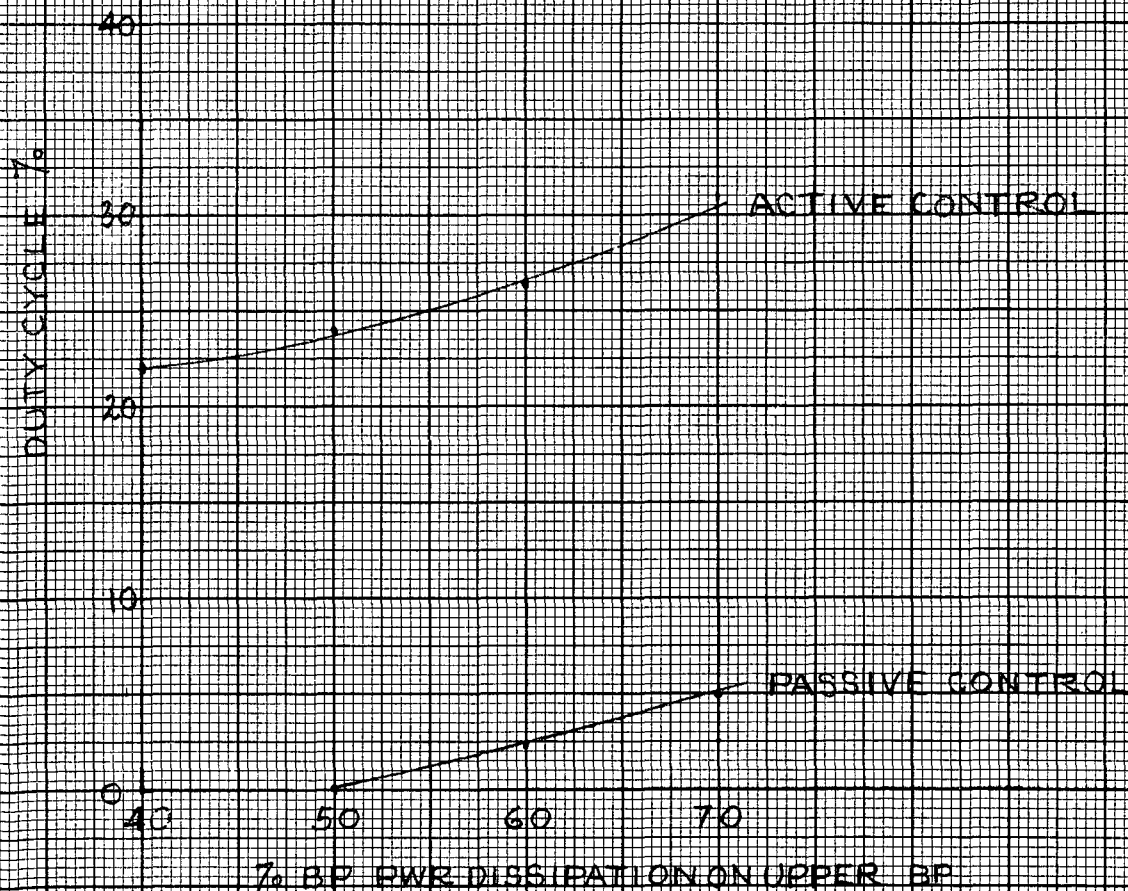
AMPERE-HOUR METER

1.0 GENERAL

The Ampere Hour Meter performs the integration of battery current to provide an accurate indication of the "state of charge" of the battery. Battery recharge ampere-hours are used to cancel discharge ampere-hours. Correction of battery efficiency as a function of battery temperature is also provided. The system capacity relative to 100% depth of discharge is 18 ampere hours, however the inherent surplus capacity of the up-down counters used provides registration up to 655.35% before overflow occurs. The system operates over a current range of 100 mA to 10 amperes with the charge/discharge ratio adjustable from 1.04 to 1.50. Two telemetry signals are developed by the system. One channel indicates the state of charge in percent with 100% equivalent to 18 ampere hours. The second channel indicates peak depth of discharge in percent with 100% equivalent to 18 ampere hours.

1.1 AMPLIFIER

A block diagram of the SOC system is shown in Figure 1. The battery current is resistively sensed and is amplified by the input amplifier to provide voltage V_c (which is scaled at 1.0 volts/ampere). Charge current provides a positive level for V_c; discharge a negative level. Current sense is detected and a direction control signal supplied to the counter, gain control network, and integrator.

1.2 C/D RATIO CONTROL

The gain control network applies a scale factor K to the analog current signal V_c and also generates an opposite polarity signal. The scale factor is fixed (0.5) for discharge currents and is adjustable from 0.48 to 0.33 to provide charge/discharge ratios of 1.04 to 1.50 for charge current. Variation of the scale factor in charge as a function of battery temperature provides temperature compensation of the C/D ratio.

The two outputs to the integrator are of equal value and opposite polarity; they each reflect the true current level and the desired C/D ratio information.

1.3 INTEGRATOR

The integrator converts the analog current signals ($\pm KV_c$) into ampere-hours (0.0018 ampere-hour per count). The integrator is unusual in that it
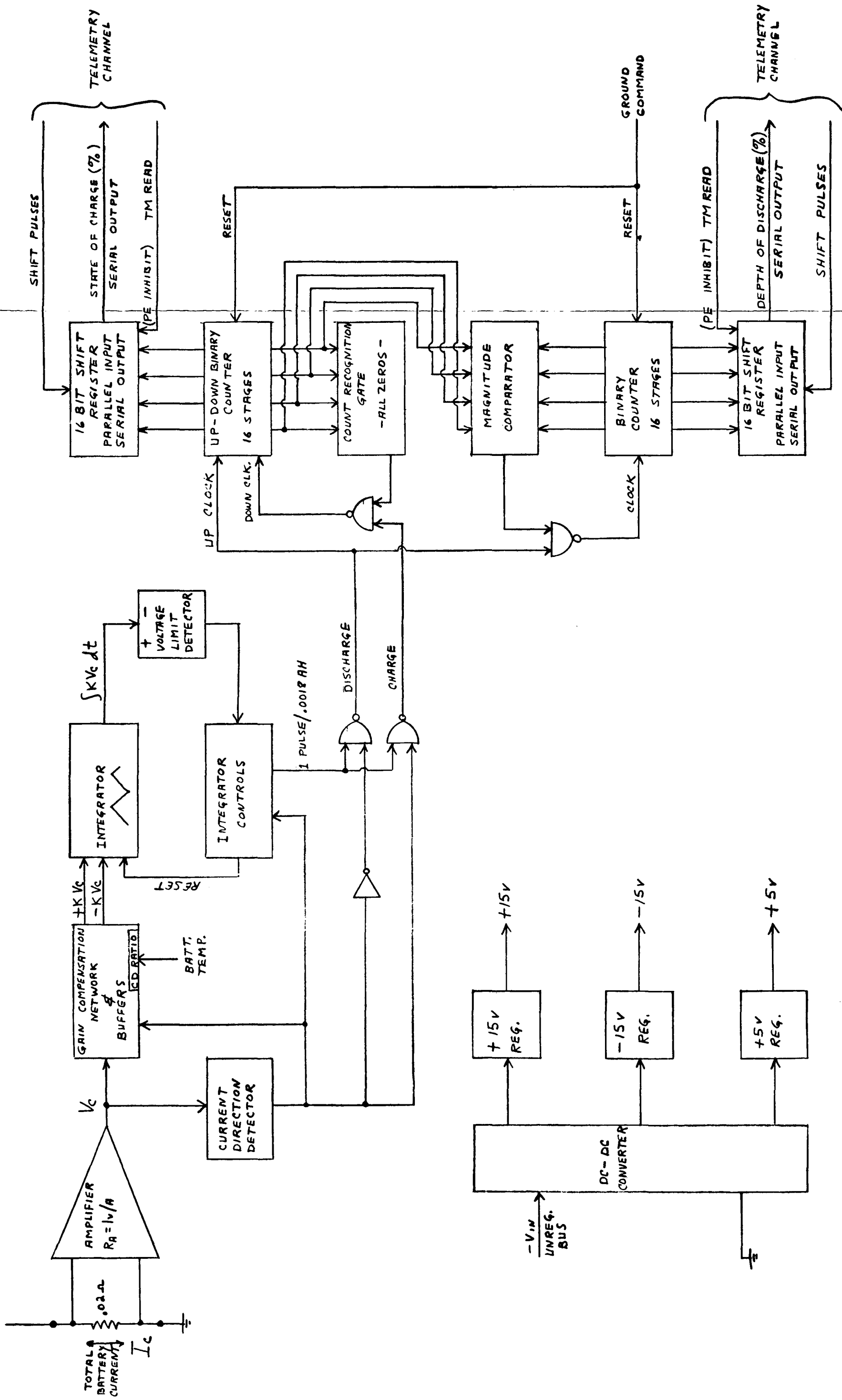
Figure 1. AE Battery State-of-Charge Monitor

FOLDOUT FRAME 1

FOLDOUT FRAME 2

does not reset in the conventional manner (i.e., discharge the capacitor to zero volts) but merely reverses direction. For example, the signal $-KV_c$ is integrated until the upper limiting voltage is reached. The limit detector signals the integrator controls which disconnect the $-KV_c$ input and connect the $+KV_c$ input causing the integrator output to ramp towards the lower limit where the direction and inputs are again reversed. Thus, the integrator output ramps between the upper and lower limits without resetting. Detection of one limit is used to supply a count pulse to the counters. This scheme has several advantages:

a. Voltage offset of the operational amplifier in the integrator adds to one input and subtracts from the other thereby tending to average out to zero over each integrator cycle.

b. Longer integrator periods are obtained for smaller capacitors and supply voltages. [1]

c. No errors are incurred due to the reset time of the integrating capacitor, and the potential problems of relay contact reliability are eliminated.

1.4 COUNTERS

The counts from the integrator (at 0.0018 ampere-hour per count) are fed to the counter logic which adds counts to the counter for discharge currents and subtracts counts from the counter for charge current. Thus, the system accumulates discharge ampere-hours which are cancelled out by charge ampere-hours (weighted by C/D ratio). When the counter returns to zero indicating the battery is fully charged, the counter is inhibited from counting below 0000. A reset command is provided to reset the system to 0000.

2.0 CIRCUIT DESCRIPTIONS (SELECTED)

2.1 AMPLIFIER

A highly stable, temperature compensated amplifier(μA 727) is used in the input amplifier to obtain the required accuracy. A μA 741 provides additional gain. Metal film resistors are used to obtain high stability. A μA 741 is also used as the current direction sensor with detection occurring at 0 $\pm$20 mA.

---

[1] For example, consider a μA 709 type amplifier with $\pm$15 volt supplies. A conventional integrator can only ramp from 0 to 12 volts before a reset is required (one cycle). The SOC integrator can ramp from -12 to $+12$ to -12 volts for one cycle (an effective ramp of 48 volts). Thus, only 1/4 the capacitance of the conventional integrator is needed.

2.2 INTEGRATOR (Reference Figure 2)

Normal and inverted analog current signals are applied through MOSFET switches (S1 and S2) to the input of the integrator (Z6). These MOSFET switches are driven by opposite sides of a flip-flop (Z9) so that only one input can be connected at any one time. The flip-flop is connected such that each time the positive or negative comparator (Z7 or Z8) detects the integrator output has reached the limit, the flip-flop changes state thus reversing the state of the MOSFET switches.

Thus, the input signal polarity reverses and the integrator ramps in the other direction. The direction of battery current flow in the 0.02 ohm shunt has no relation as to whether the integrator ramps up or down; the output of the integrator is a triangular wave rather than a saw tooth wave (conventional integrator with reset). The flip-flop is also controlled through its toggle input so that it changes state when the current through the shunt changes direction. The control gates also reverse the polarity of the integrator so that no change in state of the MOSFET switches occurs. Thus, the integrator will retrace itself thereby preventing ambiguous counts and cumulative errors.

One output of the flip-flop is also used to trigger the storage register which is an up-down counter. The direction sense of counter is controlled by the state of the current direction detector. Since the same electronics are used for both charge and discharge, effects of long term drift will not degrade accuracy over an orbital cycle of charge and discharge.

2.3 OPERATION OF THE INTEGRATOR CONTROLS

Assume switches are shown in Figure 2 and the integrator output reaches the upper reference and "gets" the flip-flop at T1-X. The output now begins to ramp down towards the lower limit.
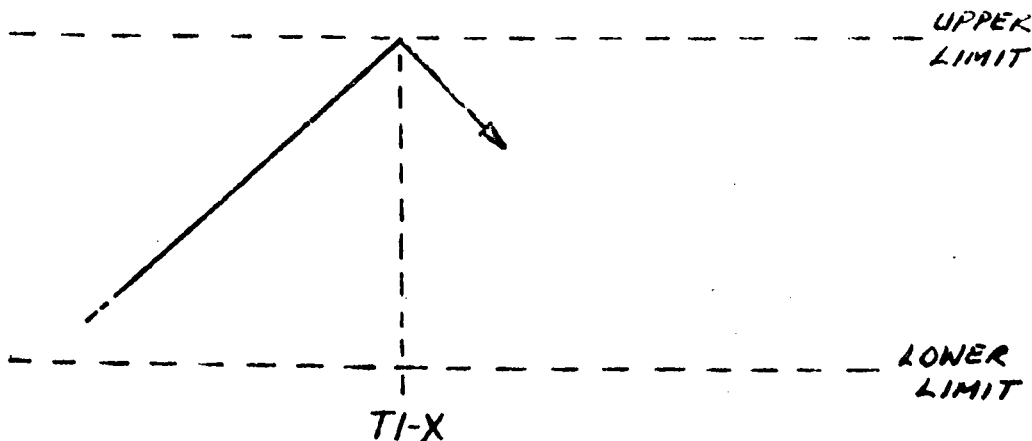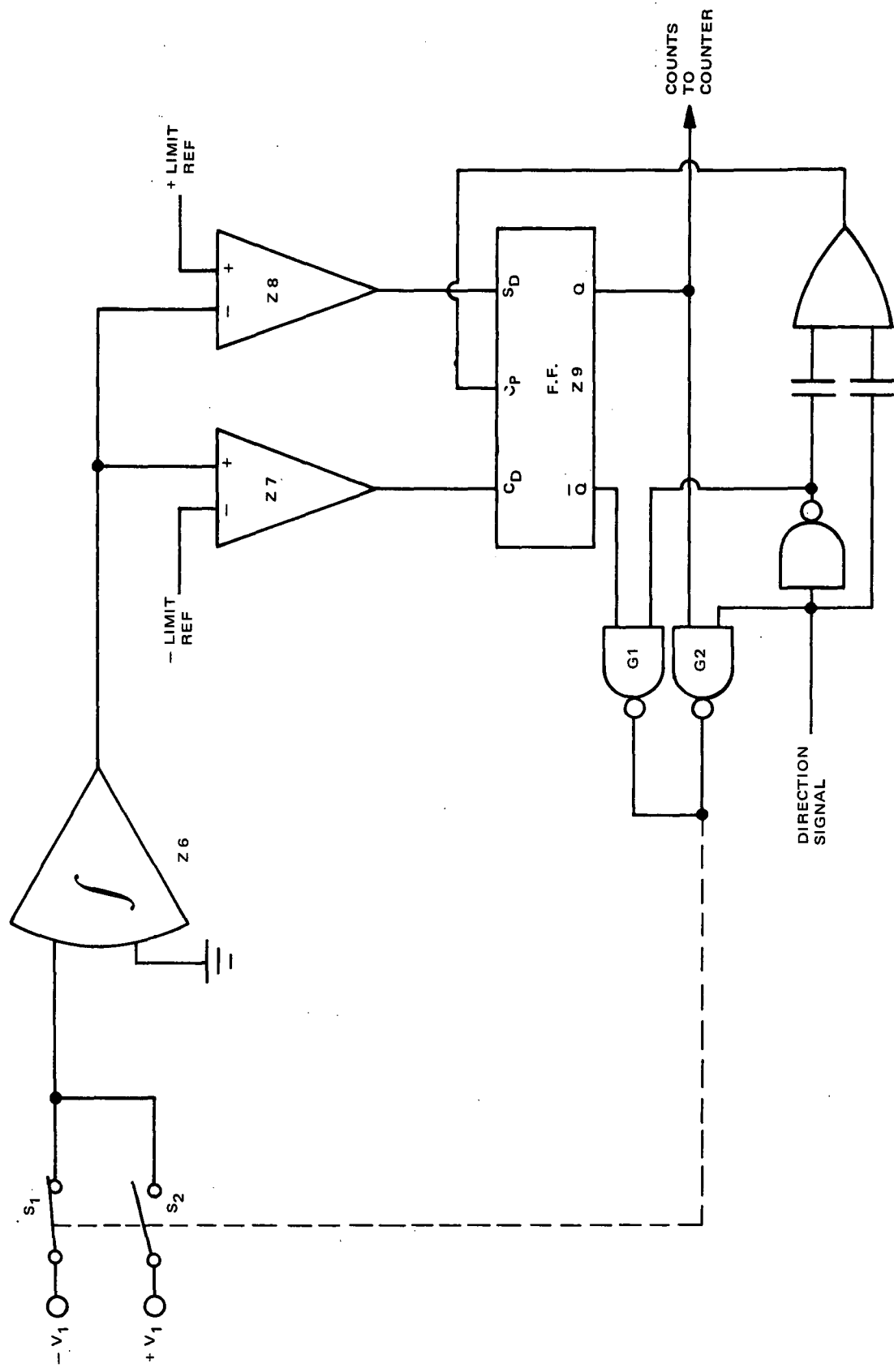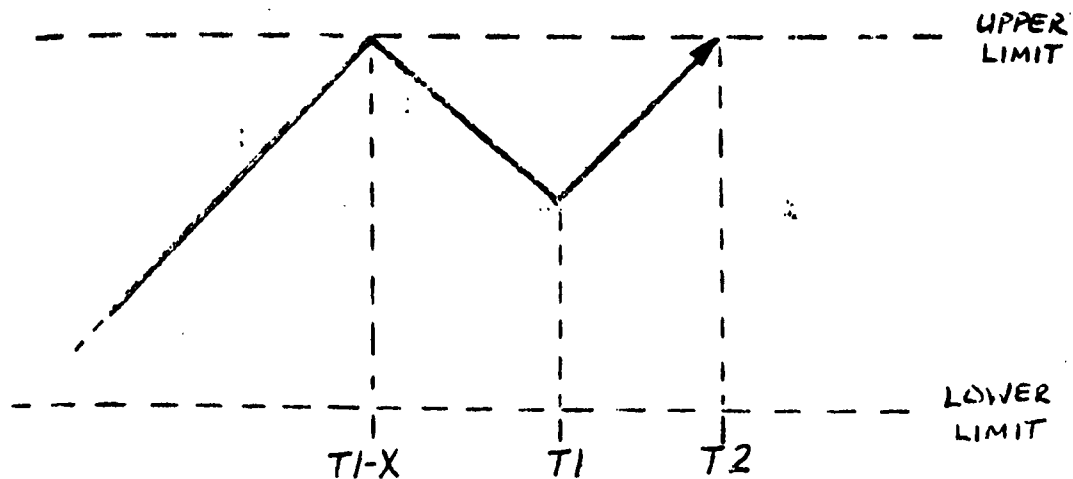
Figure 2. Integrator Controls

Assume the direction of current in the shunt reverses at time T1. With no change in the state of S1, S2, or the flip-flop, the integrator would reverse direction and approach point T2 (retrace previous integration).

When the integrator reaches the upper limit at time T2, the flip-flop cannot be "set" to reverse the states of S1 and S2 because it was previously "set" at time T1-X. Therefore, the sense of the integrator must be reversed. Gates G1 and G2 respond to a direction signal by reversing the gating of flip-flop Z9 to the switches S1 and S2. Now, with S1 open and S2 closed, the integrator will continue to ramp towards the lower limit.
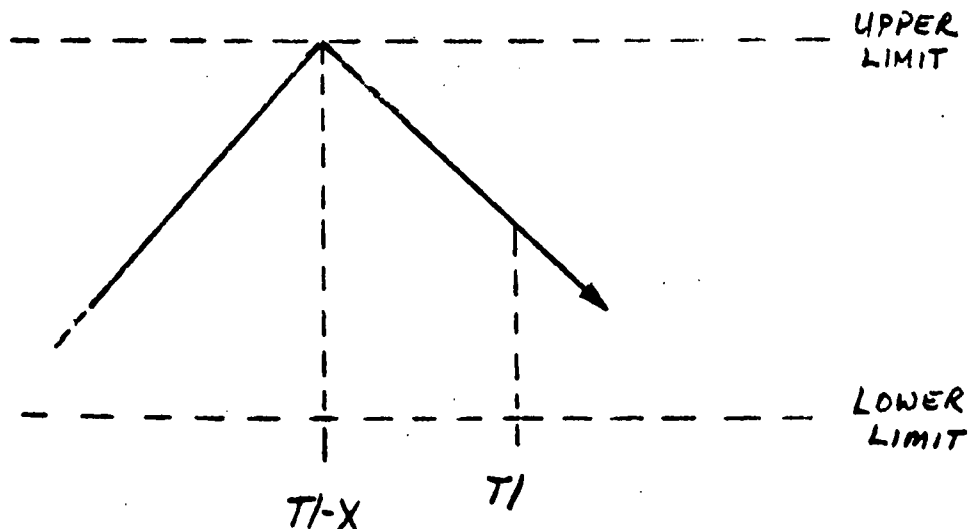
Continuation of the ramp direction is undesirable because it creates a condition whereby cumulative errors may be introduced at each battery current reversal. To alleviate this problem, the flip-flop must be toggled each time the battery current changes direction. This toggle action will again cause S1 and S2 to change state and the integrator will now ramp up. The integrator action is

now the same as it was originally except the flip-flop is now reset so that when the integrator reaches the upper limit at T2, it can be "set" and reverse the integrator ramp direction. The integrator is now forced to "re-trace" its path each time the battery current changes direction. Thus, the partial count stored in the integrator at time T1 is subtracted away before any new count pulses are generated.

2.4 STATE OF CHARGE COUNTER

The counter consists of four binary up/down counters. Total count capacity is 65,535 which is over six times the battery capacity, therefore no overflow inhibit is required in this system. When the counter contents are zero (fully-charged battery), the counter is inhibited in order to prevent overflow in this direction. The output of the counter is applied to the parallel entry of a 16 bit shift register. When telemetry read out occurs, parallel entry is inhibited and the contents of the register are shifted out in a serial format. At the end of telemetry read out, the parallel entry inhibit signal is removed and the contents of the up/down counter reappears in the shift register.

2.5 DEPTH OF DISCHARGE MONITOR

This circuit is designed to record the peak depth of discharge reached by the battery. It consists of a magnitude comparator, a binary counter, and a 16-bit shift register. If the binary counter is initially at zero, it will count all discharge pulses, during the first discharge period. During the next discharge period, the magnitude comparator continually observes the relative magnitudes of the number in the ampere-hour counter and the number stored in the binary counter (or depth-of discharge counter). When the ampere-hour number equals the depth-of-discharge number, the depth-of-discharge counter is gated on and begins counting discharge pulses. If the ampere-hour number (in discharge mode) does not reach the number previously stored in the depth-of-discharge counter, this counter will retain its previous count. As a result, the depth-of-discharge counter will always contain a number which is the maximum depth of discharge attained by the battery since the last time the counter was reset by ground command. A 16-bit shift register receives the parallel output of the depth-of-discharge counter and converts it to a serial output for ease of trans-mission.